REPORT DOCUMENTATION PAGE

The public reporting burden for this collection of information is estimated to average 1 hour per response, including the time for reviewing instructions, searching existing data sources, gathering and maintaining the data needed, and completing and reviewing the collection of information. Send comments regarding this burden estimate or any other aspect of this collection of information, including suggestions for reducing the burden, to the Department of Defense, Executive Services and Communications Directorate (0704-0188). Respondents should be aware that notwithstanding any other provision of law, no person shall be subject to any penalty for failing to comply with a collection of information if it does not display a currently valid OMB control number.
PLEASE DO NOT RETURN YOUR FORM TO THE ABOVE ORGANIZATION.

1. REPORT DATE (DD-MM-YYYY)	2. REPORT TYPE	3. DATES COVERED (From - To)
11March,2008	FINAL REPORT	From 15July03 to 14July06

4. TITLE AND SUBTITLE

ULTRAFAST TARGET RECOGNITION VIA SUPER-PARALLEL HOLOGRAPH BASED CORRELATOR, RAM AND ASSOCIATIVE MEMORY

5a. CONTRACT NUMBER

5b. GRANT NUMBER

FA49620-03-1-0408

5c. PROGRAM ELEMENT NUMBER

6. AUTHOR(S)

Dr. Selim Shahriar
EECS Department, Nortwestern University

5d. PROJECT NUMBER

5e. TASK NUMBER

5f. WORK UNIT NUMBER

7. PERFORMING ORGANIZATION NAME(S) AND ADDRESS(ES)

Northwestern University
Rebecca Crown Center
633 Clark Street, Evanston, IL 60208

8. PERFORMING ORGANIZATION REPORT NUMBER

9. SPONSORING/MONITORING AGENCY NAME(S) AND ADDRESS(ES)

AF OFFICE OF SCIENTIFIC RESEARCH
875 NORTH RANDOLPH STREET ROOM 3112
ARLINGTON VA 22203
Dr Gernot Pomrenke/NE

10. SPONSOR/MONITOR'S ACRONYM(S)

11. SPONSOR/MONITOR'S REPORT NUMBER(S)

12. DISTRIBUTION/AVAILABILITY STATEMENT

DISTRIBUTION STATEMENT A: UNLIMITED

AFRL-SR-AR-TR-08-0140

13. SUPPLEMENTARY NOTES

14. ABSTRACT

The overall objective of this project was to develop an ultrafast target recognition system using holographic techniques, as well as spin-off technologies with other applications. We report here a set of significant accomplishments towards this goal. These include: (1) demonstrations of shared hardware operation of a super-parallel holographic correlator and RAM, (2) demonstrations of a ultra-fast holographic stokesmeter for polarization imaging (3) demonstrations of off-axis transmission and reflection holographic lenses for use in the super-parallel architecture, (4) demonstrations of a translation-invariant correlation of images stored via holographic angle-multiplexing in a thick photopolymer material, (5) development of a large-area, thick, optical quality holographic recording disc capable of storing up to 2 terabyte of data, (6) demonstration of real-time, pico-second speed, translation-invariant correlation using a novel photorefractive material, and (7) demonstration of automatic target recognition of targets in a view from arbitrary altitudes and orientations during the flight of a remote-controlled aerial vehicle.

15. SUBJECT TERMS

Holographic Correlator, Automatic Target Recognition, Parallel Image Processing

16. SECURITY CLASSIFICATION OF:			17. LIMITATION OF ABSTRACT	18. NUMBER OF PAGES	19a. NAME OF RESPONSIBLE PERSON
a. REPORT	b. ABSTRACT	c. THIS PAGE			
					19b. TELEPHONE NUMBER (Include area code)

ULTRAFAST TARGET RECOGNITION VIA SUPER-PARALLEL HOLOGRAPH BASED CORRELATOR, RAM AND ASSOCIATIVE MEMORY

Final Report

Submitted by:

Prof. Selim M. Shahriar, PI
Department of Electrical and Computer Engineering
Northwestern University, Evanston, IL 60208

SUMMARY
The overall objective of this project was to develop an ultrafast target recognition system using holographic techniques, as well as spin-off technologies with other applications. We report here a set of significant accomplishments towards this goal. These include: *(1) demonstrations of shared hardware operation of a super-parallel holographic correlator and RAM, (2) demonstrations of a ultra-fast holographic stokesmeter for polarization imaging (3) demonstrations of a coherent holographic beam combiner for imaging applications, (4) demonstrations of off-axis transmission and reflection holographic lenses for use in the super-parallel architecture, (5) demonstrations of a translation-invariant correlation of images stored via holographic angle-multiplexing in a thick photopolymer material, (6) development of a large-area, thick, optical quality holographic recording disc capable of storing up to 2 terabyte of data, (7) demonstration of real-time, pico-second speed, translation-invariant correlation using a novel photorefractive material, (8) demonstration of automatic target recognition of targets in a view from arbitrary altitudes and orientations during the flight of a remote-controlled aerial vehicle, (9) demonstration of a multi-spectral holographic stokesemetry based imaging system, (10) demonstration of spatially-multiplexed holographic lenses with each lens having two separate channels of distinct angular and spectral transmission properties, with applications to a tristimulus filter for an eye-protection system, and (11) development of a holographic lenslet array for use in the super-parallel architecture of holographic correlator and RAM.* **Section 1** contains a summary of journal and conference papers resulting from this project. *We have published 21 papers and made 24 conference presentation.* **Section 2** contains a brief description of these accomplishments. *Three students have received their Ph.D. degrees based on the work reported here.* **Section 3** contains the conclusion, the status of technology transfer and outlook for future work.

20080331065

1

SECTION 1: PUBLICATIONS

1.A. JOURNAL PUBLICATIONS

1. "Demonstration of a Super-Parallel Holographic Optical Correlator for Ultrafast Database Search," M.S. Shahriar, M. Kleischmit, R. Tripathi, and J. shen, Opt. Letts. **28,** 7, pp. 525-527(2003).

2. "Shared hardware alternating operation of a super-parallel holographic optical correlator and a super-parallel holographic RAM", M.S. Shahriar, Renu Tripathi, M. Huq, and J.T. Shen, Opt. Eng. **43** 1856-1861(2004).

3. "Ultra-fast Holographic Stokesmeter for Polarization Imaging in Real Time," M. S. Shahriar, J. T. Shen, R. Tripathi, M. Kleinschmit, Tsu-Wei Nee, Soe-Mie F. Nee, Optics Letters, Vol. 29 Issue 3 Page 298 (February 2004)

4. "Polarization of holographic grating diffraction. II. Experiment," Tsu-Wei Nee, Soe-Mie F. Nee , M. W. Kleinschmit , M. S. Shahriar, JOSA A, Vol. 21 Issue 4 Page 532 (April 2004).

5. "Demonstration of a simple technique for determining the M/# of a holographic substrate by use of a single exposure," H. N. Yum, P. R. Hemmer, R. Tripathi, J. T. Shen, M. S. Shahriar, Optics Letters, Vol. 29 Issue 15 Page 1784 (August 2004).

6. "Highly polarization-sensitive thick gratings for a holographic stokesmeter", M. S. Shahriar, J. T. Shen, M. A. Hall, R. Tripathi, J. K. Lee, and A. Heifetz, Opt. Commun. (Accepted for Publication, 2004).

7. "Demonstration of a coherent holographic beam combiner", M.S. Shahriar, R. Tripathi, J.T. Shen, H.N. Yum, and P.R. Hemmer, Opt. Lett. (Submitted, 2004).

8. "Demonstration of a Thick Holographic Stokesmeter", J-K Lee, J.T. Shen, A. Heifetz, R. Tripathi, and M.S. Shahriar, Opt. Lett. (Submitted, 2004).

9. "Translation-invariant correlation of images stored via holographic angle-multiplexing in a thick photopolymer material", A. Heifetz, J.T. Shen, J-K Lee, R. Tripathi, and M.S. Shahriar, Opt. Commun. (Submitted, 2004).

10. "Prism-coupled lenslet array for a super-parallel holographic correlator", M.S. Shahriar , R. Tripathi, J.T. Shen, and A. Heifetz, Opt. Lett. (Submitted, 2004).

11. "Demonstration of High Quality Off-Axis Transmission and Reflection Holographic Lenses in a Thick Photopolymer Material," M. Andrews , A. Heifetz, J. T. Shen , J-K. Lee, R. Tripathi, M.S. Shahriar, Opt. Commun. (submitted, 2004).

12. "Translation-Invariant Object Recognition System Using an Optical Correlator and a Super-Parallel Holographic RAM", A. Heifetz, J.T. Shen, J-K Lee, R. Tripathi, and M.S. Shahriar, Opt. Engineering. (Accepted for Publication, 2005).

13. "Highly polarization-sensitive thick gratings for a holographic stokesmeter", M. S. Shahriar, J. T. Shen, M. A. Hall, R. Tripathi, J. K. Lee, and A. Heifetz, Opt. Commun. Volume 245, Issue 1-6, p. 67-73 (January, 2005).

14. "Demonstration of a coherent holographic beam combiner", H.N. Yum, P.R. Hemmer, A. Heifetz, J.T. Shen, J-K. Lee, R. Tripathi, and M.S. Shahriar Opt. Lett. (accepted, 2005)..

15. "Demonstration of a Thick Holographic Stokesmeter", J-K Lee, J.T. Shen, A. Heifetz, R. Tripathi, and M.S. Shahriar, Opt. Comm, (accepted, 2005).

16. "Prism-coupled lenslet array for a super-parallel holographic correlator and RAM", J.T. Shen, J-K. Lee, A. Heifetz, G.S, Pati, and M.S. Shahriar. Opt. Comm. (Submitted, 2005)

17. "Multiplexed Holographic Lenses with Dual Channels for Each Grating in a Thick Photopolymer Material," M. Andrews , A. Heifetz, J. T. Shen , J-K. Lee, R. Tripathi, M.S. Shahriar, Opt. Engineering. (submitted, 2005).

18. "Shift-Invariant Real-Time Edge-Enhanced VanderLugt Correlator Using Video-Rate Compatible Photorefractive Polymer," A. Heifetz, G.S. Pati, J.T. Shen, J.-K. Lee, M.S. Shahriar, C. Phan, and M. Yamomoto, submitted to Optics Commuinations (2005).

19. "Directional Correlation Between Input and Output Beams In A Dynamic Shift-Invariant Thick Hologram," A. Heifetz, G.S. Pati, J.-K. Lee, J. T. Shen, M.S. Shahriar, C. Phan, M. Yamamoto J. Opt. Soc. Am. A (submitted, 2005).

20. "A Pulse Area Theorem for Coupled Wave Equations in Thick Dielectric Gratings," A. Heifetz, G.S. Pati, J. T. Shen, J.-K. Lee, M.S. Shahriar, submitted to J. Phys. B. (2005).

21. "Experimental Realization of A Spectrally Multiplexed Holographic Stokesmeter," Jong-Kwon Lee, John.T. Shen, Alex. Heifetz, and M.S. Shahriar, submitted to Optics Letters (2005).

1.B. CONFERENCE PUBLICATIONS

1. "Quantum Versus Super-Parallel Holographic Database Search," M.S. Shahriar, presented at the SPIE Aerosense Meeting, Orlando, FL, 2003.

2. "Ultrafast Database Search Using Holographic Memory Vs. Quantum Computing," M.S. Shahriar, SPIE Photonic West, San Jose, CA, 2003. **(Invited Paper)**,

3. ""Imaging Stokesmeter utilizing holographic diffraction gratings," M.S. Shahriar, R. Tripathi, M. Kleinschmit, and T. Nee, presented at CLEO, Baltimore, MD, 2003.

4. "Demonstration of a super-parallel holographic RAM using the super-parallel holographic optical correlator architecture," M.S. Shahriar, R. Tripathi, M. Huq, and J.T. Shen, presented at CLEO/IQEC, San Fancisco, CA (2004).

5. "Holographic Stokesmeter Using Polarization-Sensitive Volume Gratings," M.S. Shahriar, J.T. Shen, Renu Tripathi, J.K Lee, and M.A. Hall, presented at CLEO/IQEC, San Fancisco, CA (2004).

6. "Demonstration of a single exposure technique for determining the M/# of a holographic substrate," H.N. Yum, P.R. Hemmer, R. Tripathi, J. T.

Shen, and M.S. Shahriar, presented at the CLEO/IQEC, San Fancisco, CA (2004).

7. "A Hybrid Correlator and RAM Using Super-Parallel Holography," M. Andrews, M. Huq, J. Shen, R. Tripathi, and M.S. Shahriar, presented at the SPIE Photonics West, San Jose, CA (2004). (**Invited Paper**).

8. "Spatio-Angular Parallelism in a Holographic Correlator and Random Access Memory," M.S. Shahriar, J.T. Shen, R. Tripathi, J-K. Lee, and A. Heifetz, presented at the OSA Annual Meeting, Rochester, NY (2004),

9. "Holographic Polarimeter Utilizing the Polarization Dependency of Thick Holographic Substrates," M.S. Shahriar, J.T. Shen, J-K. Lee, R. Tripathi, and A. Heifetz, presented at the OSA Annual Meeting, Rochester, NY (2004).

10. "High speed data search and pattern identification using a hybrid super-parallel holographic RAM-JTC geometry," M.S. Shahriar, Renu Tripathi, J.T. Shen, A. Heifetz, J-K. Lee, to be presented at SPIE Aerosense, 2005 (**Invited Paper**).

11. "A Landmark Identification Based Navigation System using A Hybrid Holographic Correlator" M.S. Shahriar, A. Heifetz, J.T. Shen, J-K. Lee, R. Tripathi, to be presented at SPIE, Photonics West, 2005, San Jose, CA (**Invited Paper**).

13. "Demonstration of a Thick Holographic Stokesmeter," M.S. Shahriar, J-K. Lee, J. T. Shen, A. Heifetz, R. Tripathi, submitted to CLEO 05, Baltimore, MD.

14. "Demonstration Of A Coherent Holographic Beam Combiner," M.S. Shahriar, R. Tripathi, J.T. Shen, H.N. Yum, P.R. Hemmer, submitted to CLEO 05, Baltimore, MD

15. "Translation-Invariant, High-Fidelity Correlation of Images Stored via Holographic Angle-Multiplexing in a Thick Polymer," M. S. Shahriar, A. Heifetz, J.T. Shen, J-K. Lee, R. Tripathi, submitted to CLEO 05, Baltimore, MD

16. "High speed data search and pattern identification using a hybrid super-parallel holographic RAM-JTC geometry," M.S. Shahriar, Renu Tripathi, J.T. Shen, A. Heifetz, J-K. Lee, presented at SPIE Aerosense, 2005 (**invited**)..

17. "A Landmark Identification Based Navigation System using A Hybrid Holographic Correlator" M.S. Shahriar, A. Heifetz, J.T. Shen, J-K. Lee, R. Tripathi, presented at SPIE, Photonics West, 2005, San Jose, CA (**invited**)

18. "Demonstration of a Thick Holographic Stokesmeter," M.S. Shahriar, J-K. Lee, J. T. Shen, A. Heifetz, R. Tripathi, presented at CLEO/QELS, Baltimore, MD, May 2005.

19. "Demonstration of a Multiwave Coherent Holographic Beam Combiner in a Polymeric Substrate," Ho Yum, Philip Hemmer, Alexander Heifetz, John Shen, Jong-Kwon Lee, Renu Tripathi, Selim M. Shahriar, to be presented at the OSA Annual Meeting, Tucson, AZ, October, 2005.

20. "Spectrally Scanned Polarimetric Imaging Using a Thick Holographic Stokesmeter," Jong-Kwon Lee, John Shen, Alexander Heifetz, Renu Tripathi, Selim M. Shahriar, to be presented at the OSA Annual Meeting, Tucson, AZ, October, 2005.

21. "Poly(Methyl Methacrylate)-Based Material for Thick Holographic Memory Plates and Ultra-Narrow Filters," John Shen, Jong-Kwon Lee, Alexander Heifetz, Gour Pati1, Renu Tripathi, John Donoghue, Shih Tseng, Selim M. Shahriar, to be presented at the OSA Annual Meeting, Tucson, AZ, October, 2005.

22. "Holographic Eye for UAV Navigation" M.S. Shahriar, to be presented at the SPIE Defense and Security Symposium, Orlando, FL, April 2006 **(invited)**

23. "Demonstration Of A Spectrally Multiplexed Holographic Stokesmeter," Jong-Kwon Lee, John.T. Shen, Alex. Heifetz, and M.S. Shahriar," to be presented at CLEO, 2006, Long Beach, California.

24. "Shift-Invariant Real-Time Edge-Enhanced VanderLugt Correlator Using Video-Rate Compatible Photorefractive Polymer," A. Heifetz, G.S. Pati, J.T. Shen, J.-K. Lee, M.S. Shahriar, C. Phan, and M. Yamomoto, to be presented at CLEO, 2006, Long Beach, California.

SECTION 2: TECHNICAL DETAILS

In Part A, we describe our accomplishments in the following areas:

- *Demonstration of shared hardware operation of a super-parallel holographic correlator and RAM,*
- *Demonstration of a ultra-fast holographic stokesmeter for polarization imaging*
- *Demonstration of a coherent holographic beam combiner for imaging applications,*
- *Demonstration of off-axis transmission and reflection holographic lenses for use in the super-parallel architecture*
- *Demonstration of a translation-invariant correlation of images stored via holographic angle-multiplexing in a thick photopolymer material.*

In Part B, we describe our accomplishments in the following areas:

- *Development of a large-area, thick, optical quality holographic recording disc capable of storing up to 2 terabyte of data,*
- *Demonstration of real-time, pico-second speed, translation-invariant correlation using a novel photorefractive material,*
- *Demonstration of automatic target recognition of targets in a view from arbitrary altitudes and orientations during the flight of a remote-controlled aerial vehicle,*
- *Demonstration of a multi-spectral holographic stokesemetry based imaging system,*
- *Demonstration of spatially-multiplexed holographic lenses with each lens having two separate channels of distinct angular and spectral transmission properties, with applications to a tristimulus filter for an eye-protection system*
- *Development of a holographic lenslet array for use in the super-parallel architecture of holographic correlator and RAM.*

A. DETAILS OF WORK DONE

A.1 COMBINED OPERATION OF THE SUPER-PARALLEL HOLOGRAPHIC OPTICAL CORRELATOR (SPHOC) AND THE SUPER-PARALLEL HOLOGRAPHIC RAM (SPHRAM)

For a practical missile recognition and tracking system, it is useful to have a high-speed random access memory (RAM) to complement the Super-Parllalel Holographic Optical Correlator (SPHOC) we have developed. For example, the RAM will be used to retrieve the targeting information for intercepting a missile once it is indentified by the holographic correlator. However, the speed of a conventional RAM, which accesses data serially, is too slow for this application. Here, we show how a super-fast RAM can be realized by simply operating the SPHOC in reverse. Called the super-parallel holographic random access memory (**SPHRAM**), this device and the SPHOC can be operated alternately using essentially the same hardware, and potentially the same data base. Thus, the SPHRAM offers a solution to the problem of identifying a fast RAM for the targeting application, without necessarily adding a separate device.
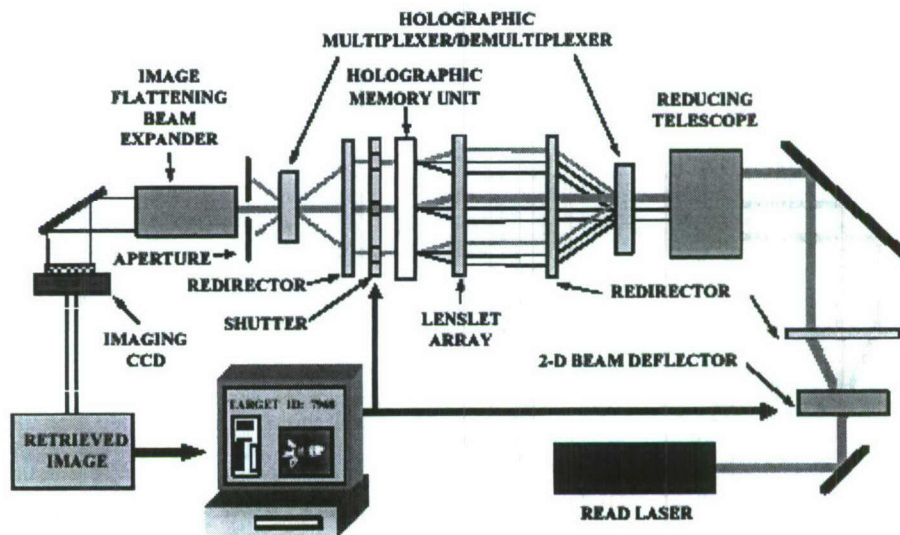
Figure 1 Schematic illustration of the Super-Parallel Holographic RAM (SPHRAM) architecture. A specificmemory page is read out by using the two coordinates: the storage angle and spatial location. The storage angle is sent to the 2-D beam deflector which deflects the read-laser to the appropriate angle. The beam is projected onto the appropriate location on the holographic multiplexer which produces N copies which are projected onto the holographic redirector. The redirector deflects each beam into the appropriate position on the lenslet array, which converts the position information into an angle. The angle generates an image from each spatial location of the HMU. The shutter array allows only the desired data-page to pass. The data is directed through the de-multiplexer, through the image- flattening beam expander and finally onto the imaging CCD array.

The basic idea of the SPHRAM is illustrated in Figure 1. As stated above, the functioning of this device is similar to an SPHOC operated in reverse. Briefly, the holographic memory unit (HMU) is recorded with the database of interest, using multiple spatial locations, each of which contains a set of images that are angularly multiplexing in two dimensions. When operating the RAM, the user enters as coordinates the spatial position and the angle of storage of the image of interest. The position coordinate is used to open the corresponding element of a shutter array. The number of elements in the shutter array is the same as the number of spatial locations in the HMU, and the locations are matched. Shutter arrays of this type are available commercially, with individually addressable ferroelectric liquid crystals, for example, with a very fast switching time. The extinction ratio of these shutters can be as high as 10s. MEMS based microdeflectors can also be used for this shutter array, which will have a virtually perfect extinction. (Alternatively, the shutter array can be eliminated from this architecture if one uses a two photon memory, where only the location of interest is illuminated by the activation laser frequency.)

Data Read-Out From Location 3X2
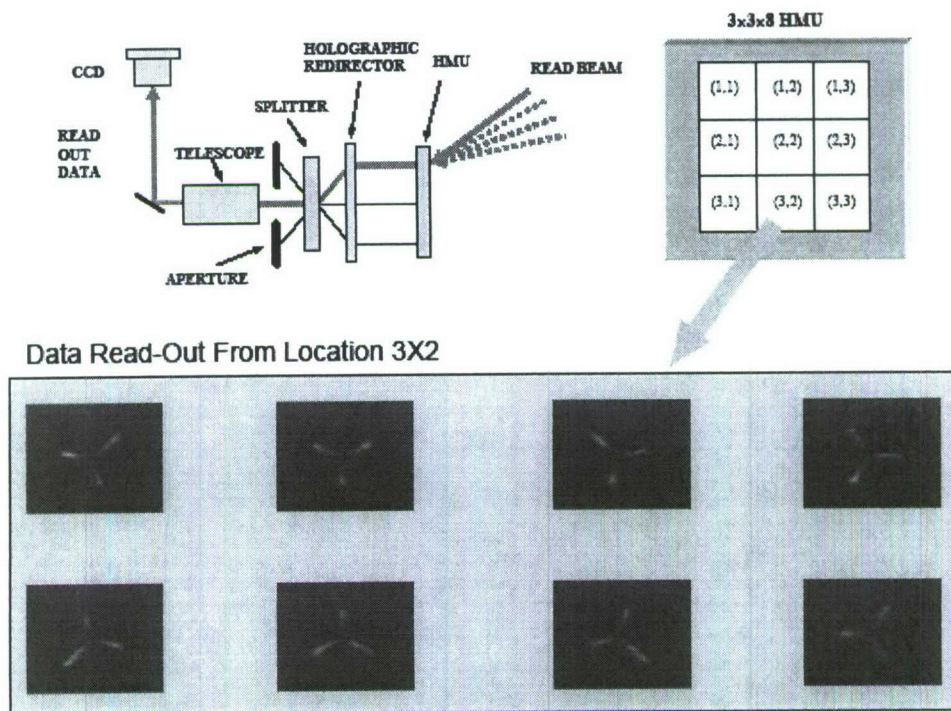
Figure 2: Examples of data pages retrieved through a simplified version of the SPHRAM architecture, using a pair of galvo-mounted mirrors for deflections. For the database, we used an existing HMU (holographic memory unit) which has 9 locations, in a 3X3 arrangement, each location containing 8 images multiplexed angularly. The redirectors and the splitter (multiplexer) used are the same as the ones created before for demonstrating the SPHOC architecture. The bottom of the figure shows a typical set of data retrieved using this setup. Similar data were also retrieved from the other locations (not shown).

The angular coordinate for the image is sent to a beam deflector (e.g., using a pair of acousto-optic or electro-optic deflectors), which orients the read beam at the desired angle, which in turn is translated to a specific position by the redirector. (Alternatively, one could simply use an SLM, but it would reduce the amount of light available for read-

out). The combination of the reducing telescope, the multiplexer, the redirector, and the lenslet array produces a copy of the read beam simultaneously at each of the locations; this is the key feature of the SPHRAM. As such, the image stored at this angle will be recalled from each location. The shutter array will block all but one of these images, and the redirector and the demultiplexer will send the wanted image to the CCD camera. We have recently demonstrated the feasibility of one part of this concept here, by using a pair of galvo-mounted mirrors for deflections. The geometry used by us for the demonstration is shown in figure 2. For the database, we used an existing HMU which has 9 locations, in a 3X3 arrangement, each location containing 8 images multiplexed angularly. The redirectors and the splitter (multiplexer) used are the same as the ones created before for demonstrating the SPHOC architecture. The bottom of the figure shows a typical set of data retrieved using this setup. Similar data were also retrieved from the other locations (not shown).
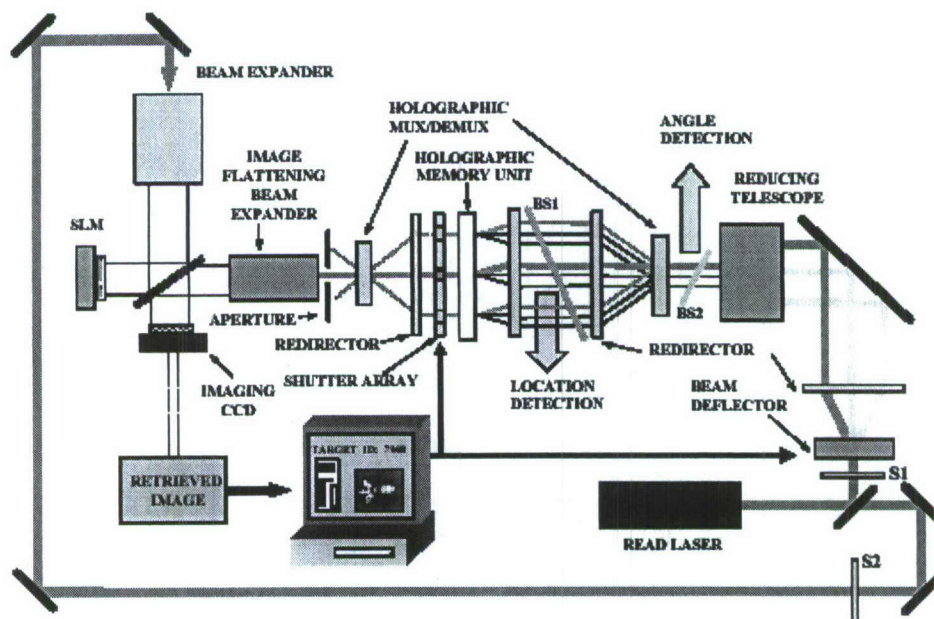
Figure 3: *Schematic illustration of an architecture that can be used as either an SPHOC or an SPHRAM, using potentially the same database. During the operation as an SPHOC, all the elements of the shutter array are open, shutter S1 is closed, and shutter S2 is open. Beams reflected by the beam splitter BS1 is used for location detection (see the SPHOC architecture for details, suppressed here for simplicity), and the beams reflected by the beam splitter BS2 is used for angle detection (again, see the SPHOC architecture for details, suppressed here for simplicity). During the operation as an SPHRAM, S1 is opened, S2 is closed, and the elements of the shutter array are opened selectively according to the address of the data page to be retrieved.*

Note that a simple modification of this architecture will allow one to operate the same system as the SPHOC as well. This is illustrated in figure 3. During the operation as an SPHOC, all the elements of the shutter array are open, shutter S1 is closed, and shutter S2 is open. Beams reflected by the beam splitter BS1 is used for location detection, and the beams reflected by the beam splitter BS2 is used for angle detection. During the

operation as an SPHRAM, S1 is opened, S2 is closed, and the elements of the shutter array is opened selectively according to the address of the data page to be retrieved.

A.2 A TRANSLATION-INVARIANT JOINT-TRANSFORM CORRELATOR FOR USE WITH THE SPHRAM.

In order to compensate for scale and rotation variance in optical correlation, a huge database of images may be used for reliable identification. Performing the correlations in a translation-invariant manner greatly reduces the size of the required database and speeds up the search process. A major disadvantage of the SPHOC in the present form is that it is difficult to achieve translation-invariant correlation because the SPHOC utilizes a thick holographic grating material to allow for two-dimensional angle-multiplexing[9,10]. Operating the SPHRAM with a translation-invariant joint-transform correlator (JTC)[2,4] based on a dynamic material answers the challenge of fast correlation with large databases. Images retrieved from the SPHRAM and used as the effective correlation filters in the JTC can be updated at a high rate, and the query images can be correlated with each filter in a translation-invariant manner. The schematics of the SPHRAM architecture combined with the JTC are presented in Figure 1 (for a detailed description of the SPHRAM operation see Reference 8).
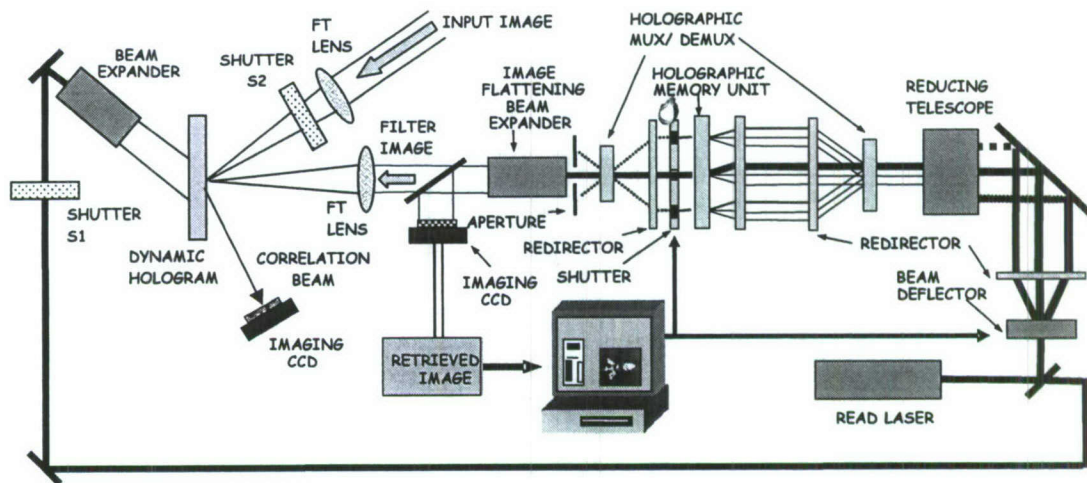
Figure 1.. End goal architecture of SPHRAM combined with JTC

The input image is encoded on the laser beam using a spatial light modulator (SLM) (not shown in the diagram). At the same time, a filter image is retrieved from the SPHRAM. The Fourier transforms of the input and the filter images are recorded in the dynamic holographic medium. During this process the shutter S1 is closed, while the shutter S2 is open. For practical parameters, it will take about 1 µs to read an image from the SPHRAM and about 1 µs to write the joint Fourier-transform onto the dynamic recording medium. Next, the shutter S2 is closed and the shutter S1 is open, thus

allowing the read beam to diffract from the grating and to produce a correlation beam. The correlation spot is captured with a CCD camera, and the dynamic holographic gratings containing the joint Fourier-transform is erased. Approximately 3 μs is needed for the CCD camera recording, and about 10 μs is needed to erase the grating in a typical high-speed material. This results in a total time of approximately 15 μs for a single correlation, which corresponds to an operating rate of 67 kHz. Once the match is found, the joint Fourier-transform grating does not need to be erased right away, allowing for subsequent translation-invariant correlation of the target.

In order to implement the SPHRAM/JTC system we need to identify the holographic material for high density and high quality permanent data storage needed to construct the SPHRAM, as well as the fast-response dynamic holographic material needed for JTC. We have already identified the photopolymer-based Memplex® thick holographic material developed by Laser Photonics Technology Inc. (Amherst, NY)[11] as the medium for high capacity and a high efficiency holographic memory. This material can have a very high M# (>20), and holograms written in this material can survive at room temperature for many years without noticeable degradation[12,13]. To the best of our knowledge, the fastest dynamic material currently available in the visible wavelength range is the photorefractive $Sn_2P_2S_6$ crystal[14,15] (abbreviated as SPS). Translation invariant JTC in a thick medium such as an SPS crystal can be realized by making use of the high angular bandwidth in the plane perpendicular to the plane of the object. Before we proceed to construct the translation-invariant SPHRAM with a JTC, we have to verify the ability of storing high quality angle-multiplexed holograms in a sample of the Memplex® material that we will subsequently refer to as the holographic memory unit (HMU), and performing a reliable translation-invariant correlation of the images reconstructed from the HMU.

We present the results of an elementary demonstration of the key components of the future SPHRAM/JTC system. In this experiment, the images were stored in the Memplex® HMU via 1-D angle-multiplexing, and later retrieved from the HMU to perform translation-invariant correlation with a static thin holographic filter in the VanderLugt filter-correlator architecture[2,3]. The experimental setup is shown in Figure 2.
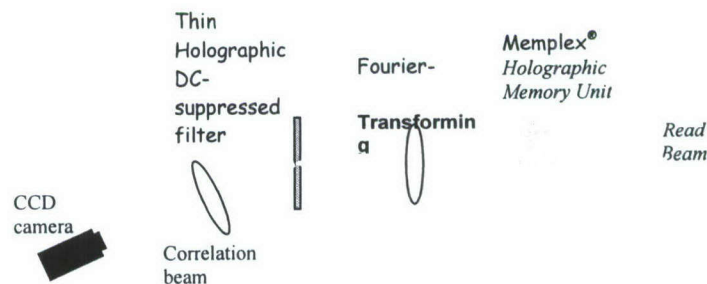

Figure 2. Setup for the translation-invariant Vanderlugt filter-correlator for the images retrieved from the HMU

In the image writing stage (not shown in the diagram), the HMU is treated as a 3x3 matrix of spatial locations, with a mask exposing one spatial location at a time. Different sets of about 20 images each are stored via angle-multiplexing in the horizontal dimension at each of the nine spatial locations of the HMU using a frequency-doubled ND:YAG laser operating at 532nm. Although we recorded images at nine spatial locations on the HMU, we would use only one spatial location containing a set of 23 binary images of snapshots of a MiG-25 fighter jet linearly translated to different locations on the frame for the translation-invariant correlation experiment. In Figure 3 one can see a sample of the original binary image.

Figure3. Original binary MiG-25 image.

A set of samples of the images reconstructed from the HMU and recorded with a CCD camera is presented in Figure 4.
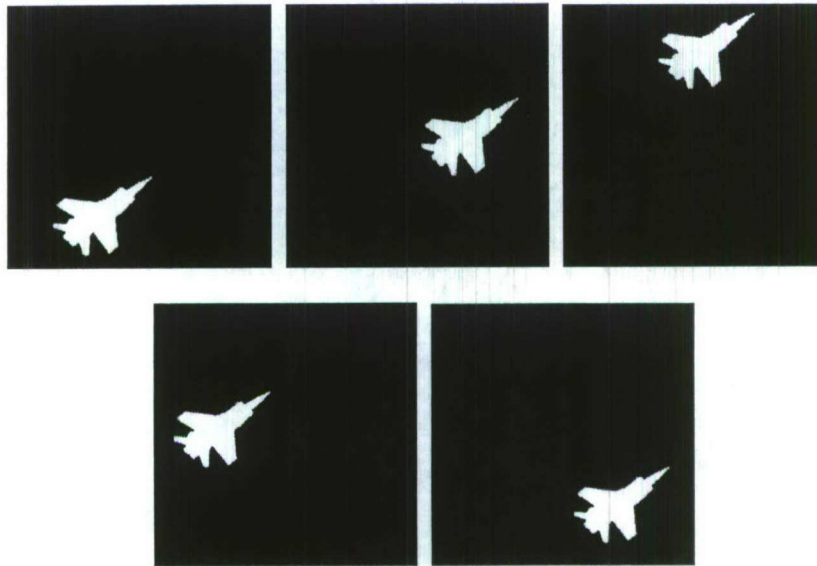
Figure 4. Samples of MiG-25 images moving in a loop pattern reconstructed from the HMU.

We note that there was no cross talk between the angle-multiplexed images at the same location or images at different spatial locations. The reconstructed images had a very high quality, which is essential for building a reliable SPHRAM correlator system.

We stored only 23 images of the MiG-25 jet, but in principle, in a 2mm thick plate, we could store up to 1000 2-D angle multiplexed images at a single spatial location[15].

The thin holographic filter used in the VanderLugt architecture contains a DC-suppressed Fourier transform of the MiG-25 jet image centered in the frame. This filter was prepared with VRP-M thin holographic plates made by Slavich using the same laser operating at the same wavelength as used for recording images in the HMU. We achieve the DC-suppression of the recorded Fourier transform by employing the DC saturation technique[3]. The edge-enhanced image reconstructed from the thin filter is shown in Figure 5.

Figure5. Edge-enhanced image reconstructed from the thin holographic filter.

The DC-suppression of the Fourier transform is needed to eliminate the chance of correlations with wrong objects[17]. The thin filter was separately tested for its correlation selectivity. Scanning the angle of the read beam incident on the same spatial location of the HMU, the images of the MiG-25 jet translated to different locations in the frame in a loop pattern are retrieved from the HMU. The correlation spot captured on the CCD camera indicates the position of the jet on the frame plane. Superimposing the successive correlation CCD frame grabs produces a trace of the trajectory of the jet, presented in Figure 6a.

(a)   (b)
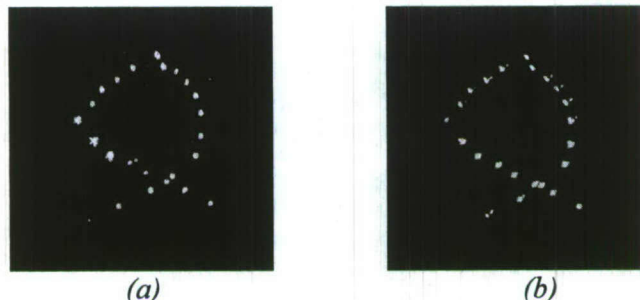
Figure 6. superimposed thresholded correlation spots showing a loop-pattern trace produced when the image source is (a) HMU and (b) SLM

For comparison of the data quality, another VanderLugt correlator is constructed, where instead of the HMU, the same images of the MiG-25 jet now come directly from the SLM. The same thin holographic filter is used for correlation. As before, a tracing trajectory of the jet is produced. The loop-pattern trajectory obtained with the images coming from the SLM is presented in Figure 6b. We see that the trajectories produced from the two experiments are essentially identical.

We have demonstrated that we can write high quality angle-multiplexed holograms in the holographic memory unit (HMU) based on the Memplex® material. We have also shown that we can perform a reliable translation-invariant correlation of the

13

images retrieved from the HMU, presently using the VanderLugt filter-correlator architecture. We will next proceed to implement the super-parallel holographic random access memory (SPHRAM) with a high-density data storage and fast data retrieval, and use it in conjunction with a joint-transform correlator (JTC) based on fast-response photorefractive crystals.

References for Sections A.1 and A.2

1. W.W. Goj, *Synthetic Aperture Radar for Electronic Warfare*, Artech House, Norwood, MA (1993).
2. J. W. Goodman, *Introduction to Fourier Optics*, McGraw-Hill, New York (1996).
3. A.B. VanderLugt, *Optical Signal Processing*, Wiley, Somerset, NJ (1992).
4. *Selected Papers on Optical Pattern Recognition Using Joint Transform Correlation*, M.S. Alam, Ed., SPIE Milestone Series MS157/HC, SPIE Press, Bellingham, WA (1999).
5. *Selected Papers on Optical Pattern Recognition*, F.T.S. Yu, Ed., SPIE Milestone Series MS156/HC, SPIE Press, Bellingham, WA (1999).
6. A.J.B. Hassaun, "Holographic correlation improves on DSP by six orders of magnitude," Laser Focus World 38, 44 (2002).
7. M.S. Shahriar, R. Tripathi, M. Kleinschmit, J. Donoghue, W. Weathers, M. Huq, and J.T. Shen, "Superparallel Holographic Correlator for Ultrafast Database Searches," Opt. Lett. **28**, 525-527 (2003).
8. M.S. Shahriar, R. Tripathi, M. Huq, J.T. Shen, "Shared-Hardware Alternating Operation of a Super-Parallel Holographic Optical Correlator and a Super-Parallel Holographic Random Access Memory," Opt. Eng. **43**, 1856-1861 (2004).
9. Q.B. He, P. Yeh, L.J. Hu, S.P. Lin, T.S. Yeh, S.L. Tu, S.J. Yang, K. Hsu, "Shift-Invariant Photorefractive Joint-Transform correlator using Fe:LiNbO$_3$ Crystal Plates," Appl. Opt. **32**, 3113-3115 (1993).
10. C. Gu, J. Hong, S. Campbell, "2-D Shift-Invariant Volume Holographic Correlator," Opt. Comm. **88**, 309-314 (1992).
11. R. Burzynski, D.N. Kumar, M.K. Casstevens, D. Tyczka, S. Ghosal, P.M. Kurtz, J.F. Weibel, "New Photopolymer for Holographic Optical Storage Technology," Proc. SPIE **4087**, R.A. Lessard, G.A. Lampropoulos Eds., 741-753 (2000).
12. H.N. Yum, P.R. Hemmer, R. Tripathi, J.T. Shen, M.S. Shahriar, "Demonstration of a Simple Technique for Determining the M# of a Holographic Substrate Using a Single Exposure," Opt. Lettt. **29**, 1784 (2004).
13. M.S. Shahriar, J. Riccobono, M. Kleinschmit, J.T. Shen, "Coherent and incoherent beam combination using thick holographic substrates," Opt. Comm. **220**, 75-83 (2003).
14. D. Haertle, G. Gaimi, A. Haldi, G. Montemezzani, P. Günter, A.A. Grabar, I.M. Stoika, Yu. M. Vysochanskii, "Electro-Optical properties of Sn$_2$P$_2$S$_6$," Opt. Comm. **215**, 333-343 (2003).
15. R. Ryf, G. Montemezzani, P. Günter, A.A. Grabar, I.M. Stoika, and Yu. M. Vysochanskii, "High-frame-rate joint Fourier-transform correlator based on Sn$_2$P$_2$S$_6$ crystal," Opt. Lett. **26**, 1666-1668 (2001).

16. H. Kogelnik, "Coupled Wave Theory for Thick Hologram Gratings," The Bell Syst. Tech. J. **48**, 2909-2947 (1969).

17. A. Pu, R. Denkewalter, D. Pasltis, "Real-time vehicle navigation using a holographic memory," Opt. Eng. **36**, 2737-2746 (1997).

A.3. **PRISM-COUPLED LENSLET ARRAY FOR A SUPER-PARALLEL HOLOGRAPHIC CORRELATOR**

In many pattern-recognition and target tracking applications, the speed of the detection system is of critical importance [1-3]. Optical correlation techniques in which the data pages are compared in parallel can offer an improvement over electronic digital signal processing methods that are serial in nature [4-8]. Volume holographic correlators can have an even larger advantage when a multiplexing scheme is used so that all the data pages stored in one location are queried simultaneously.

We have recently presented an initial demonstration of a super-parallel holographic correlator that represents a further advancement of this parallelism [9-10]. This SPHOC uniquely identifies N images from a database using only $O(\sqrt{N})$ number of detector elements, in a time scale that can be of the order of $1\,\mu$ sec. The spatial location and the reference beam angle for the matched image are identified by using a spatio-angular decoupling architecture, consisting of a combination of a lenslet array, a holographic redirector, a demultiplexer, and two CCD arrays. The key component in the spatio-angular decoupling architecture is a lenslet array that redirects and collimates the output correlation beams. We have derived the phase transformation that is required of this device as well as estimate the necessary parameters and dimensions as well as possible methods of construction. This prism-coupled lenslet array will also be used in reverse in a super parallel holographic RAM [11].

The architecture for the SPHOC is shown in figure 1 [9,11]. First, rXs (r by s) number of images are stored in each spatial location of the holographic memory unit (HMU) via two-dimensional angular multiplexing, where r is the number of horizontally multiplexed images, and s is the number of vertically multiplexed images. The process starts by expanding the collimated beam from a read laser in order to match the size of the SLM. The target image is gathered by a camera or by a SAR (synthetic aperture radar) in a battle theater for example. (Alternatively, the target could represent an object-to-image data map, which requires a much smaller amount of information to represent the image, in a rotation invariant way). This image is sent to the SLM via a high-speed data bus. The beam reflected from the face of the SLM carries this image. This reflected beam is now passed through the image flattening beam reducer (IFBR), which is a combination of two lenses. It reduces the image size by the ratio of the focal lengths of the two lenses, and projects a very slowly diverging version of the SLM image at the face of the next element: the holographic demultiplexer/multiplexer (HMDX). The HDMX is a device that produces nXm copies (which is the number of spatial locations on the HMU) of the input image, in as many angular directions. Such a device can be constructed simply by writing nXm plain wave holograms over the entire volume.

The output beams from the HDMX are now passed through the holographic redirector (HR). This role of this device is to redirect the output beams from the HMDX

into nXm images propagating parallel to the axis. The nXm identical copies of flattened images now impinge on the HMU, one at each spatial location. If the image matches one in one of these locations, a diffracted beam proportional to the correlation will emanate from that location at a particular angle. Here, we show all the possible diffraction beams (in one dimension, for simplicity of drawing), keeping in mind that only one of these beams (shown by the bold line) will be produced for a given image. The rest of the architecture identifies the (a) spatial location, and (b) the angle beam corresponds to. These two pieces of information will identify uniquely which image we have matched. The beams coming out of the HMU need to be collimated in the direction normal to the HMU. This can be achieved via the use of a prism-coupled lenslet array in which different prisms can be coupled to the different elements of the lenslet array depending on the angle of the beam emerging from the HMU i.e., each prism has a unique angle of deflection to make the beam symmetrical to the corresponding lens optic axis. In this manner, all emerging beams will be propagating parallel to the optic axis of the general system.

The beams emerging from the lenslet array, are now split into two components by a beam splitter. One component goes through another lenslet array and is focused onto an nXm array of CCD elements (CCDA). Identifying the detector that sees the highest signal yield the information about which spatial location the matched image is in. The other part of the beam goes through another HR (Holographic Redirector). The HR simply redirects all the incident batches to a central point, without focusing the beams coming from the same spot with respect to one another, as shown. These beams are now passed through another HMDX, which is identical to the one used at the input, but now operating in reverse. However, the reverse operation has the potential problem that additional beam patterns (weaker than the one generated along the axis) will also be produced. An aperture can be used to eliminate these unwanted spots. After the filter, we use a beam expander to match the size of the second CCD array, which contains rXs number of elements, corresponding to the number of angles used in the two-dimensional angular multiplexing during the writing stage. The element of the CCD that sees the brightest signal yields the information about the angle of the matched image. Data gathered from the detector array and the CCD array, properly thresholded, can be sent through a digital logic circuit to yield the absolute identity of the image we have matched. For practical parameters mentioned above, the whole process will take less than a μ sec.

In the above description, we made the simplifying assumption that only one image in a given spatial location will be matched for a certain query image. For the practical system however, it is likely that there will be multiple correlation beams of varying intensities diffracting from each spatial location. The angles between the different images in the HMU must be small in order to provide the maximum storage capacity, and thus the multiple correlation beams will be overlapping in addition to traveling at different angles. The prism-coupled lenslet array is designed to separate the correlation beams and redirect them so that they propagate in the same direction along the optic axis of the system.

Figure 2 illustrates the possible correlation beam overlap for one spatial location. A lens at each spatial location will be used to provide separation in the focal plane. The result of the differing angles of the beams will be a 2D array of spots in the focal plane. Figure 3 shows the geometry for one possible correlation beam. We will use the

geometry in figure 4 and analyze the phase transformation using Fourier optics [12,13]. The beam will undergo a phase transformation

$$t_{lens}(x) = \exp\left(-i\frac{k}{2f}(x+x_0)^2\right) \tag{1}$$

This can be expanded and viewed as the sum of three consecutive phase transformations:

$$t_{lens}(x) = \exp\left(-i\frac{k}{2f}x^2\right)\exp\left(-i\frac{k}{2f}2x_0x\right)\exp\left(-i\frac{k}{2f}x_0^2\right) \tag{2}$$

Thus the beam sees a constant phase shift, a linear phase shift, and a quadratic phase shift. The linear phase shift acts in a manner analogous to that of a prism, redirecting the beam, while the quadratic phase shift acts as a lens, focusing the beam. We can express a plane wave traveling at angle θ by $U = \exp(i2\pi\upsilon_0 x)$ where $\upsilon_0 = \sin\theta/\lambda$. Therefore, the field directly after the separating lens is:

$$U_{after} = \exp\left(i2\pi\left(\upsilon_0 - \frac{k\,x_0}{2\pi f}\right)x\right)\exp\left(-i\frac{k}{2f}x^2\right) \tag{3}$$

where we have dropped the constant phase factors. Using the Fresnel integral to propagate this field to the z=f and z=f+L planes, we find that the field at z=f+L is:

$$U_{final} = \exp\left(i\frac{k}{2L}x^2\right)\exp\left(-i2\pi\frac{f}{L}\left(\upsilon_0 - \frac{x_0}{\lambda f}\right)x\right) \tag{4}$$

This yields the information on the focal length lens we will need to cancel the quadratic phase term, as well as the angle of the prism needed to cancel the linear phase term, thus producing a plane wave traveling parallel to the optic axis. By keeping track of all the constant phase terms added by the prisms, lenses, and free-space propagation, we can also add a phase compensator plate to the lenslet array. The final array will consist of a quadratic phase correction, a linear phase correction, and a phase plate, yielding at its output collimated plane waves traveling along the optic axis, in phase. Figure 5 illustrates the layout of the full device. Figure 6 shows the device as part of a three element SPHOC/SPHRAM.

References for Section A.3

1. R.O. Duda, P.E. Hart, and D.E. Stork, "*Pattern Classification*", Wiley-Interscience (2000).
2. S. Theodoridis, and K. Koutroumbas, "*Pattern Recognition, Second Edition*", Academic Press (2003).
3. W.W. Goj, "*Synthetic-Aperture Radar and Electronic Warfare*", Artech House (1993).
4. N. Collings, "*Optical Pattern Recognition Using Holographic Techniques*", Pearson Addison Wesley (1988).
5. M. S. Alam (Ed.), "*Selected Papers on Optical Pattern Recognition Using Joint Transform Correlation*", SPIE Milestone Ser. **MS157/HC**, SPIE Press (1999).
6. F.T.S. Yu (Ed.), "*Selected papers on Optical Pattern Recognition*", SPIE Milestone Ser. **MS156/HC**, SPIE Press (1999).
7. M.J. Murdocca and B. Sugla, "Design of an optical random access memory", *Appl. Opt.* **28**(1) 182 (1989).
8. P.M. Birch, F. Claret-Tournier, D. Budgett, R. Young, and C. Chatwin, "Optical and electronic design of a hybrid digital-optical correlator system", *Opt. Eng.* **41**(1) 32-40 (2002).
9. M.S. Shahriar, R. Tripathi, M. Kleinschmit, J. Donoghue, W. Weathers, M. Huq, J.T. Shen "Superparallel holographic correlator for ultrafast database searches", *Opt. Lett.* **28**(7), 525-527 (2003).
10. A. J.-B. Hassaun, "Holographic Correlation Improves on DSP by Six Orders of Magnitude", *Laser Focus World* (July 2002).
11. M.S. Shahriar, R. Tripathi, M. Huq, J.T. Shen, "Shared-hardware alternating operation of a super-parallel holographic optical correlator and a super-parallel holographic random access memory", *Opt. Eng.* **43**(8) 1856-61 (2004).
12. J.W. Goodman, "*Introduction to Fourier Optics*", McGraw-Hill (1996).
13. A. Vanderlugt, "*Optical Signal Processing*", Wiley-Interscience (1992).
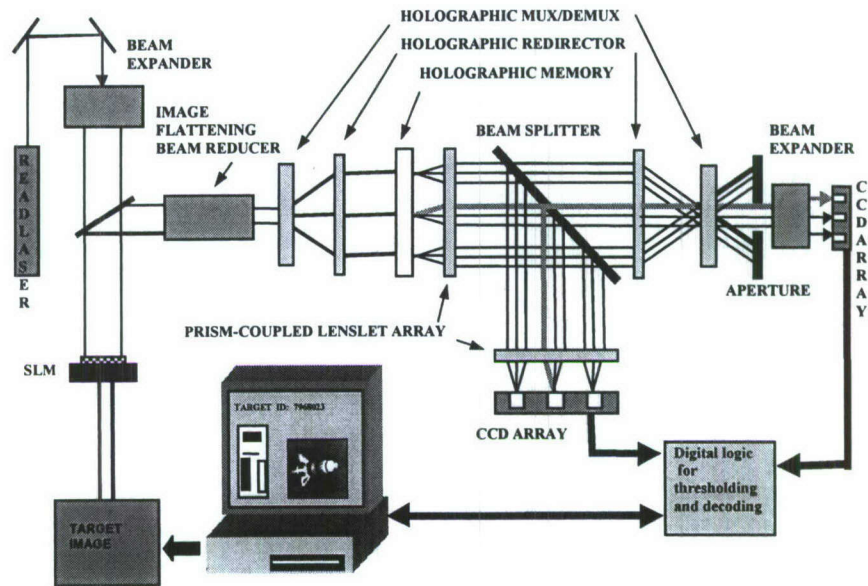
Figure 1: SPHOC Architecture
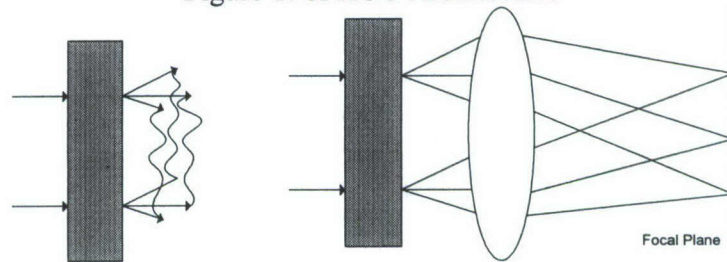
Figure 2: a) Overlapping correlation beams b) lens to separate and focus
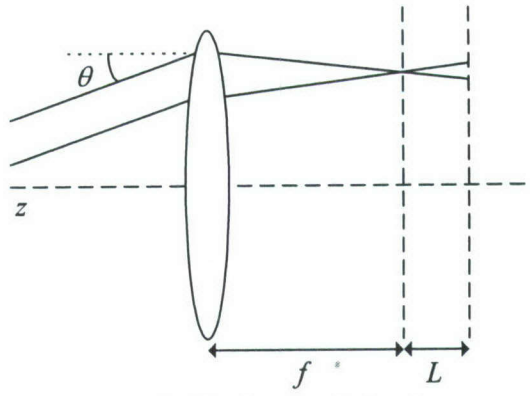
Figure 3: Single correlation beam
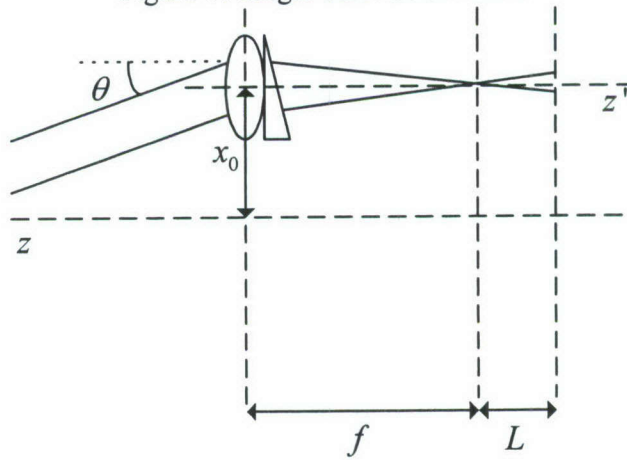
Figure 4: Phase transformation equivalent
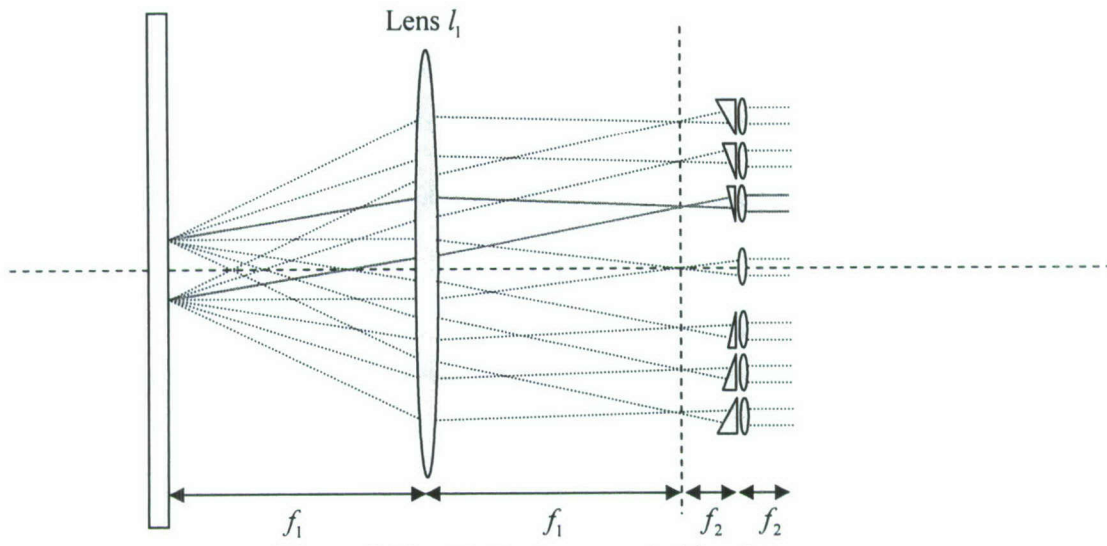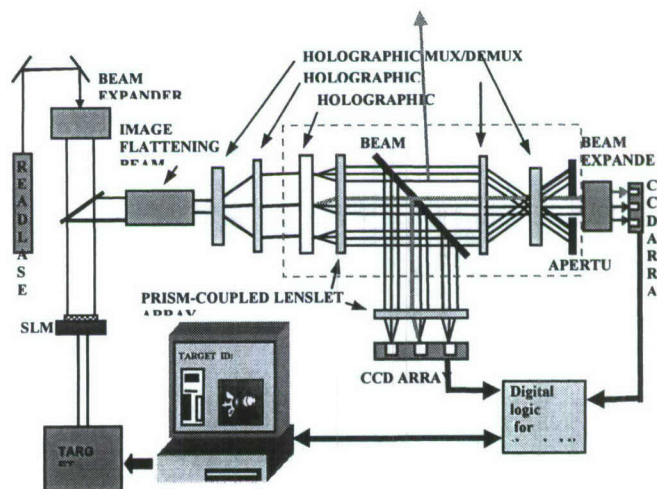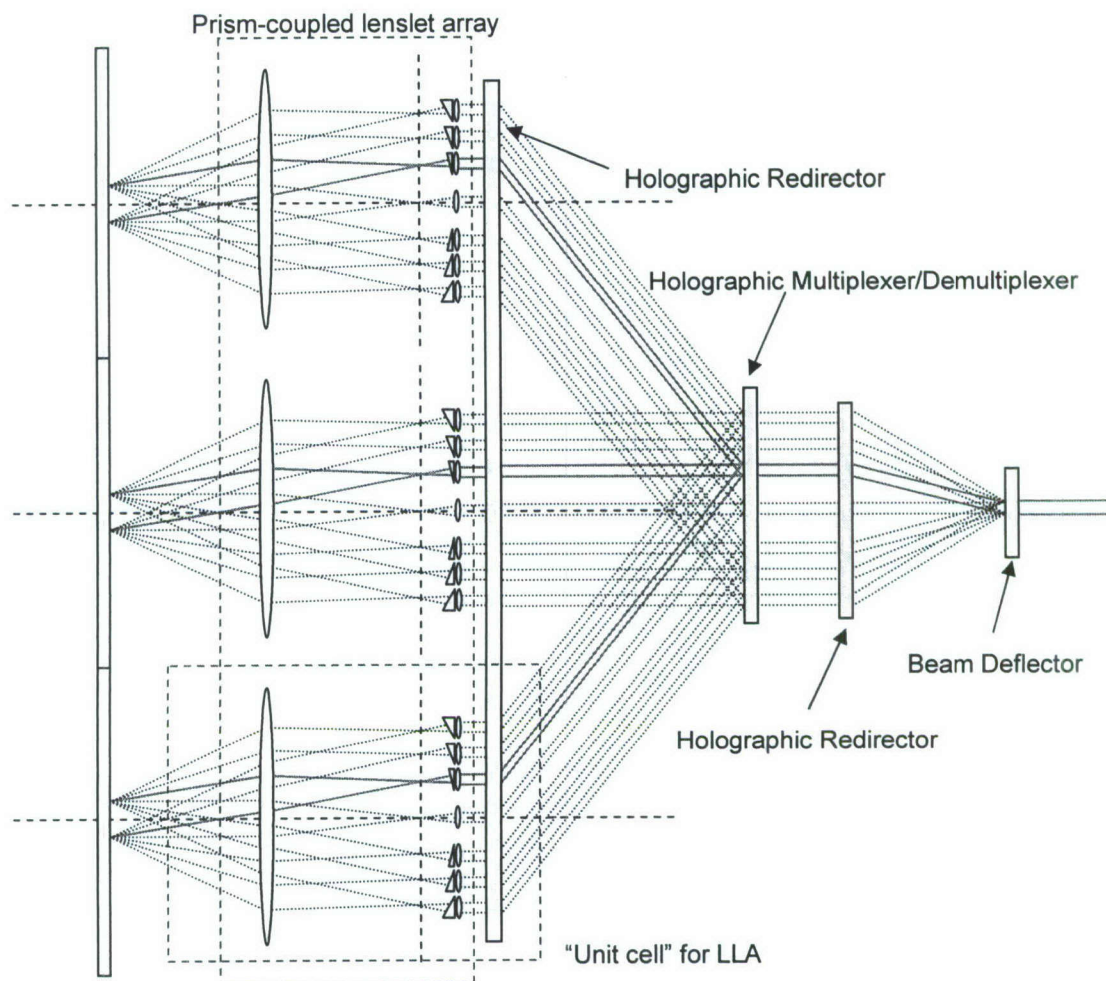
Figure 5: Detail of prism-coupled lenslet array

Figure 6: Prism-coupled LLA as part of the SPHOC architecture

A. 4. DEMONSTRATION OF A THICK HOLOGRAPHIC STOKESMETER FOR POLARIZATION IMAGING IN CONJUNCTION WITH HOLOGRAPHIC CORRELATION

Polarization imaging [1-3] can discriminate a target from its background in situations where conventional imaging methods fail. Identifying the components of the polarization of light reflected from a target allows one to construct an image that corresponds to the target's unique polarimetric signature. This is useful in applications ranging from target recognition to vegetation mapping [4-7]. Identifying the Stokes vector of the scattered light completely characterizes the polarization of light [8]. Current architectures for such a Stokesmeter include mechanical quarter-wave plate/linear polarizer combinations, photodetectors with polarization filtering gratings etched onto the pixels, and liquid crystal variable retarders [9-14]. The mechanical system is limited by the fact that it must rotate the angle between the wave-plate and polarizer before determining each Stokes parameter. The etched photodetector systems cannot resolve the complete Stokes vector at this time. The liquid crystal variable retarder system is similar to the mechanical sensor but with a liquid-crystal display replacing the wave plates and polarizers. This method is still sequential and the time required to reset the display limits the device operation to ~10 Hz. Systems based on the wave plate/polarizer architecture that split the beam into four parts and calculate the parameters in parallel [15] require four times as many optical components. Polarization gratings method that uses multiply diffracted and dispersed orders[16] can measure all four Stokes parameters in parallel but always needs the order blocking filters to prevent overlapping between the multiple diffraction orders of the beam, which gives rise to the scattering problems. Thus, it is not suitable for a polarimetric imaging system.

A holographic Stokesmeter can be used to resolve all four Stokes components in parallel and at a high speed [17]. For a typical thick holographic grating, the response time of the device can be on the order of 10 ps. This removes the device as the bottleneck in the imaging system and instead the desired signal-to-noise ratio and detector parameters set the upper limit on the imaging process. The holographic Stokesmeter [17] consists of two sets of two multiplexed volume gratings in a combination with a quarter-wave plate. The incoming beam is split and one half diffracts from the first set of multiplexed gratings, while the second half passes through the quarter-wave plate before diffracting from the second set of multiplexed gratings. Measurements of the four diffracted intensities are used in a set of pre-weighted equations to determine the four Stokes parameters. This architecture can be analyzed using a set of Mueller matrices for each grating which then yields the measurement matrix of the system. This allows one to take into account the Fresnel reflection and the grating diffraction and pre-determine the weights for the system of equations that determines the Stokes vector.

The holographic Stokesmeter takes advantage of the fact that volume gratings are polarization sensitive. This can be seen from a coupled-wave analysis of thick gratings [18], and the recent papers about the holographic grating diffraction [19,20]. Separating the diffraction efficiency into its s- and p- polarization components, one is able to analyze the architecture with Mueller matrices and arrive at a compact measurement matrix for the system:

$$
\begin{bmatrix} I_{t1} \\ I_{t2} \\ I_{t3} \\ I_{t4} \end{bmatrix} = \begin{bmatrix} A_1+B_1 & (A_1-B_1)\cos(2\gamma_1) & (A_1-B_1)\sin(2\gamma_1) & 0 \\ A_2+B_2 & (A_2-B_2)\cos(2\gamma_2) & (A_2-B_2)\sin(2\gamma_2) & 0 \\ A_3+B_3 & (A_3-B_3)\cos(2\gamma_1) & 0 & -(A_3-B_3)\sin(2\gamma_1) \\ A_4+B_4 & (A_4-B_4)\cos(2\gamma_2) & 0 & -(A_4-B_4)\sin(2\gamma_2) \end{bmatrix} \begin{bmatrix} I \\ Q \\ U \\ V \end{bmatrix} \quad (5)
$$

The values of A and B are specified by the grating itself. The Bragg angle and the slant of the grating will determine the Fresnel coefficients while the angle and the slant plus the index modulation depth, the thickness of the substrate, and the readout wavelength will determine the s- and p- components of the diffraction efficiency. The angles γ_1 and γ_2 denote the two different rotations of the substrate. I, Q, U, and V are determined by measuring the diffracted intensities I_{t1-4} and solving the matrix equation (1). In order for the system to be well conditioned [21,22], the diffraction efficiencies of the four gratings need to be chosen properly along with the other parameters.

We performed the measurements of the Stokes parameters using a holographic Stokesmeter made from a 2mm thick Memplex [23] sample with a 532nm frequency doubled Nd:YAG laser. We employed two sets of multiplexed gratings using rotation angles of $\gamma_1 = -4°$ and $\gamma_2 = 4°$. Both sets of the two multiplexed gratings were written at external angles of 40° and 54° for the first and second gratings respectively, with the reference beam at a 2° angle. Fig.1 displays the diffraction efficiencies of the holographic samples. It shows the polarization-sensitive diffraction efficiencies of 0.242, 0.211, 0.235, and 0.202 for the s- polarized state, and 0.147, 0.133, 0.148, and 0.113 for the p-polarized state. These diffraction efficiencies yield contrast ratios of 39.8%, 45.6%, 43.0%, and 45.5% respectively. Using the above parameters we constructed the measurement matrix for our system.

The experimental readout setup for the holographic Stokesmeter is illustrated in Fig.2 (a). We considered three different polarizations of the input beam: horizontal linear [1,1,0,0], linear [1,-0.55,0.84,0], and elliptical [1, 0.9, -0.25, -0.36]. These polarizations states can be realized by passing the laser beam through a half- wave and a quarter-wave plates rotated by the appropriate angles. The intensity of each of the four diffracted beams was measured, and used in the measurement matrix to determine the original Stokes vector. These values were then compared to a conventional measurement of the Stokes parameters.

For comparison, the values of the Stokes parameters describing the input polarization states were measured with a quarter- wave plate and a linear polarizer. This setup is illustrated in Figure 2 (b). In this conventional method, we need to measure the four different intensities I (0,0), I(45,0), I(45,90) and I(90,0) by changing the angle of the linear polarizer, and inserting the quarter wave plate. Here, θ of I (θ,Φ) is the angle of the half wave plate, and Φ of I (θ,Φ) is the quarter wave plate retardation. The output intensity for this method is given as:

$$I_{out}(\theta,\Phi) = (1/2)* [I + Q*\cos(2\theta) + U*\cos(\Phi)*\sin(2\theta) + V*\sin(\Phi)*\sin(2\theta)] \quad (6)$$

From these intensity measurements we can calculate the Stokes parameters:

$$I = I(0,0) + I(90,0)$$
$$Q = I(0,0) - I(90,0)$$
$$U = 2 I(45,0) - I(0,0) - I(90,0)$$
$$V = (2 I(45,90) - I(0,0) - I(90,0)) / P^2$$

(7)

where P^2 is the absorption factor related to the quarter wave plate.

Fig.3 displays the measured average values and the standard deviations of I, Q, U and V for the each method. Although the result for the holographic Stokesmeter has a slightly larger error than the result for the QWP/linear polarizer, the average values are approximately equal to the assumed values within the error range. Errors from the holographic Stokesmeter result in the variation of the values of I and Q by a margin of 1% to 5%. Variations of the U and V values are in the range of 3% to 16%. For comparison, all the Stokes parameters from the conventional method have a variation of less than 4%. The reasons for the larger error range of the holographic Stokesmeter compared with the conventional method can be seen from an analysis of the robustness of this holographic Stokesmeter. Our Stokesmeter shows lower contrast ratio of 40% to 50%. According to our previous simulation results for the C/R versus error level, a higher contrast ratio gives a lower error rate. We expect a Stokesmeter made using such gratings to be more error tolerant.

As the next step in the development of the performance of the holographic Stokesmeter, we suggest an improved architecture that consists of a single set of multiplexed gratings and two electro-optic modulators (EOM), as shown in Fig.4(a). The first EOM plays the same role as the quarter-wave plate in the current architecture, namely to interchange the U and V parameters. In order to use only one holographic optical element (HOE), we have to reverse the polarization states of the input beams (s-polarization into p-polarization and p-polarization into s-polarization) by rotating the fast axis of the second EOM of 45° with respect to that of the first EOM. Fig.4 (a) also shows the driving voltage scheme for the EOMs with the frequency of ~ 10GHz. This will produce a well conditioned measurement matrix. Since there is 0V sent to the EOMs during T_1, the input beam enters the HOE without changing the polarization state. Then, the measured intensities from the diffracted beams will give us the information about the first two rows of the measurement matrix in Eq(1). The intensity measurement for the reversed polarization states of the input beams after interchanging U and V parameters during T_2 yields the information about the third and fourth rows of the measurement matrix in Eq(1). This new holographic Stokesmeter will be simpler and more reliable than current one because it requires fewer optical elements. In addition, it only requires splitting the incident power once, as opposed to twice in most architectures. Fig 4(b) shows the entire polarimetric imaging system. The input image is diffracted by the HOE and is directed and imaged onto the two FPAs using a 4f imaging system. After we gather all four intensity measurements taken during the periods of T_1 and T_2 for each pixel of the FPA arrays, we can construct the polarimetric image by manipulating the signals with precalibrated field programmable gate arrays (FPGA). We are currently in the process of demonstrating the holographic Stokesmeter with the new architecture using high contrast ratio samples.

References for Section A.4

1. J.L. Pezzaniti, and R.A. Chipman, "Mueller matrix imaging polarimetry," *Opt. Eng.* **34** 1558 (1995).

2. K.P. Bishop, H.D. McIntire, M.P. Fetrow, L. McMackin, "Multispectral polarimeter imaging in the visible to near-IR, Targets and Backgrounds: Characterization and Representation," *Proc. SPIE* **3699,** 49 (1999).

3. G.P. Nordin, J.T. Meier, P.C. Deguzman, and M.W. Jones, "Micropolarizer array for infrared imaging polarimetry," *J. Opt. Soc. Am.* **A 16,** 1168 (1999).

4. L.J. Denes, M. Gottlieb, B. Kaminsky, and D. Huber, "Spectro-polarimetric imaging for object recognition," *Proc. SPIE,* **3240,** 8 (1998).

5. T. Nee, S.F. Nee, "Infrared polarization signatures for targets," *Proc. SPIE* **2469,** 231 (1995).

6. W.G. Egan, "Polarization in remote sensing," *Proc. SPIE* **1747,** 2 (1992).

7. Curran, P.J., "Polarized visible light as an aid to vegetation classification," *Remote Sens. Environ.* **12,** 491-499, (1982).

   8. A. Gerrard, J.M. Burch, "Introduction to Matrix Methods for Optics," Dover Publications, NY (1974).

9. R.M.A. Azzam, "Photopolarimeter using two modulated optical rotators," *Opt. Lett.* **2,** 148 (1977).

10. D.H. Goldstein, " Mueller matrix dual-rotating retarder polarimeter," *Appl. Opt.* **31,** 6676 (1992).

11. C.S.L. Chun, D.L. Fleming, W.A. Harvey, and E.J.Torok "Polarization Sensitive Infrared
    Sensor for Target Discrimination," *Proc. SPIE* **3121** (1997).

12. J.L. Pezzaniti, R.A. Chipman, " High-resolution Mueller matrix imaging polarimetry for
    understanding high-resolution optoelectronic modulators," *Proc. SPIE* **2297,** 468 (1994).

13. J.S. Tyo, T.S. Turner, Jr., "Imaging spectropolarimeters for use in visible and infrared remote
    sensing," *Proc. SPIE* **3753,** 214 (1999).

14. J.M. Bueno, P. Artal, "Double-pass imaging polaimetry in the human eye," *Opt. Lett.* **24**, 64
    (1999).

15. V. L.Gamiz, " Performance of a four channel polarimeter with low light level detection,"
    Proc. SPIE **3121** (1997).

16. S. Krishnan, S. Hampton, J. Rix, B. Taylor, and R.M.A.Azzam,"Spectral polarization measurements by use of the grating division of amplitude photopolarimeter," *Appl. Opt*. **42**, 1216(2003).

17. M.S. Shahriar, J.T. Shen, R. Tripathi, M. Kleinschmitt, T. Nee, S.F. Nee, "Ultra-fast Holographic Stokesmeter for Polarization Imaging in Real Time," *Opt, Lett*, **29**, 298 (2004).

18. H. Kogelnik, "Coupled wave theory for thick hologram gratings," *Bell Syst. Tech. J.* **48** 2909
    (1969).

19. Tsu-Wei Nee, Soe-Mie F. Nee, " Polarization of holographic grating diffraction. I. General theory," *J. Opt. Soc. Am.* **A 21**, 523 (2004).

20. T.W. Nee, S.F.Nee , M.W. Kleinschmit , M. S. Shahriar, " Polarization of holographic grating diffraction. II. Experiment," *J. Opt. Soc. Am.* **21**, 532 (2004).

21. A. Ambirajan, D.C. Look, "Optimum angles for a polarimeter," *Opt. Eng.* **34,** 1651-1655
    (1995).

22. D.S. Sabatke, A.M. Locke, M.R. Descour, W.C. Sweatt, J.P. Garcia, E.L. Dereniak, S.A.
    Kemme, G.S. Phillips, "Figures of merit for complete Stokes polarimeter optimization,"
    Proc. SPIE **4133,** 75-81 (2000).

23. Burzynski, D.N. Kumar, S. Ghosal, and D.R. Tyczka, "Holographic Recording Material,"
    U.S Patent No. **6,344,297** (2002).
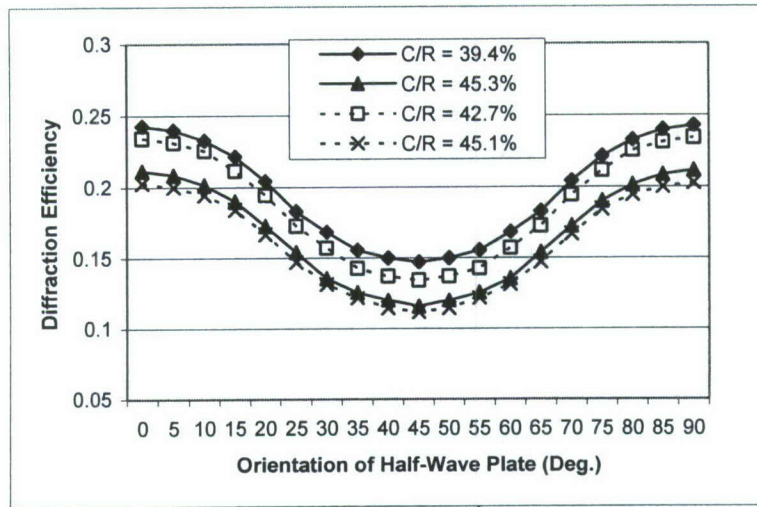
Figure 1: Diffraction efficiencies vs. incident polarization of the two multiplexed
holographic Stokesmeter gratings

(a)   (b)
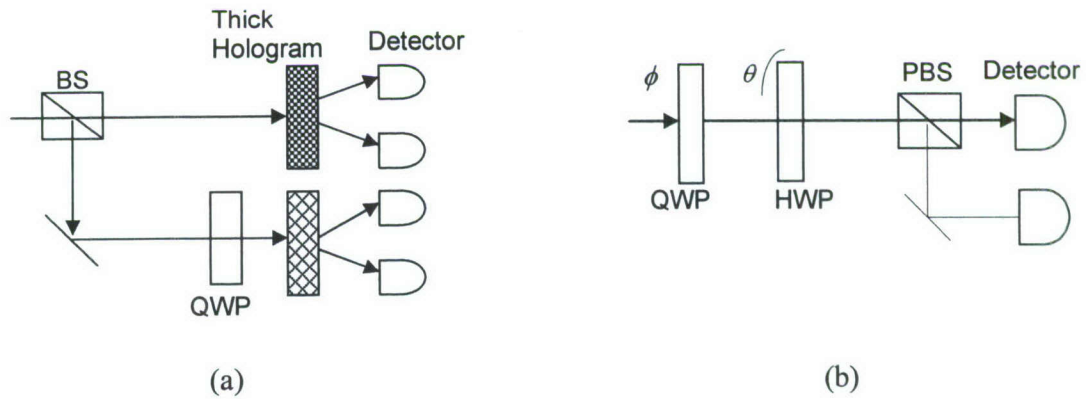
Figure 2: Readout setup for (a) holographic Stokesmeter (b) Conventional method using QWP/ linear polarizer
(QWP: Quarter-Wave Plate, HWP: Half-Wave Plate, PBS: Polarization Beam Splitter)
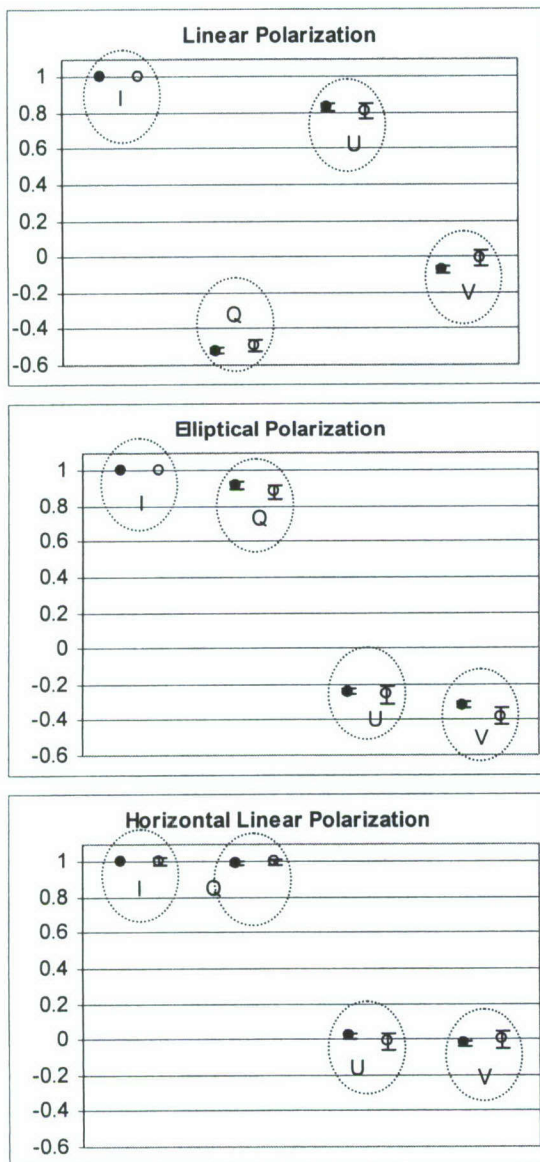
Figure.3: The measured average values and the standard deviations of I, Q, U and V by the two methods for the three different polarization states of the input beam (holographic Stokesmeter: white circles, quarter wave plate / linear polarizer: black circles)
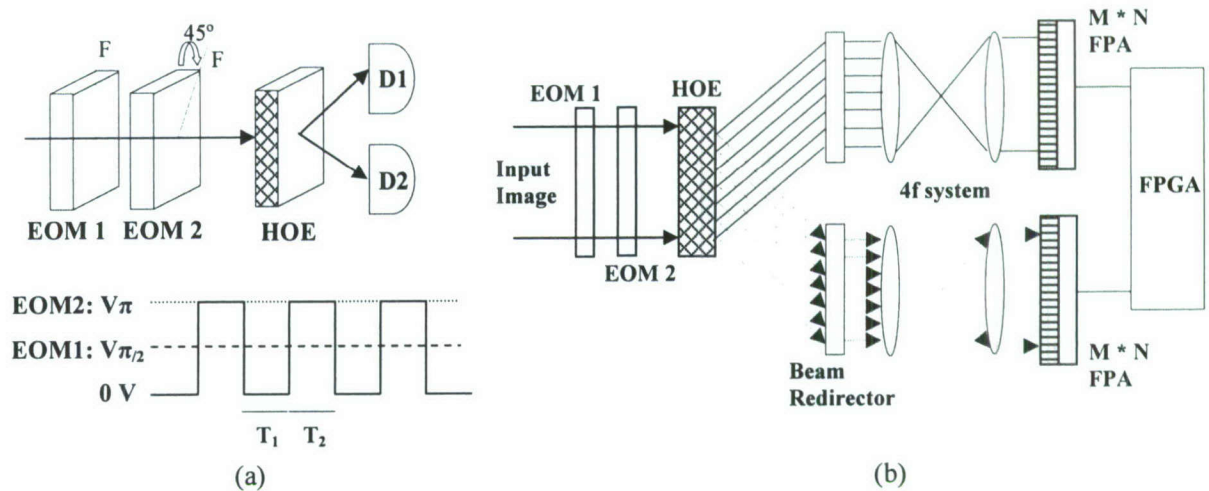
Figure.4 (a) Top: Suggested new architecture of holographic Stokesmeter Bottom: input signal scheme for the EOMs (b) Polarimetric imaging system using holographic Stokesmeter D: Detector, EOM: electro-optic modulator, F: Fast axis, FPA: M X N focal plane array, HOE: holographic optical element (thick hologram with two multiplexed gratings)

A. 5. DEMONSTRATION OF A SIMPLE TECHNIQUE FOR DETERMINING THE M/# OF A HOLOGRAPHIC SUBSTRATE USING A SINGLE EXPOSURE

The dynamic range of a holographic medium is an important parameter in determining the storage density and diffraction efficiency for holographic memory systems and holographic beam combiners [1-4]. In these applications, many holographic gratings are multiplexed in the medium at the same spatial location. The M/# is a parameter that defines the dynamic range of the holographic medium; it is essentially $\pi/2$ times the ratio of the maximum achievable index modulation and the index modulation corresponding to a unity diffraction efficiency grating. The existing techniques [4-8] to measure the M/# require one to write many holograms on the material. We have developed a potentially simpler technique to determine the M/# for a holographic recording material and we present simulated and experimental results for a photopolymer-based holographic recording medium.

Typically, illumination of a holographic substrate with a spatially periodic, sinusoidal intensity pattern produces a periodic index modulation $n(x) \equiv n_o + n' \cos(K x)$ where n_o is the spatially averaged index of refraction of the medium, n' is the index modulation depth, and K represents the wave number of the grating. When a laser beam of wavelength λ illuminates this grating at the Bragg angle, the diffraction efficiency η is given by [9]

$$\eta = \frac{I_d}{I_o} = \sin^2\left(\frac{\pi n' \alpha d}{\lambda}\right) \tag{1}$$

where I_o is the input intensity, I_d is the diffracted intensity, d is the thickness of the substrate and α is the obliquity factor determined by the orientation of the grating. A characteristic scale for the index modulation is $n_c \equiv \lambda/(2\alpha d)$, so that η becomes

$$\eta = \sin^2\left(\frac{\pi}{2} \frac{n'}{n_c}\right); \qquad \eta = 1 \quad \text{for} \quad n' = n_c \tag{2}$$

In many situations the modulation depth [4] can be modeled as

$$n' = n_m \left[1 - \exp\left(-\frac{t}{\tilde{\tau}}\right)\right] \tag{3a}$$

where t is the exposure time, $\tilde{\tau}$ is a time constant that depends on the material sensitivity and the intensity of the writing laser beams, and n_m is the maximum index modulation. A convenient way to quantify the value of n_m is through the use of the M/#, which can be defined as $M/\# = (\pi n_m)/(2 n_c)$. For notational convenience, we define a scaled version of this expression

$$Q \equiv \frac{n_m}{n_c}; \text{ so that } M/\# = \left(\frac{\pi}{2}\right)Q \tag{3b}$$

When Q is an integer, it represents essentially the maximum number of orthogonal, unit diffraction efficiency gratings that can ideally be written in a given spatial location.

Consider a situation where N equalized diffraction efficiency gratings are multiplexed on a single substrate using the Bragg (angle or wavelength) orthogonality condition. For $N \gg Q$ the diffraction efficiency for each grating can be approximated by

$\eta \cong \left(\pi^2 / 4\right)\left(Q/N\right)^2$ [4,5]. More generally, if the diffraction efficiencies of the gratings are not identical, it is possible to define and measure the M/# of the material from the relation [4,5]

$$Q \approx \sum_{i=1}^{N} \sqrt{\eta_i} \,, \qquad \eta_i \ll 1 \tag{4}$$

Although one can measure the M/# using one exposure for certain cases[5,7], in general to measure the M/# using this approach may require one to write many holograms. As an alternative method, one can also use the fact that the diffraction efficiency of a single grating in the small index modulation limit is a quadratic function (to a first order) of the exposure time, described by

$$\eta(t) \approx Q^2 \left(\frac{t^2}{\tilde{\tau}^2}\right)\left(\frac{\pi^2}{4}\right) \tag{5}$$

which follows directly from eqns. 2, 3a, and 3b. The M/# can thus be determined from the curve that defines the diffraction efficiency of a single hologram as a function of exposure time. This method also requires recording many successive holograms with different exposures on the holographic substrate.[4]

We have developed a potentially simpler approach to determine the M/# from a single recording on the holographic medium. To illustrate this method, we first combine eqns. 2 and 3a in order to express the diffraction efficiency as a function of time:

$$\eta(t) = \sin^2\left(\frac{\pi}{2} Q\left[1 - \exp\left(-\frac{t}{\tilde{\tau}}\right)\right]\right) \tag{6a}$$

Now, according to the generalized optical pumping model [4] the saturation rate $(\tilde{\tau}^{-1})$ depends linearly on the intensity of the radiation for writing the grating: $\tilde{\tau}^{-1} = \beta \tilde{I}$, where β is the sensitivity of the medium, and $\tilde{I}$ is the amplitude of the intensity modulation defined as

$$I \equiv \tilde{I}\left(1 + \cos(K_G x)\right) \tag{6b}$$

with K_G being the grating vector. For typical values of $\tilde{I}$ used, the value of β can be assumed to be a constant. If the value of $\tilde{I}$ depends on position $\vec{r}$ as well, then we can write

$$\eta(t, \vec{r}) = \sin^2\left(\frac{\pi}{2} Q\left[1 - \exp\left(-\beta \tilde{I}(\vec{r})t\right)\right]\right) \tag{7}$$

As a specific example, let us consider a situation when two equal intensity, coherent Gaussian beams write a grating in the holographic medium. The intensity distribution will be:

$$I(\vec{r}) = 2 I_o \exp\left(-2r^2 / \omega_o^2\right)\left[1 + \cos\left(\vec{K}_G \cdot \vec{r}\right)\right]; \quad \vec{K}_G = \vec{K}_1 - \vec{K}_2 \tag{8}$$

where $\vec{K}_1$ and $\vec{K}_2$ are the propagation wave vectors, I_o is the intensity at the center of each beam, and ω_o is the Gaussian beam radius of each writing beam. Comparing eqn. 8 with eqn 6b, we find: $\tilde{I} = 2 I_o \exp\left(-2r^2 / \omega_o^2\right)$. When this expression is used in eqn. 7, the resulting diffraction efficiency is given by

$$\eta(t, \vec{r}) = \sin^2\left(\frac{\pi}{2} Q\left[1 - \exp\left(-f(r) t / \tau\right)\right]\right); \quad 0 \le f(r) \le 1 \tag{9}$$

where $f(r) = \exp\left(-2r^2/\omega_o^2\right)$, and $\tau = 1/2\beta I_o$. Across the spatial profile of the writing beams, the value of f(r) varies from 1 in the center for r = 0 to a value of 0 for $r \gg \omega_o$.

Now, if $t/\tau \approx 5$, for example, then at r=0, $\exp\left(-f(r) t/\tau\right)$ approaches zero. However, for r>>ω_o, $f(r) \ll 1/5$ and $1 - \exp\left(-f(r) t/\tau\right)$ approaches unity. This argument holds for larger value of t/τ as well. Thus for $t/\tau \geq 5$, the quantity $1 - \exp\left(-f(r) t/\tau\right)$ varies *monotonically* from one to zero. Therefore, the total number of circular fringes is on the order of Q/2 for $t/\tau \geq 5$. Accordingly, we note that for the proper exposure time one can be sure to observe the full number of fringes. To be more precise, let us express Q as follows:

$$Q = 2m + n + \alpha; \quad \alpha<1, \; n=0, \text{ or } 1 \tag{10}$$

In this notation, α is the fractional part of Q, while n determines if Q is odd or even. Consider first the case where n=0, and α=0: In this case, for $t/\tau \geq 5$, the number of full circular fringes equals m with a null at the center. Consider next the situation where n=1, and α=0. In this case, the number of full circular fringes will still be m, but there will be a peak at the center. Finally, for $\alpha \neq 0$, the efficiency at the center will have a dip if n=1, and a peak if n=0. The actual value of the efficiency at the center reveals the value of α.

We studied the phenomenon using simulations. Fig 1 shows the result for exposure time dependence of the diffraction efficiency for an even Q value material with a plane wave read-out. This result shows the expected dark center for an even Q material. Fig 2 shows the simulation result for diffraction for a material with an odd Q value plus a fractional part. As expected there is an intensity peak at the center of the diffraction pattern and a dip due to the fractional part. The value at the center yields the value of the fractional α as 0.2, resulting in a Q value of 11.2 which corresponds to an M/# value of 17.584.

To show the principle of operation experimentally, we used a dye-doped polymeric Memplex ® [10] material. This material had a Q value of 6 as claimed by the manufacturer. Fig 3 shows the combined setup for hologram writing, and readout. Writing was done with a frequency doubled Nd:YAG laser (λ=532 nm) and readout was performed with a He-Ne laser operating at 632.8 nm. This material required baking after holographic exposure. During the experiment, the exposure times were gradually increased. After the exposure, the material was baked until the number of observable interference fringes reached maximum. Table 1 shows the results for a series of exposures for the holographic substrate. It shows that as we reach the optimum limit for holographic exposure, the number of interference fringes visible in the diffracted beam reach a maximum (3 in this case). Thus, the Q for our material is ~ 6. This value of Q yields the M/# of the material as 9.42.

References for section A.5:

1. M.-P. Bernal, H. Coufal, R.K. Grygier, J.A. Hoffnagle, C.M. Jefferson, R.M. Macfarlane, R.M. Shelby, G.T. Sincerbox, P. Wimmer, and G. Wittman, "A precision tester for studies of holographic optical storage materials and recording physics", *Appl. Opt.* **35** 2360 (1996).

2. L. Solymar, D.J. Webb, A. Grunnet-Jepson, and W. Solymar, Eds. *"The Physics and Applications of Photorefractive Materials"*, Oxford Series in Optical and Imaging Sciences **11** (1996).

3. L. Dhar, A. Hale, H. Katz, M.L. Schilling, M.G. Schnoes, and F.G. Schlling, "Recording media that exhibit high dynamic range for digital holographic data storage", *Opt. Lett.* **24**(7) 487 (1999).

4. Shahriar M.S., Riccobono J., Kleinschmit M., and Shen J.T., "Coherent and incoherent beam combination using thick holographic substrates", *Opt. Commun.* **220** 75 (2003).

5. Mok F.K., Burr G.W., and Psaltis D., "System metric for holographic memory systems", *Opt. Lett.* **21** 896 (1996).

6. G.W. Burr, W.-c. Chou, M.A. Neifeld, H. Coufal, J.A. Hoffnagle, and C.M. Jefferson, "Experimental evaluation of user capacity in holographic data-storage systems", *Appl. Opt.* **37**(23) 5431 (1998).

7. G. J. Steckman, R. Bittner, K, Meerholz, D. Psaltis, "Holographic multiplexing in photorefractive polymers", *Opt. Comm.* **185** p13 (2000).

8. Psaltis D., Brady D., and Wagner K., "Adaptive optical networks using photorefractive crystals", *Appl. Opt.* **27** 1752 (1988).

9. H. Kogelnik, "Coupled wave theory for thick hologram gratings", *Bell Syst. Tech. J.* **48** 2909 (1969).

10. R. Burzynski, D.N. Kumar, S. Ghosal, and D.R. Tyczka, *"Holographic Recording Material"*, U.S. Patent No. **6,344,297** (2002).
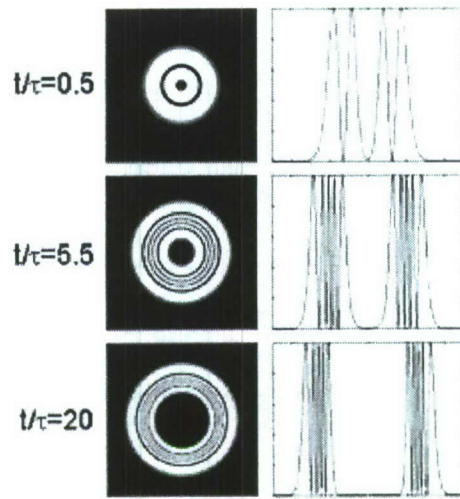
Fig 1   Simulation result showing the evolution of diffracted pattern as a function of holographic exposure for an even Q (m=5, n=0, α=0 in eqn 10) value material with a plane wave read-out beam. Normalized diffraction efficiency is plotted versus radial distance.
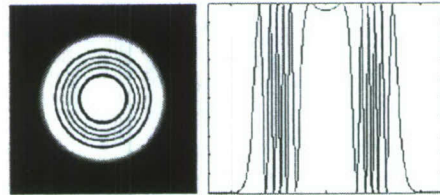
Fig. 2   Simulation result for the diffraction pattern for fractional Q with a plane wave read-out beam (m=5, n=0, α=0.2 in eqn 10). Normalized diffraction efficiency is plotted versus radial distance.
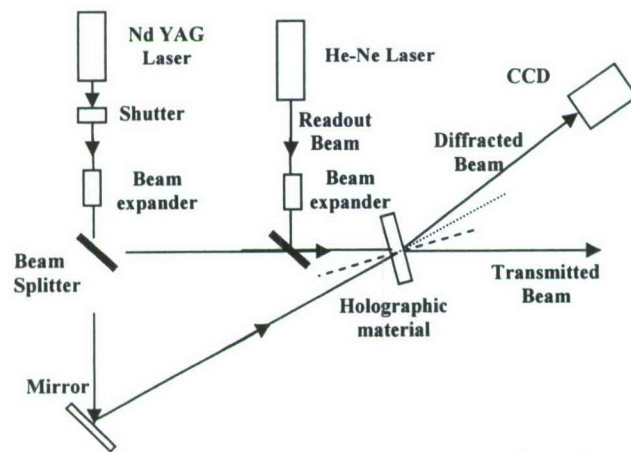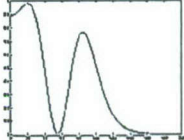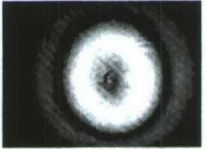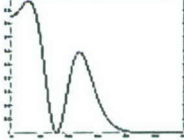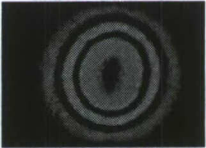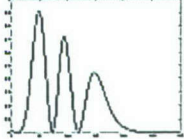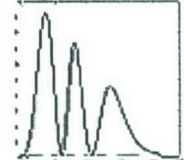
Fig. 3: Writing and Read-out Geometry

S.N.	Exp. Time	Diffracted Image	Profile of the Diffracted Image
1	26 sec		
2	32 sec		
3	52 sec		
4	64 sec		

Table 1: Experimentally observed diffraction pattern for 4 different exposures. As one reaches the optimum limit for holographic exposure, the number of interference fringes visible in the diffracted beam each a maximum.

A.6. DEMONSTRATION OF A COHERENT HOLOGRAPHIC BEAM COMBINER FOR APPLICATIONS TO IMAGE MULTIPLEXING AND DEMULTIPLEXING

A holographic beam combiner (HBC) [1] has applications in combining the output from multiple laser sources to a single output. It can alternately function as a beam splitter, or a beam coupler [1,2]. These functionalities can be achieved both coherently and incoherently. Thick holographic materials are used in incoherent beam combination due to narrow spectral selectivity of the gratings allowing one to multiplex a higher number of gratings compared to a thin material.

The coupled wave theory for thick holographic gratings [3] describes the diffraction efficiency of a volume hologram and provides solutions for the amplitudes of the signal and reference waves. Volume gratings cause an energy interchange between the incoming reference wave and the outgoing signal wave at or near the Bragg angle. The coupled-wave theory has been extended to verify the diffraction efficiencies of a refractive index modulated holographic material with two sets of incoherently superimposed gratings used for beam splitter and beam combiner modes [4-9], and to consider multiple gratings recorded sequentially by one reference wave and object waves in a lossless holographic material under Bragg-matching condition. [1,8]

We have investigated the influence of the variation of phase angle difference between adjacent input waves on the intensity of the output wave for a case of N input waves which have equally separated phase angles in an incoherent beam combiner. We use a coupled-wave analysis to perform a simulation, which agrees with the experimental beam combiner demonstrated here.

Figure 1 shows the schematic illustration of the reconstruction of object waves illuminating N multiplexed gratings with a reference wave. The derivation of the coupled-wave equations for multiple gratings is not shown here for brevity, but can be seen in references [2, 3]. We assume that the recording material is infinite in the x and y directions, and that all waves polarizations are in the y direction. Z is the propagation direction. In addition, we neglect second derivatives assuming that there is no cross-talk between different diffracted orders and consider the absorption to be zero, i.e., we consider only the refractive index modulations. The coupled-wave equations can be written as

$$C_0 S_0' = -j \sum_{h=1}^{N} \kappa_h S_h$$

$$C_h S_h' + j \vartheta_h S_h = -j \kappa_h S_0$$

(8)

The parameters C_0 and C_h are the obliquity factors defined as $C_0 = \rho_{0z}/\beta$, $C_h = \rho_{0h}/\beta$ where $\beta = n\omega/c$ and the propagation vectors ρ_0 and ρ_h are related to the grating vector K by $\vec{\rho}_h = \vec{\rho}_0 - \vec{K}_h$, S_0 and S_h are the amplitudes of the reference and hth object waves respectively, ϑ_h is the dephasing constant given by $\vartheta_h = (\beta^2 - \rho_h^2)/2\beta = 0$, under Bragg matching conditions. The parameter κ is the coupling constant $\kappa = \pi n_h/\lambda$ where n_h is the amplitude of the refractive index modulation.

The grating strength v_h for the h_{th} grating can be written as

$$v_h = \frac{\pi m_h d}{\lambda \sqrt{C_R C_h}} \tag{2}$$

where C_R and C_h are the obliquity factors for the reference and the hth object wave respectively.

N gratings can be incoherently multiplexed by recording sequential holograms with a fixed reference wave and N angularly separated object waves [3,4]. In a beam-combiner, the N object waves illuminate the structure at their respective Bragg angles and reconstruct the reference wave.

We study the influence of the variation of phase angle difference between adjacent input waves on the intensity of the output wave for the case that N input waves have equally separated phase angles in the beam combiner mode. We consider a constant phase angle variation from one object wave to another. The boundary conditions at $z=0$ are $S_0(0)=0$, $S_1(0)=1$, $S_2(0)=e^{j\phi}$, $S_3(0)=e^{j2\phi}$, ... $S_N(0)=e^{j(N-1)\phi}$ where ϕ is the phase difference between adjacent waves. The amplitude of S_0 at $z=d$ becomes

$$S_0(d) = -\frac{1}{2}\sqrt{\frac{\prod\limits_{h=1}^{N} C_h}{C_0 \gamma}} \left[\sum_{h=1}^{N} \kappa_h e^{j(h-1)\phi}\right]\left[\exp\left(j\sqrt{\frac{\gamma}{N}} d\right) - \exp\left(-j\sqrt{\frac{\gamma}{N}} d\right)\right] \tag{3}$$

where the parameter γ is defined as $\gamma = \sum\limits_{h=1}^{N}\left(\prod\limits_{k=1}^{N} C_k\right)\kappa_h^2 \Big/ C_h$

Intensity of the output wave can be written as

$$I = S_o(d) S_o^*(d) \tag{4}$$

In the analysis of intensity profiles of the output waves using simulation, it is assumed that grating strengths for N holograms are equalized to the value at which the beam combiner shows maximum diffraction efficiency. A holographic beam splitter with N superimposed gratings divides an incident wave into N partial waves with equalized maximum diffraction efficiencies when the N grating strengths satisfy the equation

$\left(\sum\limits_{h=1}^{N} v_h^2\right)^{\frac{1}{2}} = \frac{\pi}{2}$ where $v_h = \pi n_h d \big/ \lambda\sqrt{C_R C_h}$ [2-4]. By a time-reversal argument, the beam

combiner must show maximum efficiency at the same grating strength at which the holographic beam splitter reaches maximum diffraction efficiency. Therefore the equalized grating strength for N superimposed holograms is $v_1 = v_2 = ...$

$= v_{N-1} = v_N = v = \pi\big/2\sqrt{N}$.

Fig 2a shows the output intensity of a six- beam combiner as a function of equalized grating strength for the case when all the input waves are in phase. Fig 2b shows the output intensity as a function of phase angle between adjacent waves when the equalized grating strength is set to three different values of v: two, four, and six (similar to that shown in fig 2a). The output beam intensity reaches a value equal to the sum of the

intensities of individual input beams when all the input beams are in phase. From fig 2b we see that the finesse corresponds to the number of input waves. The finesses of the six- and nine- beam combiners are double and triple of that of a three- beam combiner. The height of peak decreases as the grating strength reduces to the value of 0.2500. The finesses of three peaks have the same value of 6.

Figure 3 shows the experimental setup for hologram writing and readout. A frequency-doubled Nd:YAG laser (λ=532nm) was used both for writing and reading the holograms. The material used in the study was a dye-doped polymer Memplex ® [10]. We recorded four holograms in the first sample and six holograms in the second sample using angular multiplexing and exposure schedule. The incident reference beam S_0 was fixed for all exposures. The angle difference between consecutive object waves is kept constant.

In the readout, a beam illuminates the holograms at the common Bragg angle for the reference beam which reconstructs beams S_1-S_N simultaneously. Tables 1 shows the transmitted and diffracted images of the 4 and 6 superimposed holograms, exposure schedules, and simulation results. In Table 1, the diffraction image of S_2 shows low efficiency as compared with that of S_1, S_3, S_4 and a fringe in the bright region inside the ring because of mode hopping of the laser during the 2nd exposure.

The combination of six waves was performed with the 2nd sample. Figure 4 describes the experimental set-up using a plano-convex lens. The input wave from Nd-YAG laser illuminates holograms in the direction of reference S_0 and is split into 6 waves. The waves represented by solid lines are propagating in the beam splitter mode. The flat surface of the lens faces the holograms which is the point source of the split six waves. Therefore both surfaces contribute to refractions to minimize spherical aberrations. The six waves are paralleled by the lens and reflected by mirror. The incident angle displacement between adjacent object waves is constant during hologram recording. The phase angles of six diffracted waves can be distributed with equal separation ϕ. The six reflected waves illuminate the hologram in the beam combiner mode. The combined beam is partially reflected by a beamsplitter. The partially reflected beam is monitored by a photo detector while the mirror is adjusted to vary the phase difference. The waves represented by dashed lines are propagating in the beam combiner mode.

The sum of the intensity of individual split beam defined as $6I_0$ measured as 760mV after the splitter but before the lens in Fig. 4. I_0 notes the average intensity of each individual beam. At this point, the undeflected beam was measured as 20mV. It was determined from the simulation that the maximum height of peak which can be theoretically obtained by our holographic beam combiner is 734 mV. Figure 5 shows the intensity of the partially reflected combined beam measured by photodetector. It is noted from the 3rd and 4th peak on the left that the half width covers 0.7 fractional divisions in one rectangular box and the distance between peaks is 4 fractional divisions. The measurement yields the finesse of 6 beam combiner as 5.7 which is approximately equal to the value theoretically estimated. We can confirm all 6 input waves contribute to beam combining. The height of the highest peak is measured as 265mV at the detector in Fig 6. The beamsplitter in Fig. 4 reflects 61.54% of the incoming light. Therefore the intensity

of the combined beam is calculated as 475.6mV corrected for reflection from hologram surface. The experimental output is lower than the theoretically expected output of 734mV.

The degradation of the efficiency of holographic beam combiner can be caused by the following reasons. There may be a loss of coupling into the reconstructed wave because of partial diffraction back into the 6 objective waves (S_1-S_6). The input wave may also illuminate a location which is deviated from the center of a hologram. The grating strength degenerates along the radius of the hologram showing the Gaussian distribution of the writing beam. Therefore, illumination with the center of reading beam on the center of the hologram without deviation results in high diffraction efficiency. The error of angle displacement during holographic recording can bring about phase angle difference variation between adjacent beams. Because of this, phase angle mismatch always exists to a certain degree. All input beams can neither be in-phase simultaneously nor fully combined.

References for section A.6

1. M.S. Shahriar, J. Riccobono, M. Kleinschmit, J.T. Shen, "Coherent and incoherent beam combination using thick holographic substrates", *Optics Comm.* **220** 75-83 (2003).
2. J. Zhao, X . Shen, and Y. Xia, "Beam splitting, combining, and cross coupling through multiple superimposed volume-index gratings," *Opt. &Las. Tech.* **33**, 23-28, (2001).
3. H. Kogelnik, "Coupled wave theory for thick hologram gratings", *Bell Syst. Tech. J.* **48** 2909 (1969).
4. S. K. Case, "Coupled wave theory for multiply exposed thick holographic gratings," *J. Opt. Soc. Am.* **65**, 724-729 (1975).
5. R. Magnusson, and T. K. Gaylord, "Analysis of multiwave diffraction of thick gratings," *J. Opt. Soc. Am.,* **67**, 1165-1170, (1977)
6. J. Zhao, P. Yeh, M. Khoshnevisan , and I . McMichael, "Diffraction properties of vector synthetic volume index gratings," *J. Opt. Soc. Am. B* **17**, 898-903, (2000).
7. H. Kobolla, J. Schmidt, J. T. Sheridan, N. Streibl and R. Völkel, "Holographic optical beam splitters in dichromated gelatin," *J. Mod. Optic,* **39** (4), 881-887, Apr. (1992).
8. J.E. Ludman, J. Riccobono, N. Reinhand, I., Yu. Korzinin, M.S. Shahriar, H.J. Caulfield, J. Fournier, and P.R. Hemmer, "Very thick holographic nonspatial filtering of laser beams", *Optical Engineering*, **36** 1700 (1997).
9. L. Solymar and D.J. Cooke, "Volume Holography and Volume Gratings", (London : Academic Press) Chap.8.2 (1981).
10. R. Burzynski, D.N. Kumar, S. Ghosal, and D.R. Tyczka, "*Holographic Recording Material*", U.S. Patent No. **6,344,297** (2002).
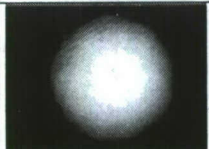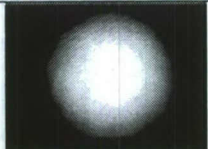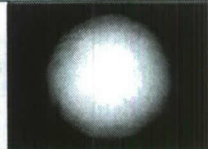
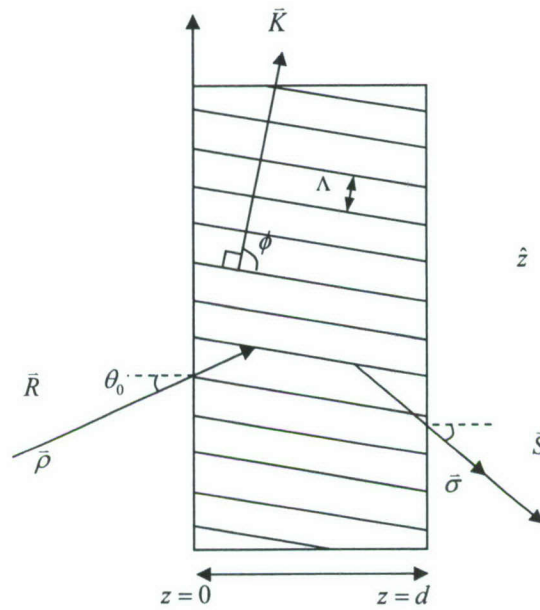Table 1. Experimentally observed diffraction patterns for six superimposed gratings S1-S6.

Fig 1. Schematic illustration of the reconstruction of object waves illuminating on superimposed multiple gratings with a reference wave
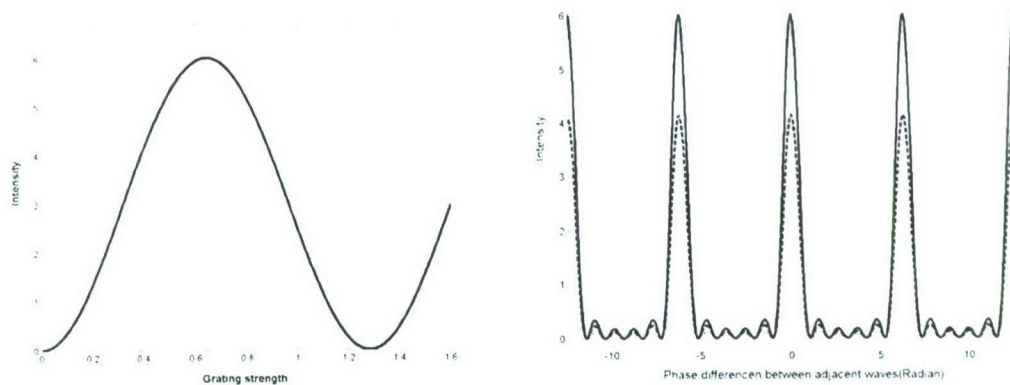
Fig 2(a)   Simulation results showing the intensity of output wave as a function of equalized grating strength ν. Six input waves have unit intensity and are in-phase. φ is set to 0 in eqn 3.

(b)   Simulation result showing the intensity of output wave as a function of phase angle between adjacent waves for three values of ν. Solid line for ν=0.6409, dashed line for ν=0.3850, and dot line for ν= 0.2500 in eqn 3.
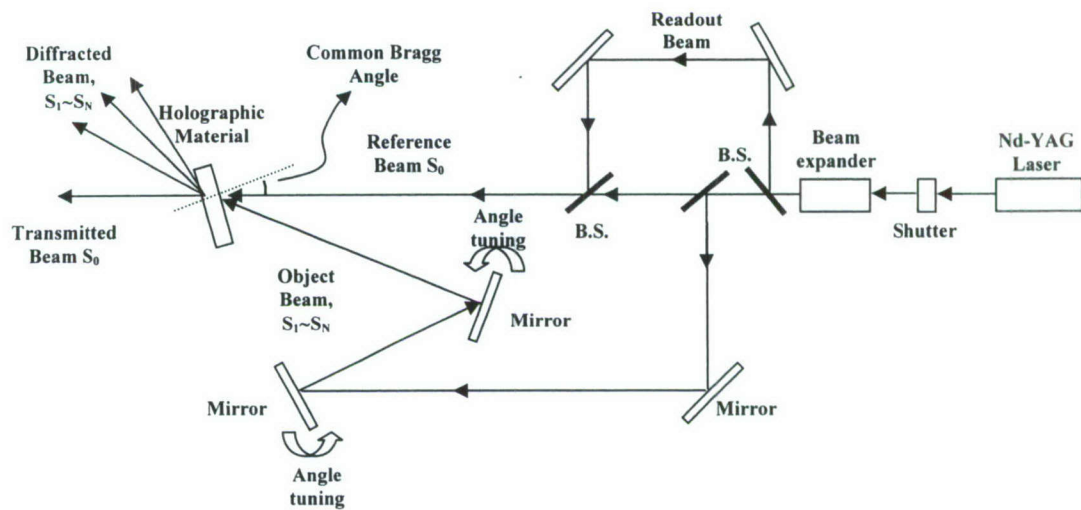
Figure 3: Recording set-up with Nd-YAG laser using the angular multiplexing and Read-out with the identical laser
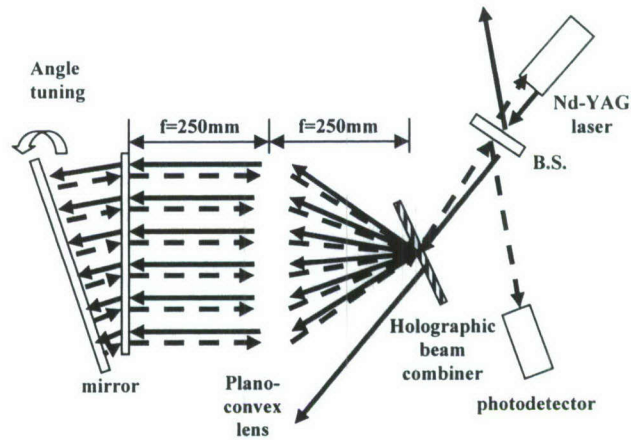
Figure 4: Experimental setup for six- beam combining with the 2nd sample which has six superimposed gratings and functions as holographic beam combiner. The focal length of lens is 25cm.
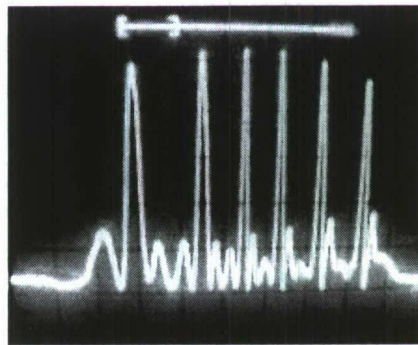

Figure 5: Intensity measured at the photodetector using the experimental setup shown in Fig 4. One longitudinal division of rectangular box is 50 mV. One lateral division is 0.1s. The D.C offset of photodetector is -100 mV.

B. DETAILS OF WORK DONE

B.1 Shift-Invariant Real-Time Edge-Enhanced VanderLugt Correlator Using Video-Rate Compatible Photorefractive Polymer

Optical data storage continues to attract significant interest because it offers the possibility of creating large image databases that can be searched at a high speed because of the parallelism in optics. A massive optical memory system can be realized by dense holographic storage achievable with multiplexing techniques, of which spatio-angular multiplexing (SAM) is the most straightforward and effective one[1-5]. The super-parallel holographic ROM (SPHROM) is the architecture proposed by our group to implement dense SAM with fast retrieval, capable of storing up to 2TB of data[3-5]. Search of the holographic memory is typically accomplished with a shift-invariant Fourier Transform (FT) based correlator[6]. The two types of a simple correlator are the joint transform (JTC) and matched spatial filter or VanderLugt (VLC) correlators, either of which can be implemented in real-time by degenerate four wave-mixing in a photorefractive material[7,8]. Physical implementation of any mathematically shift-invariant correlator requires that the holographic material possesses sufficient angular bandwidth. This requirement can be fulfilled by using a thin photorefractive (PR) material.

The diagram in Figure 1 shows our proposed system, consisting of the SPHROM coupled with a shift-invariant real-time VLC. The correlation is performed in the VLC architecture to achieve a much higher image recognition system operational speed than what a JTC architecture would allow[8,9]. The PR grating is written by the FT of the query image and a reference plane wave at the speed limited by the response of the PR material. However, once the grating for a particular query image has been written, the rest of the searching process happens at the speed with which the probe beam, carrying the FT of the images retrieved from the SPHROM, diffracts from the grating.

Here we describe our demonstration of 2-D (horizontal and vertical) shift invariant correlation[10] using recently invented bis-triarylamine side-chain polymer matrix[11,12] 37µm thick PR polymer composites operating at 532nm. The gratings in our experiment were written by beams intersecting in the horizontal plane. The material samples for our experiment were provided by Nitto Denko Technical Corp. (NDT). We consider this PR polymer material to be the prime candidate for the implementation of a shift-invariant search of the SPHROM, because this material has a demonstrated capability of stable dynamic video-rate operation and a long shelf lifetime at room temperature[11]. A previously reported PR polymer VLC was constructed from PVK-based PR polymer[9], a material in which deterioration of PR properties was observed after prolonged use[10]. In addition, the experiment reported in [9] relied on a cross-hairs filter to perform edge-enhanced correlation. In our experiment, edge-enhancement was achieved in real time by adjusting the intensities of the writing beams[13,14]. Our experiment was performed with a PR polymer sample with a large transverse area of 1.5" in diameter, using an ND:YAG frequency doubled solid-state pumped Verdi laser, operating at 532nm.

Prior to the correlation experiment, we measured the angular bandwidth of the PR polymer sample by performing incoherent phase conjugation readout in a degenerate

four-wave mixing configuration. The diagram illustrating the experimental setup is presented in Figure 2. The sample consisted of the PR polymer composite with an average refractive index n_0=1.6 sandwiched between Indium Tin Oxide (ITO) electrode-coated glass plates. An external DC field was applied across the sample. We determined experimentally that the maximum diffraction efficiency was obtained at a 3kV bias. The grating was written by two s-polarized, collimated gaussian beams A_1 and A_2, incident on the hologram at 60° and 30° to normal in the air, respectively. The writing beams were each 5mW in power, with spot diameters of 5mm. Because of the Fresnel refraction in glass, the actual angles of incidence of the beams A_1 and A_2 in the material were 35° and 20°, respectively. An asymmetric writing beams arrangement was needed so that the gratings K-vector would make an angle with the poling field direction. The p-polarized probe beam A_3 at 2mW power with a 5mm spot size was incident on the grating, aligned to be exactly counter-propagating to the writing beam A_1. The phase-conjugated beam A_2^* was reconstructed with p-polarization. A diffraction efficiency of about 1% was observed (when reading the grating with a He-Ne laser at 633nm, a diffraction efficiency close to 40% was observed). After passing through the half-wave plate, A_2^* became s-polarized, and subsequently it was reflected by the polarizing beam splitter (PBS) cube. Note that all the PBS cubes mentioned in this paper transmit p-polarized beams and reflect s-polarized beams.

In order to measure the angular bandwidth of the PR polymer sample, the probe beam was scanned with the help of computer-controlled galvo mirrors (see Figure 2). The two-mirror galvo system, sweeping at an average rate of 15rad/s, was designed to keep the probe beam at a fixed spot on the hologram, while changing the angle of incidence. Since the beam A_2^* was also sweeping through a large angle, a 2-f to 2-f single lens imaging system was set up to keep A_2^* on the detector. The signal was detected with a Thorlabs PDA55 10MHz bandwidth photodetector. One can see from Figure 3 that the angular bandwidth in the air measured between the first nulls of the sinc function for our sample is about ten degrees.

The theory plot was obtained from the coupled wave equations for lossless transmission dielectric gratings[15]. Since the range of angular deviations from the Bragg angle was quite large during the experiment, we did not follow the usual approach of Taylor series expansion in the small parameter $\Delta\theta$. Instead, all the relevant parameters were recalculated using the defining equations each time the incident angle was changed. Under the stated experimental conditions we observed Bragg diffraction. To confirm that diffraction in our samples was in the Bragg regime, we calculated the values of $Q = 2\pi\lambda d/n_0\Lambda^2$ (Klein-Cook) and $\rho = \lambda^2/\Lambda^2 n_0 n_1$ (Raman-Nath) parameters[16,17]. Here d is the sample thickness, n_1 is the amplitude of the refractive index modulation and Λ is the grating periodicity. We determined that $n_1 \approx 3\times10^{-4}$ by measuring the diffraction efficiency at the Bragg angle. We obtained $Q \approx 36$ and $\rho \approx 300$, which satisfy the conditions for the Bragg regime that both Q>>1 (thick grating) and $\rho >> 1$ (weak modulation).

The diagram detailing the experimental setup of the shift-invariant VLC demonstration is shown in Figure 4. Expanded laser beams with spot sizes of 1" diameter were used in the correlation experiment. The query image of a MIG-25 jet (Figure 5(a))

was encoded on the expanded laser beam wit the help of a Boulder Nonlinear Systems 512x512 pixel reflective FLC SLM with a pixel size 15x15µm. The filter image of a MIG-25 jet was retrieved from the Memplex® photopolymer-based holographic memory. A CCD capture of the retrieved image is shown in Figures 6(a) and 7(a). A real-time grating in the PR polymer was written with an s-polarized FT query image beam and an s-polarized plane wave. The probe beam carrying the FT of the filter image was p-polarized. The writing beams carried about 5mW of optical power each, while the probe beam was about 0.5mW. A quarter-wave plate and the mirror shown in the diagram in Figure 4 by dashed lines were installed on flip mounts. The purpose of these two components was to monitor the power ratio of the signal and reference beams in order to produce an edge-enhanced hologram. This technique is based on the fact that most optical power of a typical image spectrum resides in the low frequencies. If the intensity of high frequencies matches the intensity of the reference beam, the intensity of the DC component significantly exceeds the intensity of the reference. Hence, the modulation depth (m) of the DC part of the spectrum is low, and the DC is not recorded well in the hologram[13]. DC suppression could be observed in real-time by retro-reflecting the reference beam with the flipping mirror through the quarter wave plate. Double passing of the s-polarized reference beam through the quarter-wave plate resulted in converting it to a p-polarized beam. The retro-reflected reference, now acting as a probe beam, diffracted from the grating, producing a phase conjugated beam carrying an edge-enhanced image that could be observed with a CCD camera. A CCD capture of the edge-enhanced SLM query image is shown in Figure 5(b). The image appears inverted with respect to the original because the phase-conjugating system acts as a 4-f system. In our experiment the SLM query image was edge-enhanced; however for a practical system a better alternative might be to store edge-enhanced images in the large optical memory database.

Once the desired level of edge-enhancement was achieved, the quarter-wave plate and the mirror were lowered so that the cross-correlation signal could be observed on the CCD camera. The CCD capture of the probe beam is shown in Figures 6(a) and 7(a). We demonstrated shift-invariance of correlation by projecting query images consisting of two MIG-25 jets, horizontally translated to the left and to the right by about 100 pixels from the center in the SLM frame (Figure 6(b)). In the experimental setup with a 250mm FT lens, this shift corresponded to $|\Delta\theta|=0.34°$ angular deviation from the Bragg angle of the DC part of the image. The correlation signal is shown in Figure 6(c). Vertical displacement of the image by 100 pixels up and down in the SLM plane is shown in Figure 7(b) and the corresponding correlation signal is Figure 7(c). We observed a considerable amount of speckle noise in the correlation, possibly because of scattering in the PR polymer. Nevertheless, the correlation signal from the PR polymer could be thresholded to produce an unambiguous spot identifying the location of the query image.

It should be noted that the spatial frequency components in the Fourier plane of the probe beam might be distributed over a large area, depending on the features of the image, the beam diameter and the focal length of the FT lens. For example, the Fourier spectrum of the MIG-25 jet image obtained from a 100x150-pixels size SLM image with a 250mm lens covers an area of about 4mm in diameter. The real-time VLC architecture is quasi-phase matched, because only the mean k-vector of the probe beam (essentially only the DC part of the spectrum) is counter-propagating to the reference beam. Higher

6

spatial frequencies that carry the information about the image contours are incident at Bragg-mismatched angles. Thus, the high spatial frequencies will not diffract from the grating unless their angle of incidence is within the allowed angular bandwidth. Therefore, it is advantageous to have a real-time material that is both thin and has a large aperture to capture the entire Fourier spectrum of an image, such as the material that we used.

In summary, we have demonstrated a real-time shift-invariant VLC with real-time edge enhancement. The VLC was implemented with a 37μ thick triarylamine-based PR polymer composite operating at 532nm wavelength. A high degree of shift-invariance in this material is possible because of the material thinness. Large values of the Q and ρ parameters indicate that coupled-wave theory is applicable to describing the diffraction process in this material. The angular bandwidth of this material was measured experimentally in degenerate four-wave mixing setup. The experimental data agrees with coupled-wave theory results.

1. S. Tao, Z.H. Song, D.R. Selviah, and J.E. Midwinter, "Spatioangular-multiplexing scheme for dense holographic storage," Appl. Opt. **34**(29), 6729-6737 (1995).

2. F. Mok, D. Psaltis, and G. Burr, "Spatially- and angle-multiplexed holographic random access memory," in *Photonics for Computers, Neural Networks, and Memories*, W.J. Miceli, J.A. Neff, and S.T. Kowel, eds., Proc. SPIE **1773**, 334-345 (1992).

3. A. Heifetz, J.T. Shen, J-K. Lee, R. Tripathi, M.S. Shahriar, "Translation-invariant object recognition system using an optical correlator and a super-parallel holographic RAM," Opt. Eng., in press (2006).

4. M.S. Shahriar, R. Tripathi, M. Huq, J.T. Shen, "Shared-Hardware Alternating Operation of a Super-Parallel Holographic Optical Correlator and a Super-Parallel Holographic Random Access Memory," Opt. Eng. **43**, 1856-1861 (2004).

5. M.S. Shahriar, R. Tripathi, M. Kleinschmit, J. Donoghue, W. Weathers, M. Huq, J.T. Shen, "Superparallel Holographic Correlator for Ultrafast Database Searches," Opt. Lett. **28**(7), 525-527 (2003).

6. M. Duelli, A.R. Pourzand, N. Collings, and R. Dändliker, "Holographic memory with correlator-based readout," IEEE J. Sel. Top. Quant. Electron. 4(5), 849-855 (1998).

7. D.M. Pepper, J. AuYeung, D. Fekete, and A. Yariv, "Spatial convolution and correlation of optical fields via degenerate four-wave mixing," Opt. Lett. 3(1), 7-9 (1978).

8. D.T.H. Liu, L.-J. Cheng, "Real-time VanderLugt optical correlator that uses photorefractive GaAs," Appl. Opt. **31**(26), 5675-5680 (1992).

9. C. Halvorson, B. Kraabel, and A.J. Heeger, B.L. Volodin, K. Meerhoz, Sandalphon, and N. Peyghambarian, "Optical computing by use of photorefractive polymers," Opt. Lett., **20**(1), 76-78, (1995).

10. C.-C. Sun, M.-S. Tsaur, W.-C. Su, B. Wang, and A.E.T. Chiou, "2-D shifting tolerance of a volume-holographic optical correlator," Appl. Opt. **38**(20), 4316-4324 (1999).

11. C. Fuentes-Hernandez, J. Thomas, R. Termine, G. Meredith, N. Peyghambarian, B. Kippelen, S. Barlow, G. Walker, S.R. Marder, M.Yamamoto, K. Cammack, K. Matsumoto, "Video-rate compatible photorefractive polymers with stable dynamic properties under continuous operation," Appl. Phys. Lett. **85**(11), 1877-1879 (2004).

12. T.-H. Chao, "Optical joint transform correlator using high-speed holographic photopolymer film,"in *Optical Pattern Recognition XVI*, D.P. Casasent and T.-H. Chao eds., Proc. SPIE **5816**, 136-143 (2005).

13. J. Feinberg, "Real-time edge enhancement using the photorefractive effect," Opt. Lett. 5, 330-332 (1980).

14. P.P. Banerjee, E. Gad, T. Hudson, D. McMillen, H. Abdeldayem, D. Frazier, and K. Matsushita, "Edge enhancement and edge-enhanced correlation with photorefractive polymers," Appl. Opt. **39**(29), 5337-5346 (2000).

15. H. Kogelnik, "Coupled wave theory for thick hologram gratings," Bell Syst. Tech. J. **48**(9), 2909-2947 (1969).

16. T.K. Gaylord and M.G. Moharam, "Thin and thick gratings: terminology clarification," Appl. Opt. **20**(19), 3271-3273 (1981).

17. M.G. Moharam and L. Young, "Criterion for Bragg and Raman-Nath diffraction regimes," Appl. Opt. **17**(11), 1757-1759 (1978).
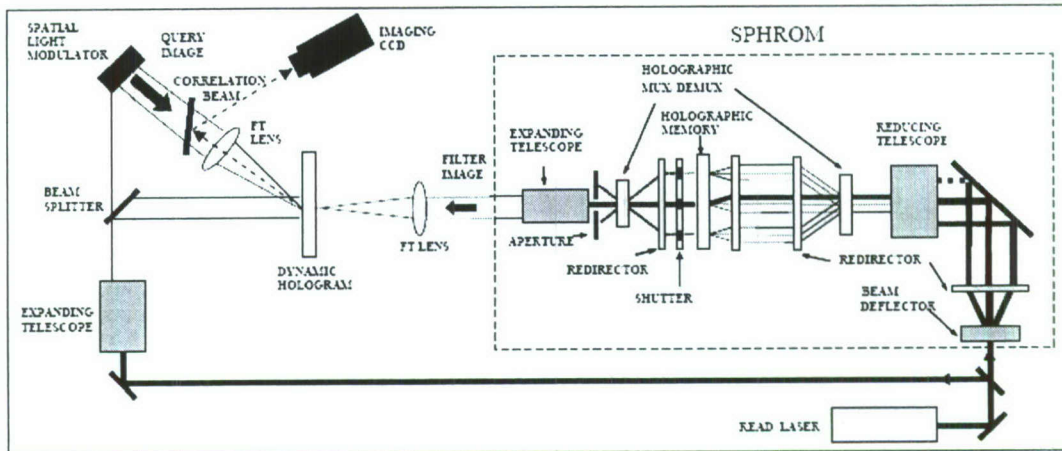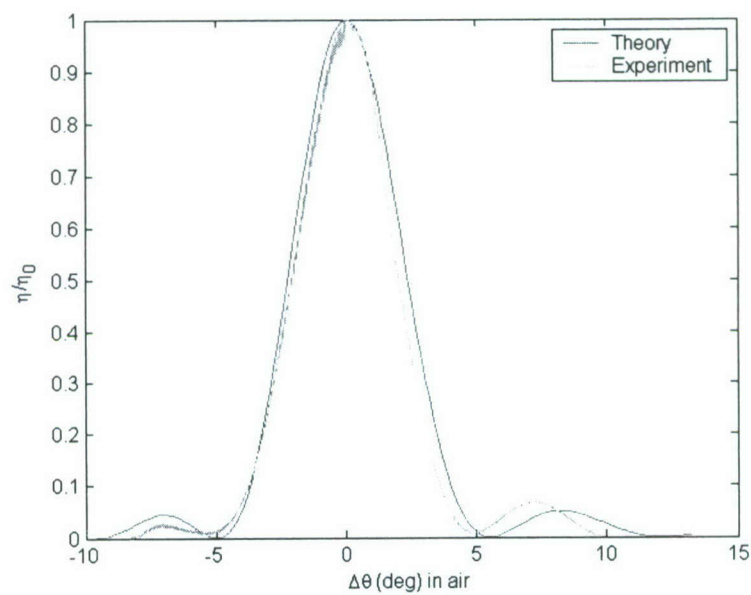
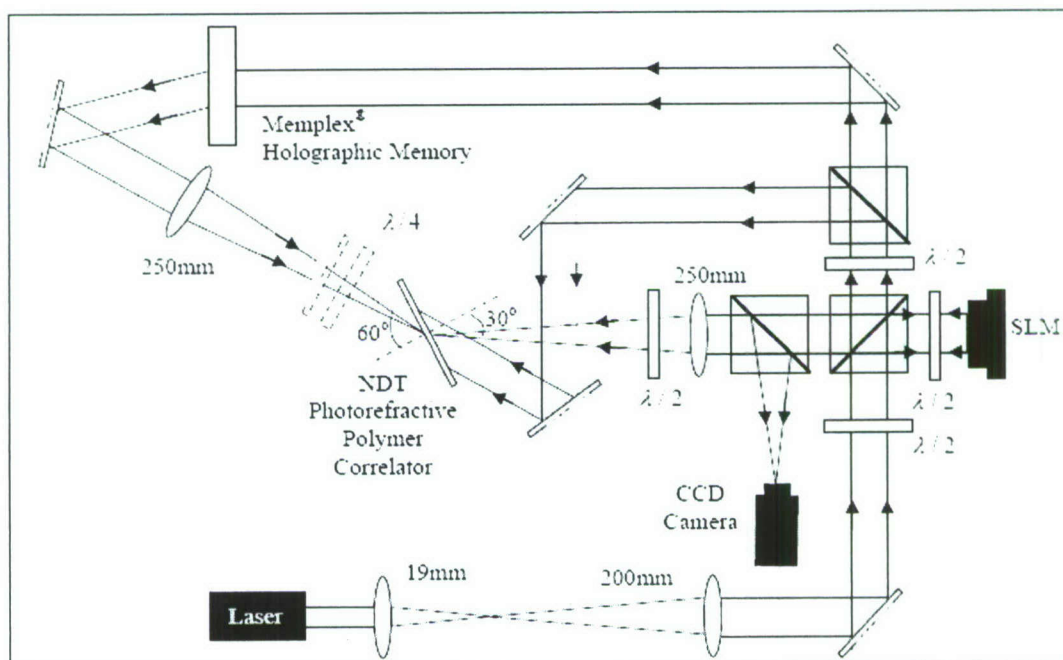**Figure 1**. Real-time VLC coupled with SPHROM
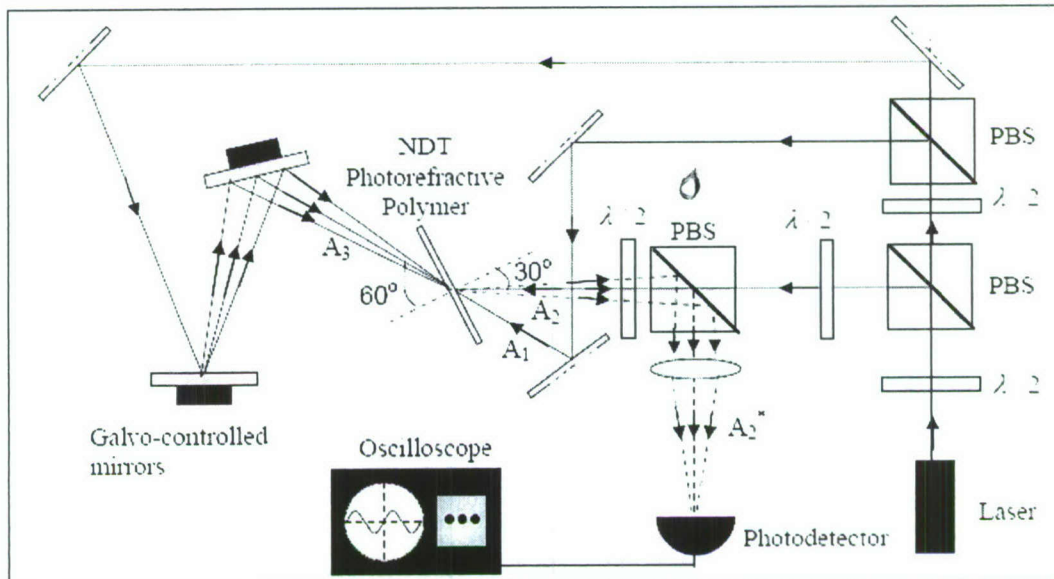
Figure 2. Experimental setup for measuring the angular bandwidth of the photorefractive polymer sample
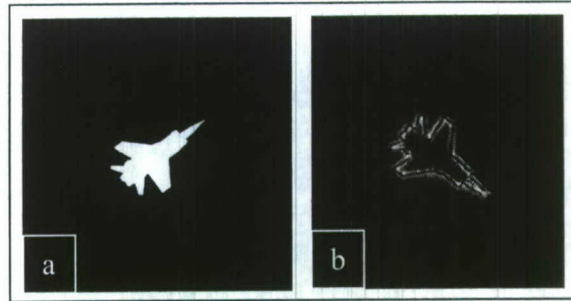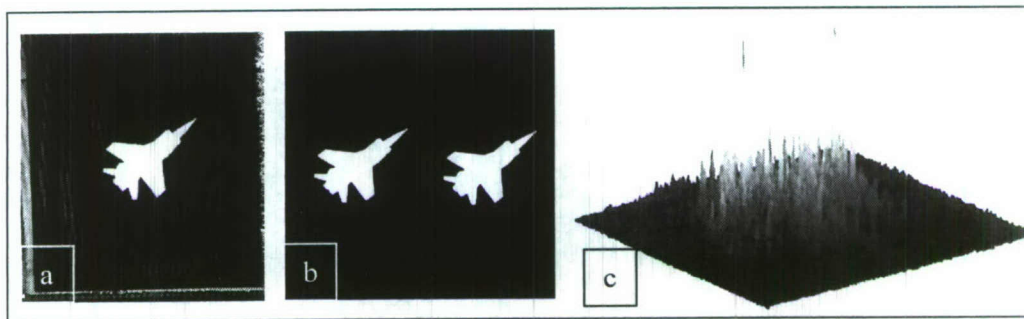
Figure 3. Experimentally measured angular bandwidth for the photorefractive polymer sample, along with the theoretical curve.
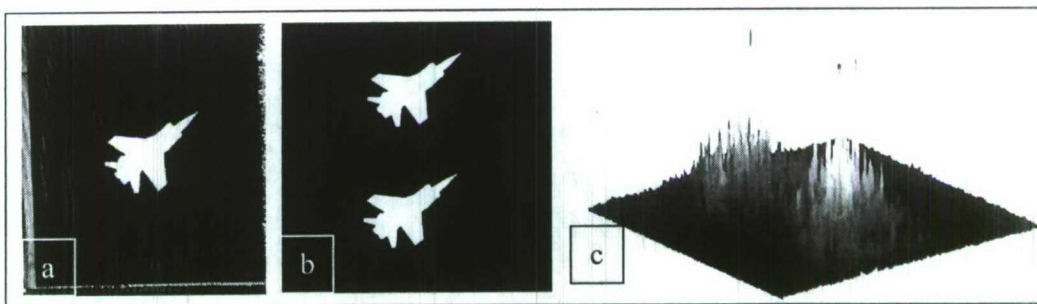

Figure 4. Experimental setup for demonstrating the shift-invariant real-time VLC.

Figure 5. (a) SLM image. (b) Edge enhanced phase-conjugated reconstruction of the SLM image.

Figure 6. Horizontal shift: (a) Memplex⁻ image, (b) SLM image, (c) correlation

Figure 7. Vertical shift: (a) Memplex® image, (b) SLM image, (c) correlation

B.2 Translation-Invariant Correlation of Images Stored via Holographic Angle-Multiplexing in a Thick Photopolymer Storage Medium

In many military and civilian applications, rapid target identification and tracking is essential[1]. Real-time target identification and recognition is usually performed by correlating an acquired image with images stored in a database. Current image identification technology relies upon digital signal processing (DSP) architectures and algorithms, which are often too slow for target interception applications because in the DSP approach, the data is compared serially, bit by bit. A holographic optical correlator (HOC)[2-5], in which images stored holographically via angle-multiplexing, offers parallel database searches much faster[6] than DSP because of the advantages derived from the inherent parallelism of optics. However, the potential of a HOC is limited by the inability to access simultaneously the angle-multiplexed images stored at more than one spatial location. A super-parallel holographic optical correlator (SPHOC)[7] solves this problem by employing spatial multiplexing achievable with the help of a special purpose lenslet array, redirectors and holographic multiplexers. Thus, the SPHOC performs optical correlations at thousands of spatial locations simultaneously, resulting in a system performance that could be millions of times faster than the DSP-based correlators. We have demonstrated that operating the SPHOC in reverse, with an addition of a shutter array to the SPHOC hardware, can serve to realize a super parallel holographic random access memory (SPHRAM)[8]. This hybrid device eliminates the need for a separate RAM for a holographic correlator-based target recognition system.

In order to compensate for scale and rotation variance in optical correlation, a huge database of images is needed for reliable identification. Performing the correlations in a translation-invariant manner greatly reduces the size of the required database and speeds up the search process. A major disadvantage of the SPHOC in the present form is that it is difficult to achieve translation-invariant correlation because the SPHOC utilizes a thick holographic grating material to allow for the angle-multiplexing[9,10]. Operating the SPHRAM with a joint-transform correlator (JTC)[2,4] based on a thin dynamic material answers the challenge of fast correlation with large databases. The image retrieved from the SPHRAM and used as the correlation filters in the JTC can be changed at a high rate, and the query images can be correlated with each filter in a translation-invariant manner. The schematics of the SPHRAM architecture combined with the JTC are presented in Figure 1 (for a detailed description of the SPHRAM operation see Reference 8). The input image is encoded on the laser beam using a spatial light modulator (SLM) (not shown in the diagram). At the same time, a filter image is retrieved from the SPHRAM. The Fourier transforms of the input and the filter images are recorded in the dynamic holographic medium. During this process the shutter S1 is closed, while the shutter S2 is open. For practical parameters, it will take about 1 µs to read an image from the SPHRAM and about 1 µs to write the joint Fourier-transform onto the dynamic recording medium. Next, the shutter S2 is closed and the shutter S1 is open, thus allowing the read beam to diffract from the grating and to produce a correlation beam. The correlation spot is captured with a CCD camera, and the dynamic holographic gratings containing the

joint Fourier-transform is erased. Approximately 3 μs is needed for the CCD camera recording, and about 10 μs is needed to erase the grating. This results in a total time of approximately 15 μs for a single correlation, which corresponds to an operating rate of 67 kHz. Once the match is found, the joint Fourier-transform grating does not need to be erased right away, allowing for subsequent translation-invariant correlation of the target.

In order to implement the SPHRAM/JTC system we need to identify the holographic material for high density and high quality permanent data storage needed to construct the SPHRAM, as well as the fast-response dynamic holographic material needed for JTC. We have already identified the photopolymer-based Memplex® thick holographic material developed by Laser Photonics Technology Inc. (Amherst, NY)[11] as the medium for high capacity and a high efficiency holographic memory. This material can have a very high M# (>20), and holograms written in this material can survive at room temperature for many years without noticeable degradation[12,13]. Our literature search shows that the fastest dynamic material currently available in the visible wavelength range is the photorefractive $Sn_2P_2S_6$ crystal[14] (abbreviated as SPS). A JTC (although not translation invariant) has already been reported operating at a rate higher than 10 kHz[15]. Before we proceed to construct the translation-invariant SPHRAM with a JTC, we have to verify the ability of storing high quality angle-multiplexed holograms in a sample of the Memplex® material that we will subsequently refer to as the holographic memory unit (HMU), and performing a reliable translation-invariant correlation of the images reconstructed from the HMU.

Here we describe the results of an elementary demonstration of the key components of the future SPHRAM/JTC system. In this experiment, the images were stored in the Memplex® HMU via 1-D angle-multiplexing, and later retrieved from the HMU to perform translation-invariant correlation with a static thin holographic filter in the VanderLugt filter-correlator architecture[2,3]. The experimental setup is shown in Figure 2. In the image writing stage (not shown in the diagram), the HMU is treated as a 3x3 matrix of spatial locations, with a mask exposing one spatial location at a time. Different sets of about 20 images each are stored via angle-multiplexing in the horizontal dimension at each of the nine spatial locations of the HMU using a frequency-doubled ND:YAG laser operating at 532nm. Although we recorded images at nine spatial locations on the HMU, we would use only one spatial location containing a set of 23 binary images of snapshots of a MiG-25 fighter jet linearly translated to different locations on the frame for the translation-invariant correlation experiment. In Figure 3 one can see a sample of the original binary image. A set of samples of the images reconstructed from the HMU and recorded with a CCD camera is presented in Figure 4. We note that there was no cross talk between the angle-multiplexed images at the same location or images at different spatial locations. The reconstructed images had a very high quality, which is essential for building a reliable SPHRAM correlator system. We stored only 23 images of the MiG-25 jet, but in principle, in a 2mm thick plate, we could store up to 1000 2-D angle multiplexed images at a single spatial location[15].

The thin holographic filter used in the VanderLugt architecture contains a DC-suppressed Fourier transform of the MiG-25 jet image centered in the frame. This filter was prepared with VRP-M thin holographic plates made by Slavich using the same laser operating at the same wavelength from as used for recording images in the HMU. We achieve the DC-suppression of the recorded Fourier transform by employing the DC

saturation technique[3]. The edge-enhanced image reconstructed from the thin filter is shown in Figure 5. The DC-suppression of the Fourier transform is needed to eliminate the chance of correlations with wrong objects[17]. The thin filter was separately tested for its correlation selectivity. Scanning the angle of the read beam incident on the same spatial location of the HMU, the images of the MiG-25 jet translated to different locations in the frame in a loop pattern are retrieved from the HMU. The correlation spot captured on the CCD camera indicates the position of the jet on the frame plane. Superimposing the successive correlation CCD frame grabs produces a trace of the trajectory of the jet, presented in Figure 6a. For comparison of the data quality, another VanderLugt correlator is constructed, where instead of the HMU, the same images of the MiG-25 jet now come directly from the SLM. The same thin holographic filter is used for correlation. As before, a tracing trajectory of the jet is produced. The loop-pattern trajectory obtained with the images coming from the SLM is presented in Figure 6b. We see that the trajectories produced from the two experiments are essentially identical.

Finally, the Memplex HMU we have used is rather small in size. For a large scale implementation of the technique demonstrated here, it is necessary to create a large – scale HMU capable of storing multi-terabytes of data. As reported previously, we have been working for a while on making such an HMU. However, the process has generally been beset by problems such as development of bubbles. Very recently, we have overcome this problem, and finally been able to make a large size HMU, encased between a pair of optical quality glass windows, with an estimated storage capacity of nearly two terabytes. This HMU is shown at the top of figure 7. The bottom part of figure 7 shows some sample images stored and recalled from this medium. The distortions appearing as fringes are due to the SLM used for the recording, and not due to any imperfections of the storage medium.

We have demonstrated that we can write high quality angle-multiplexed holograms in the holographic memory unit (HMU) based on the Memplex® material. We have also shown that we can perform a reliable translation-invariant correlation of the images retrieved from the HMU, presently using the VanderLugt filter-correlator architecture. We will next proceed to implement the super-parallel holographic random access memory (SPHRAM) with a high-density data storage and fast data retrieval, and use it in conjunction with a joint-transform correlator (JTC) based on fast-response photorefractive crystals.

References:

1. W.W. Goj, *Synthetic Aperture Radar for Electronic Warfare*, Artech House, Norwood, MA (1993).
2. J. W. Goodman, *Introduction to Fourier Optics*, McGraw-Hill, New York (1996).
3. A.B. VanderLugt, *Optical Signal Processing*, Wiley, Somerset, NJ (1992).
4. *Selected Papers on Optical Pattern Recognition Using Joint Transform Correlation*, M.S. Alam, Ed., SPIE Milestone Series MS157/HC, SPIE Press, Bellingham, WA (1999).
5. *Selected Papers on Optical Pattern Recognition*, F.T.S. Yu, Ed., SPIE Milestone Series MS156/HC, SPIE Press, Bellingham, WA (1999).
6. A.J.B. Hassaun, "Holographic correlation improves on DSP by six orders of magnitude," Laser Focus World 38, 44 (2002).
7. M.S. Shahriar, R. Tripathi, M. Kleinschmit, J. Donoghue, W. Weathers, M. Huq, and J.T. Shen, "Superparallel Holographic Correlator for Ultrafast Database Searches," Opt. Lettt. **28**, 525-527 (2003).
8. M.S. Shahriar, R. Tripathi, M. Huq, J.T. Shen, "Shared-Hardware Alternating Operation of a Super-Parallel Holographic Optical Correlator and a Super-Parallel Holographic Random Access Memory," Opt. Eng. **43**, 1856-1861 (2004).
9. Q.B. He, P. Yeh, L.J. Hu, S.P. Lin, T.S. Yeh, S.L. Tu, S.J. Yang, K. Hsu, "Shift-Invariant Photorefractive Joint-Transform correlator using Fe:LiNbO$_3$ Crystal Plates," Appl. Opt. **32**, 3113-3115 (1993).
10. C. Gu, J. Hong, S. Campbell, "2-D Shift-Invariant Volume Holographic Correlator," Opt. Comm. **88**, 309-314 (1992).
11. R. Burzynski, D.N. Kumar, M.K. Casstevens, D. Tyczka, S. Ghosal, P.M. Kurtz, J.F. Weibel, "New Photopolymer for Holographic Optical Storage Technology," Proc. SPIE **4087**, R.A. Lessard, G.A. Lampropoulos Eds., 741-753 (2000).
12. H.N. Yum, P.R. Hemmer, R. Tripathi, J.T. Shen, M.S. Shahriar, "Demonstration of a Simple Technique for Determining the M# of a Holographic Substrate Using a Single Exposure," Opt. Lettt. **29**, 1784 (2004).
13. M.S. Shahriar, J. Riccobono, M. Kleinschmit, J.T. Shen, "Coherent and incoherent beam combination using thick holographic substrates," Opt. Comm. **220**, 75-83 (2003).
14. D. Haertle, G. Gaimi, A. Haldi, G. Montemezzani, P. Günter, A.A. Grabar, I.M. Stoika, Yu. M. Vysochanskii, "Electro-Optical properties of Sn$_2$P$_2$S$_6$," Opt. Comm. **215**, 333-343 (2003).
15. R. Ryf, G. Montemezzani, P. Günter, A.A. Grabar, I.M. Stoika, and Yu. M. Vysochanskii, "High-frame-rate joint Fourier-transform correlator based on Sn$_2$P$_2$S$_6$ crystal," Opt. Lett. **26**, 1666-1668 (2001).
16. H. Kogelnik, "Coupled Wave Theory for Thick Hologram Gratings," The Bell Syst. Tech. J. **48**, 2909-2947 (1969).
17. A. Pu, R. Denkewalter, D. Pasltis, "Real-time vehicle navigation using a holographic memory," Opt. Eng. **36**, 2737-2746 (1997).
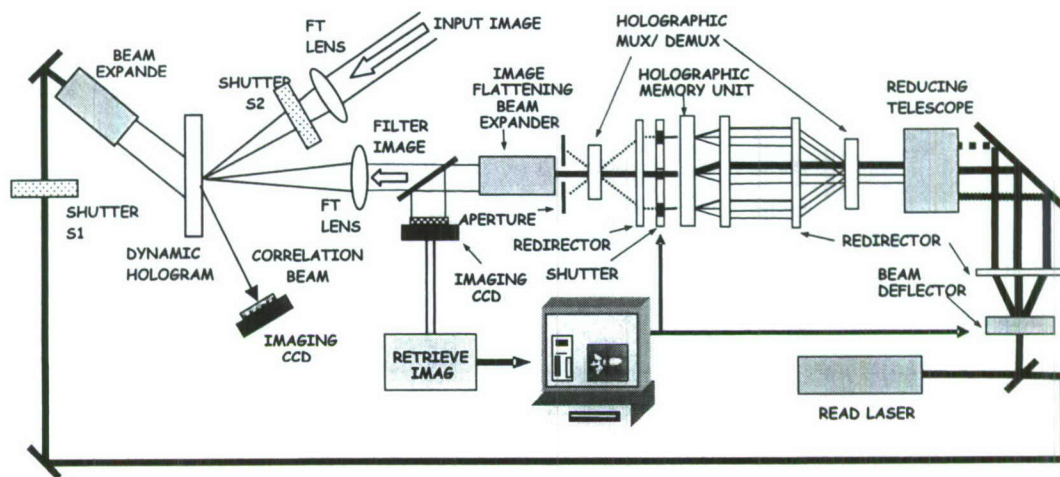
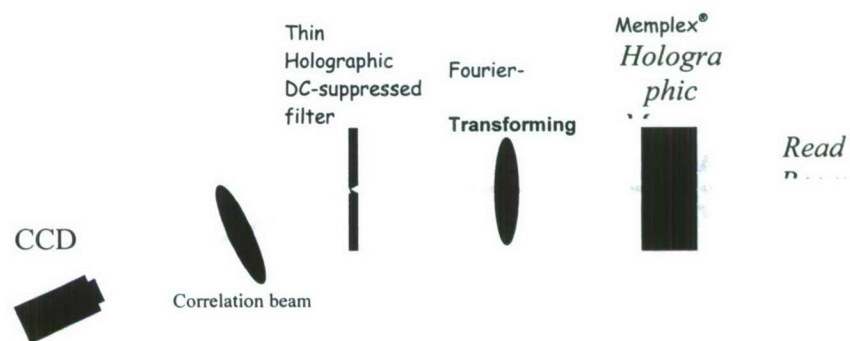Figure1. End goal architecture of SPHRAM combined with JTC

Figure 2. Setup for the translation-invariant Vanderlugt filter-correlator for the images

retrieved from the HMU

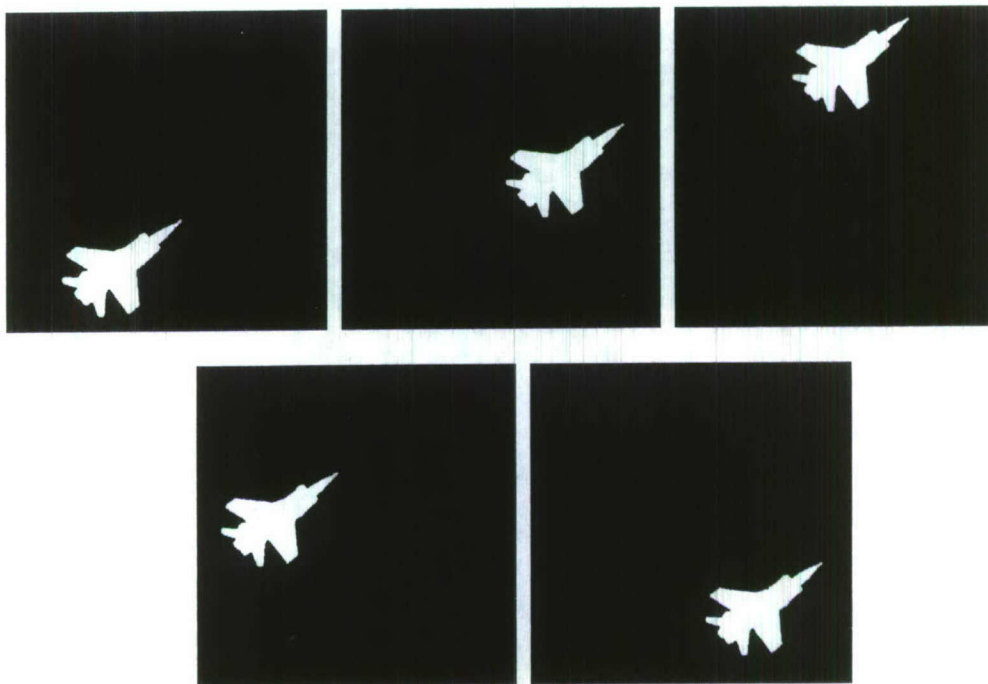Figure 3. Original binary MiG-25 image.

Figure 4. Samples of MiG-25 images moving in a loop pattern reconstructed from the HMU.
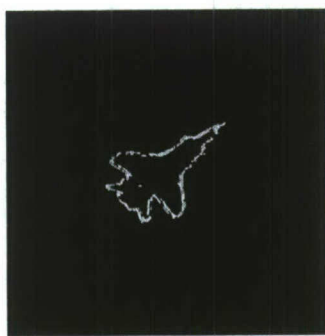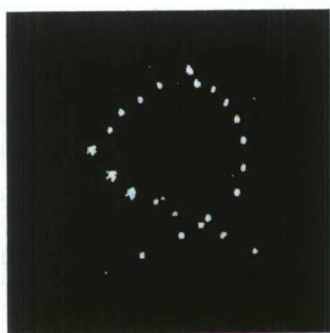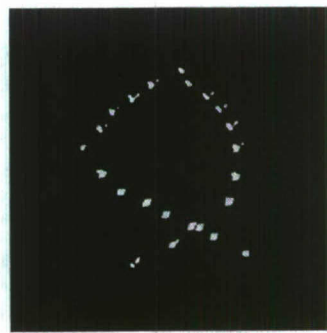
Figure 5. Edge-enhanced image reconstructed from the thin holographic filter.

(a)   (b)

Figure 6. Superimposed correlation spots showing a loop-pattern trace produced when the image source is (a) HMU and (b) SLM
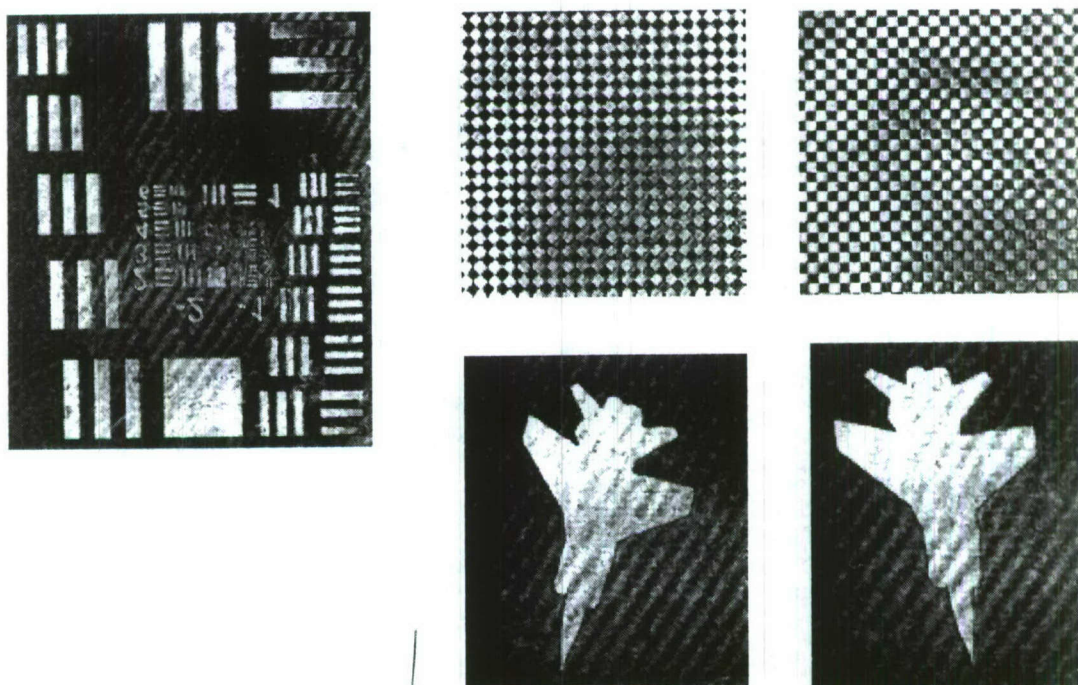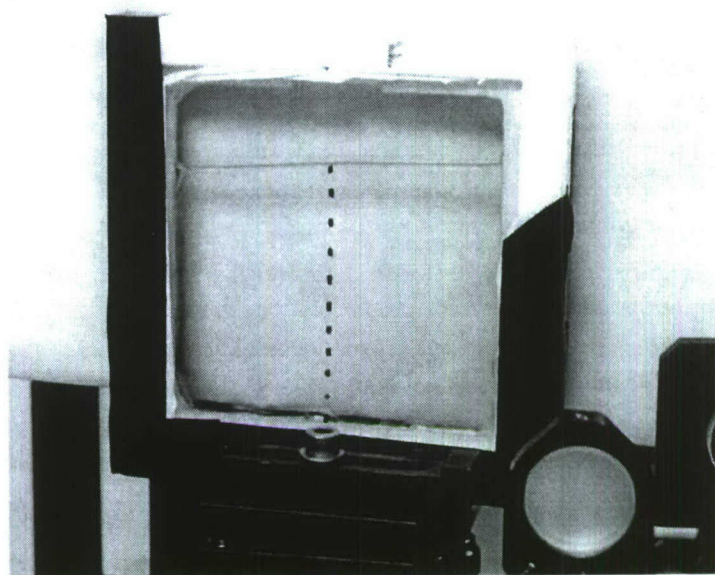
Figure 7. Top: picture of the 4 inch X 4 inch thick substrate we have developed, with high optical quality, and a storage capacity of nearly two terabyte. Bottom: sample images stored and recalled from this medium. The distortions appearing as fringes are due to the SLM used for the recording, and not due to any imperfections of the storage medium.

B.3 Directional Correlation Between Input and Output Beams In A Dynamic Shift-Invariant Thick Hologram

Optical data storage continues to attract significant interest because it offers the possibility of creating large image databases that can be searched at high speed because of the parallelism in optics. A massive optical memory system can be realized by dense holographic storage achievable with multiplexing techniques, of which spatio-angular multiplexing (SAM) is the most straightforward and effective technique[1-6]. The super-parallel holographic ROM (SPHROM) is the architecture proposed by our group to implement dense SAM with fast retrieval, capable of storing up to 2TB of data[4-6]. Search of the holographic memory is typically accomplished with a shift-invariant Fourier Transform (FT) based correlator. A VanderLugt (VLC) correlator, which can be implemented in real-time by degenerate four wave-mixing in a photorefractive material[7] is the preferred choice for searching large databases. Physical implementation of any mathematically shift-invariant correlator requires that the holographic material possesses sufficient angular bandwidth. This requirement can be fulfilled by using a thin photorefractive (PR) material.

Here, we describe the experimental study of the directional correlation between the read and diffracted beams for off-Bragg incidence in thick holographic gratings. The PR polymer material that we intend to use for constructing the VLC belongs in the category of volume gratings but possesses a large degree of shift-invariance because of its thickness[8]. Figure 1 shows the model of a hologram grating which is used for our analysis. The z-axis is chosen perpendicular to the surfaces of the medium, the x-axis is in the plane of incidence and parallel to the medium boundaries, and the y-axis is perpendicular to the paper. The fringe planes are slanted with respect to the medium boundaries at an angle ϕ. The grating vector K is oriented perpendicular to the fringe planes and is of length $K = 2\pi/\Lambda$, where Λ is the period of the grating. The fringes of the hologram grating are represented by a spatial modulation of the refractive index $n = n_0 + n_1 \cos(K \cdot r)$, where n_1 is the amplitude of the spatial modulation, n_0 is the average refractive index, and r is the radius vector. We call the reference read beam R, and the diffracted signal beam S. The propagation vectors ρ and σ contain the information about the propagation constants and the directions of propagation of R and S. Here we assume that $|\rho| = |\sigma| = \beta$, where $\beta = 2\pi n_0/\lambda$ is the average propagation constant and λ is the wavelength in free space. The propagation vector σ is forced by the grating and related to ρ and the grating vector by $\sigma = \rho - K + \Delta\sigma$, which has the appearance of a conservation of momentum equation. We introduce the mismatch vector $\Delta\sigma$ to accommodate the Bragg-mismatched readout.

The vector relations are shown in Figure 2 on the *Ewald* sphere[9], which is drawn on a plane as a circle of radius β. Bragg-matched readout ($\Delta\sigma = 0$) is shown in Figure 2 with dotted arrows. The question arises about the direction of σ for Bragg-mismatched readout. From pure physical arguments, the diffracted beam is generated by the interaction of the electromagnetic field with the grating over a semi-infinite volume. The bandwidth-uncertainty product for the diffracted beam can be written as $\Delta\sigma \cdot \Delta r = 2\pi$, where $\Delta\sigma$ represents the uncertainty in the diffracted beam wave vector σ and

$\Delta r = \Delta x \hat{x} + \Delta y \hat{y} + \Delta z \hat{z}$ represents the dimensions of the region of interaction. The grating is assumed to be infinite in the x and y directions, but has a finite thickness d in the z-direction ($\Delta x = \infty$, $\Delta y = \infty$, $\Delta z = d$). Therefore, the bandwidth uncertainty product implies that $\Delta\sigma_x = 0$, $\Delta\sigma_y = 0$, and $\Delta\sigma_z d = 2\pi$, so that $\Delta\sigma = |\Delta\sigma| \hat{z}$. The resulting vector diagram is shown in Figure 2 with solid lines.

Next, we derive the conditions imposed on the diffracted beam wave vector for Bragg-mismatched readout using the mathematical formalism of the coupled wave theory[10]. We restrict our attention to transmission lossless dielectric gratings, because gratings of this type are formed in the PR polymer composites under study. Wave propagation in the grating is described by the scalar wave equation $\nabla^2 E + k^2 E = 0$, where $E(x,z)$ is the comlex amplitude of the y-component of the electric field, which is assumed to be independent of y and to oscillate with an angular frequency ω. The propagation constant $k(x,z)$ is spatially modulated and related to the refractive index of the medium by $k^2 = (\omega n/c)^2 = \beta^2 + 2\kappa\beta(\exp(i\mathbf{K}\cdot\mathbf{r}) + \exp(-i\mathbf{K}\cdot\mathbf{r}))$, where the coupling constant κ was defined as $\kappa = \pi n_1/\lambda$, and c is the light velocity in free space. In our model the constants of the medium are independent of y. The total electric field in the grating is the superposition of the two waves $E = R(z)\exp(-i\mathbf{\rho}\cdot\mathbf{r}) + S(z)\exp(-i\mathbf{\sigma}\cdot\mathbf{r})$. The other diffraction orders violate the Bragg condition strongly and are neglected. The reference and signal waves are described by complex amplitudes $R(z)$ and $S(z)$, which vary along the z axis as a result of this energy interchange. The coupled wave theory makes an assumption that $|\mathbf{\rho}| = \beta$ and $\mathbf{\sigma} = \mathbf{\rho} - \mathbf{K}$. If the actual phase velocities differ somewhat from the assumed values, then these differences will appear in the phases of $R(z)$ and $S(z)$ as a result of the theory. The vector relation is shown in Figure 3 in the *Ewald* sphere. The general case, where the Bragg condition is not met and the length of σ differs from β, is shown in Figure 3 with solid lines. Bragg-matched diffraction is shown for reference with dotted arrows.

After inserting the expression for the modulated propagating constant into the scalar wave equation, the waves generated in the directions of $\mathbf{\rho} + \mathbf{K}$ and $\mathbf{\sigma} - \mathbf{K}$ are neglected together with all higher diffraction orders. Then we group together the terms with equal exponentials ($\exp(-i\mathbf{\rho}\cdot\mathbf{r})$ and $\exp(-i\mathbf{\sigma}\cdot\mathbf{r})$). In addition, one assumes that the energy interchange between S and R is slow. This allows neglecting R'' and S'' (slowly varying envelope approximation), where the primes indicate differentiation with respect to z. We obtain the coupled wave equations $c_R R' = -i\kappa S$ and $c_S S' + i\vartheta S = -i\kappa R$, where we introduced the obliquity parameters $c_R = \rho_z/\beta$ and $c_S = \sigma_z/\beta$, and the dephasing measure $\vartheta = (\beta^2 - \sigma^2)/2\beta$. For transmission gratings, the boundary conditions are $R(0) = 1$, $S(0) = 0$. It is straightforward to obtain the general solution of the coupled wave equations[10]. The final expressions are $S(z) = S_0(z)\exp(-i\xi z)$ and $R(z) = R_0(z)\exp(-i\xi z)$, where $S_0(z) = -i(c_R/c_S)^{1/2}(1 + \xi^2/v^2)^{-1/2}\sin\left[(\xi^2 + v^2)^{1/2} z\right]$ and $R_0(z) = i\xi/(\xi^2 + v^2)^{1/2}\sin\left[(\xi^2 + v^2)^{1/2} z\right] + \cos\left[(\xi^2 + v^2)^{1/2} z\right]$. Here we introduced the parameters $v = \kappa/(c_R c_S)^{1/2}$ and $\xi = \vartheta/2c_s$.

Note that both $R(z)$ and $S(z)$ contain a z-dependent phase $\exp(-i\xi z)$. This phase factor identifies the vector $\xi = \hat{z}\vartheta/2c_S = \hat{z}(\beta^2 - \sigma^2)/4\sigma_z$ to be a correction to the initial guess for the σ vector. Therefore, the final expression for the diffracted beam wave vector, as predicted by the coupled-wave theory, is $\sigma' = \rho - K + \xi$. Note that ξ points in the z-direction, which is consistent with the bandwidth-uncertainty product requirement. One can see from Figure 4 that in the Bragg-mismatched case, $|\sigma| \neq \beta$, which is a violation of the conservation of the wavenumber. Note that if $|\sigma| > \beta$, then ξ is pointing in the $-\hat{z}$ direction, and if $|\sigma| < \beta$ then ξ is pointing in the $+\hat{z}$ direction. That is, ξ is acting to bring the tip of the σ-vector back to the β-circle.

Let us compare the magnitude of the ξ vector with $\Delta\sigma$. Consider the case of off-Bragg incidence shown in Figure 3. From the triangle formed by vectors σ, ξ, and the radial vector of the β-circle, the law of cosines gives $\beta^2 = \sigma^2 + (\Delta\sigma)^2 - 2\sigma(\Delta\sigma)\cos(\varphi)$. Since $\cos\varphi = \sigma_z/\sigma$, we obtain a quadratic equation $(\Delta\sigma)^2 - 2(\Delta\sigma)\sigma_z + (\sigma^2 - \beta^2) = 0$ with the solution $\Delta\sigma_{1,2} = \sigma_z \pm [\sigma_z^2 - (\sigma^2 - \beta^2)]^{1/2}$. The solution with the + sign can be dropped because it corresponds to the distance to the opposite side of the circle. Writing the solution in the form $\Delta\sigma = \sigma_z - [\sigma_z^2 - (\sigma^2 - \beta^2)]^{1/2}$ we note that $(\sigma^2 - \beta^2)/\sigma_z^2 \ll 1$. For example, for the 16μm photorefractive polymer sample at the largest deviation of $\Delta\theta = 5^o$, we have $(\sigma^2 - \beta^2)/\sigma_z^2 \approx 0.05$. Therefore, we have $\Delta\sigma \approx (\sigma^2 - \beta^2)/2\sigma_z$, so that $\xi \approx \Delta\sigma/2$. Hence the tip of the vector σ' is not on the β-circle. Note that since the expression for $R(z)$ also contains the phase factor $e^{-j\xi}$, the coupled wave theory predicts that the propagation vectors of the reference wave after the gratings is $\rho' = \rho + \xi$. That is $|\sigma'| \neq \beta$ and $|\rho'| \neq \beta$, which is inconsistent with our understanding of the physical process.

There exists an approach to coupled-wave theory that explicitly assumes[11] that $|\sigma| = \beta$ and $\sigma = \rho - K + \Delta\sigma$. Here $\Delta\sigma$ is assumed to be pointing in the z-direction. Proceeding with the analysis and using the same arguments as before, one obtains a new set of coupled wave equations $c_R R' = -i\kappa S \exp(-i\Delta\sigma x)$ and $c_S S' = -i\kappa R \exp(i\Delta\sigma x)$, where $c_R = \rho_z/\beta$ and $c_S = \sigma_z/\beta$ as defined before. After some algebraic manipulations we obtain $S(z) = S_0(z)\exp(i\zeta z)$ where, $S_0(z) = -i(c_R/c_S)^{1/2} v/(\zeta^2 + v^2)^{1/2} \sin[(\zeta^2 + v^2)^{1/2} z]$, and $R(z) = R_0(z)\exp(-i\zeta z)$ where $R_0(z) = i\zeta/(\zeta^2 + v^2)^{1/2} \sin[(\zeta^2 + v^2)^{1/2} z] + \cos[(\zeta^2 + v^2)^{1/2} z]$, and we introduced the parameter $\zeta = \Delta\sigma/2$. However, just as before, the phases of $S(z)$ and $R(z)$ introduce corrections to the initially defined wave vectors, so that $\rho' = \rho + \Delta\sigma/2$ and $\sigma' = \rho - K + \Delta\sigma/2$. For the case sketched in Figure 4, $\Delta\sigma$ points in the $-z$ direction, so that we arrive at the same results as before. Thus, we conclude that Kogelnik's coupled-wave theory[10] does not provide a fully accurate description of the physical process in this context, possibly because of the approximations made in the derivations.

We performed an experiment to measure the angular deviation from the Bragg angle of the diffracted beam $\Delta\varphi$ as a function of the angular deviation of the probe beam $\Delta\theta$. We measured directional correlation of the probe and diffracted beams in a PR

polymer sample by performing an incoherent phase-conjugation readout in a degenerate four-wave mixing configuration. We used a recently invented bis-triarylamine side-chain polymer matrix[12-14] 16µm thick PR polymer composite, operating at 532nm. The material samples for our experiment were provided by Nitto Denko Technical Corp. (NDT). We consider this PR polymer material to be the prime candidate for the implementation of a shift-invariant search of the SPHROM, because this material has a demonstrated capability of stable dynamic video-rate operation and a long shelf lifetime at room temperature[12]. Our experiment was performed with a PR polymer sample with a large transverse area of 1.5" in diameter, using an ND:YAG frequency doubled solid-state pumped Verdi laser, operating at 532nm. The diagram illustrating the experimental setup is presented in Figure 2. The sample consisted of the PR polymer composite with an average refractive index n_0=1.6 sandwiched between Indium Tin Oxide (ITO) electrode-coated glass plates. External DC field was applied across the sample. We determined experimentally that the maximum diffraction efficiency was obtained at a 3kV bias.

The grating was written by two s-polarized, collimated gaussian beams A_1 and A_2, incident on the hologram at $60°$ and $30°$ to normal in the air, respectively. The writing beams were each 5mW in power, with spot diameters of 5mm. Because of the Fresnel refraction in glass, the actual angles of incidence of the beams A_1 and A_2 forming the grating in the material were $35°$ and $20°$, respectively. An asymmetric writing beams arrangement was needed so that the gratings K-vector would make an angle with the poling field direction. The p-polarized probe beam A_3 at 2mW power with a 5mm spot size was incident on the grating, aligned to be exactly counter-propagating to the writing beam A_1. A diffraction efficiency of about 1% was observed (a much higher diffraction efficiency - close to 40% - was observed when the gratings were read out with a He-Ne laser at 633 nm). The phase-conjugated beam A_2^* was reconstructed with p-polarization. After passing through the half-wave plate, A_2^* became s-polarized, and subsequently it was reflected by the polarizing beam splitter (PBS) cube. Note that all the PBS cubes mentioned in this paper transmitt p-polarized and reflect s-polarized beams. In order to measure the directionality correlation in the PR polymer sample, the probe beam was scanned with the help of computer-controlled galvo mirrors (see Figure 2). The two-mirror galvo system was designed to keep the probe beam at a fixed spot on the hologram, while changing the angle of incidence. We estimated $\Delta\varphi$ by measuring the shift of the diffracted beam spot on the ruler as we changed the angle of the probe beam by a known amount. The results are presented in Figure 5. The experimental data is shown with circles, while the theory curve was obtained using the *Ewald* diagram vector model. All the angles we measured in air. One can see that the theory is in a good agreement with the experiment.

To confirm that diffraction in our samples was in the Bragg regime, we calculated the values of $Q = 2\pi\lambda d/n_0\Lambda^2$ (Klein-Cook) and $\rho = \lambda^2/\Lambda^2 n_0 n_1$ (Raman-Nath) parameters[15]. Here d is the sample thickness, n_1 is the amplitude of the refractive index modulation and Λ is the grating periodicity. We determined that $n_1 \approx 3\times10^{-4}$ by measuring the diffraction efficiency at the Bragg angle. We obtained $Q \approx 18$ and $\rho \approx 300$, which satisfy the conditions for the Bragg regime that both Q>>1 (thick grating) and $\rho >> 1$ (weak modulation).

23

In summary, we investigated theoretically and experimentally the directionality of the wave vector of the diffracted beam in off-Bragg readout of volume holographic gratings. We measured the angular deflection of the diffracted beam as a function of the deviation of the probe beam by incoherent readout in degenerate four-wave mixing geometry using a photorefractive polymer composite. We explained our experimental results on the basis of a Ewald sphere vector diagram. In addition, we obtained the theoretical expressions for the angular dependence of the diffracted beam wavevector using the formalism of the coupled wave theory. We showed that the coupled wave theory yields results that is not completely accurate in this context, possibly because of the approximations involved. This analysis is important for construction of a working shift-invariant real-time VanderLugt correlator, because one needs to be able to predict the direction of the correlation beam.

References:

1. S. Tao, D.R. Selviah, and J.E. Midwinter, "Spatioangular multiplexed storage of 750 holograms in an Fe:LiNbO$_3$ crystal," Opt. Lett., **18**(11), 912-914 (1993).
2. S. Tao, Z.H. Song, D.R. Selviah, and J.E. Midwinter, "Spatioangular-multiplexing scheme for dense holographic storage," Appl. Opt. **34**(29), 6729-6737 (1995).
3. F. Mok, D. Psaltis, G. Burr, "Spatially- and angle-multiplexed holographic random access memory," SPIE **1773**, 334-345 (1992).
4. A. Heifetz, J.T. Shen, J-K. Lee, R. Tripathi, M.S. Shahriar, "Translation-invariant object recognition system using an optical correlator and a super-parallel holographic RAM," Opt. Eng., in press (2005).
5. M.S. Shahriar, R. Tripathi, M. Huq, J.T. Shen, "Shared-Hardware Alternating Operation of a Super-Parallel Holographic Optical Correlator and a Super-Parallel Holographic Random Access Memory," Opt. Eng. **43**, 1856-1861 (2004).
6. M.S. Shahriar, R. Tripathi, M. Kleinschmit, J. Donoghue, W. Weathers, M. Huq, and J.T. Shen, "Superparallel Holographic Correlator for Ultrafast Database Searches," *Opt. Lett.* **28**, 525-527 (2003).
7. D.M. Pepper, J.A. Yeung, D. Fekete, and A. Yariv, "Spatial convolution and correlation of optical fields via degenerate four-wave mixing," Opt. Lett. **3**(1), 7-9 (1978).
8. T.K. Gaylord and M.G. Moharam, "Thin and thick gratings: terminology clarification," Appl. Opt. **20**(19), 3271-3273 (1981).
9. G. Barbastathis and D. Psaltis, "Voume holographic multiplexing methods," in *Holographic Data Storage*, H.J. Coufal, D. Psaltis and G.T. Sincerbox eds., Springer (2000).
10. H. Kogelnik, "Coupled wave theory for thick hologram gratings," *Bell Syst. Tech. J.* **48**(9), 2909-2947 (1969).
11. P. Yeh, *Introduction to Photorefractive Nonlinear Optics*, Wiley (1993).
12. C. Fuentes-Hernandez, J. Thomas, R. Termine, G. Meredith, N. Peyghambarian, B. Kippelen, S. Barlow, G. Walker, S.R. Marder, M.Yamamoto, K. Cammack, K. Matsumoto, "Video-rate compatible photorefractive polymers with stable dynamic properties under continuous operation," *Appl. Phys. Lett.* 85(11), 1877-1879 (2004).
13. T.-H. Chao, "Optical joint transform correlator using high-speed holographic photopolymer film,"in *Optical Pattern Recognition XVI*, D.P. Casasent and T.-H. Chao eds., Proc. SPIE **5816**, 136-143 (2005).
14. A. Heifetz, G.S. Pati, J.T. Shen, J.-K. Lee, M.S. Shahriar, C. Phan, M. Yamomoto, "Shift-invariant real-time edge-enhanced VanderLugt correlator using video-rate compatible photorefractive polymer," manuscript in preparation (2005).
15. M.G. Moharam and L. Young, "Criterion for Bragg and Raman-Nath diffraction regimes," Appl. Opt. **17**(11), 1757-1759 (1978).
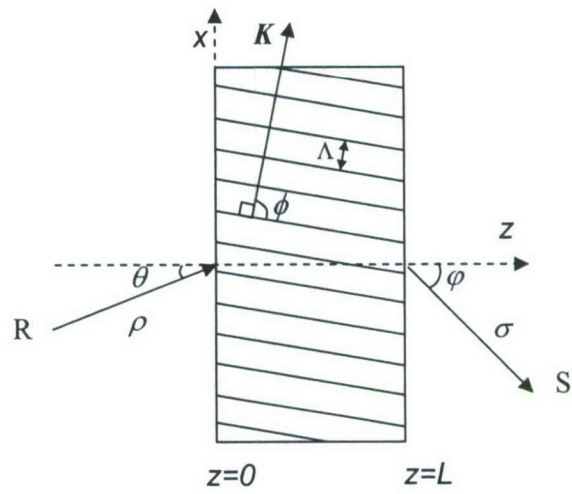
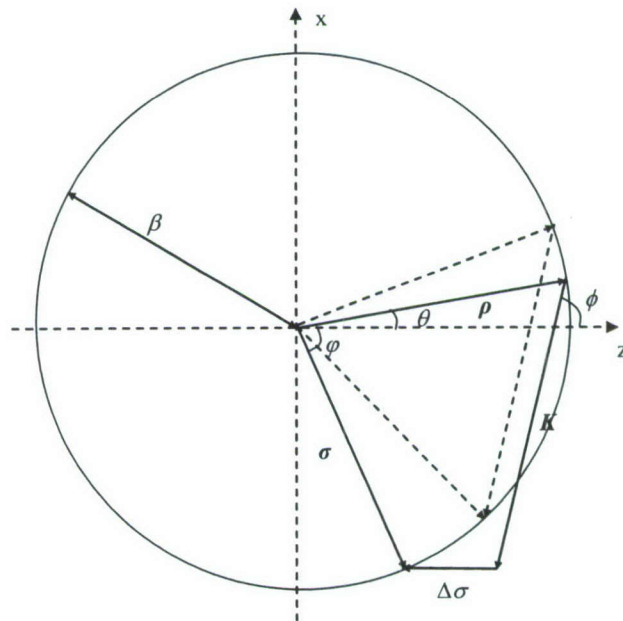Figure 1. Model of thick holographic gratings readout.

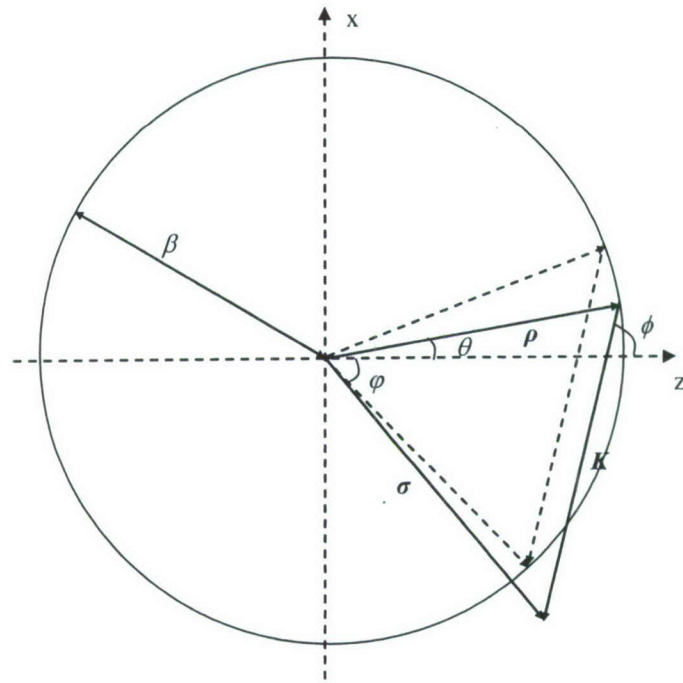Figure 2. Vector diagram obtained from bandwidth-uncertainty product relation.

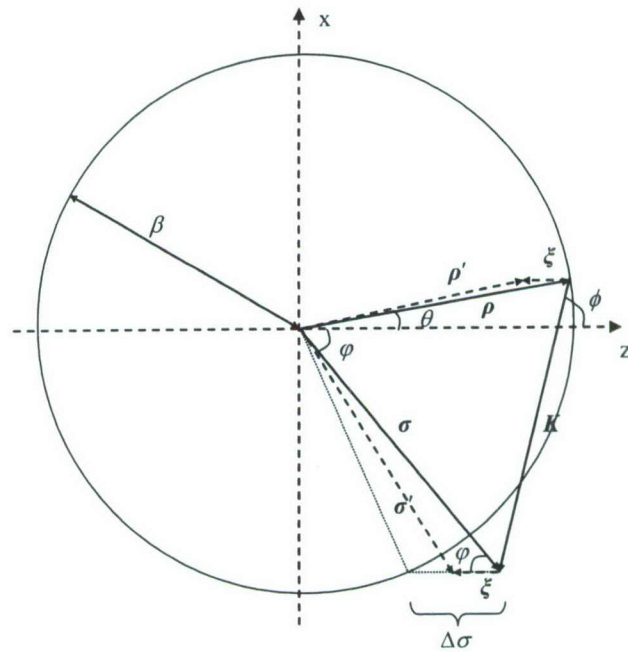Figure 3. Vector diagram corresponding to the assumptions of the coupled-wave theory.

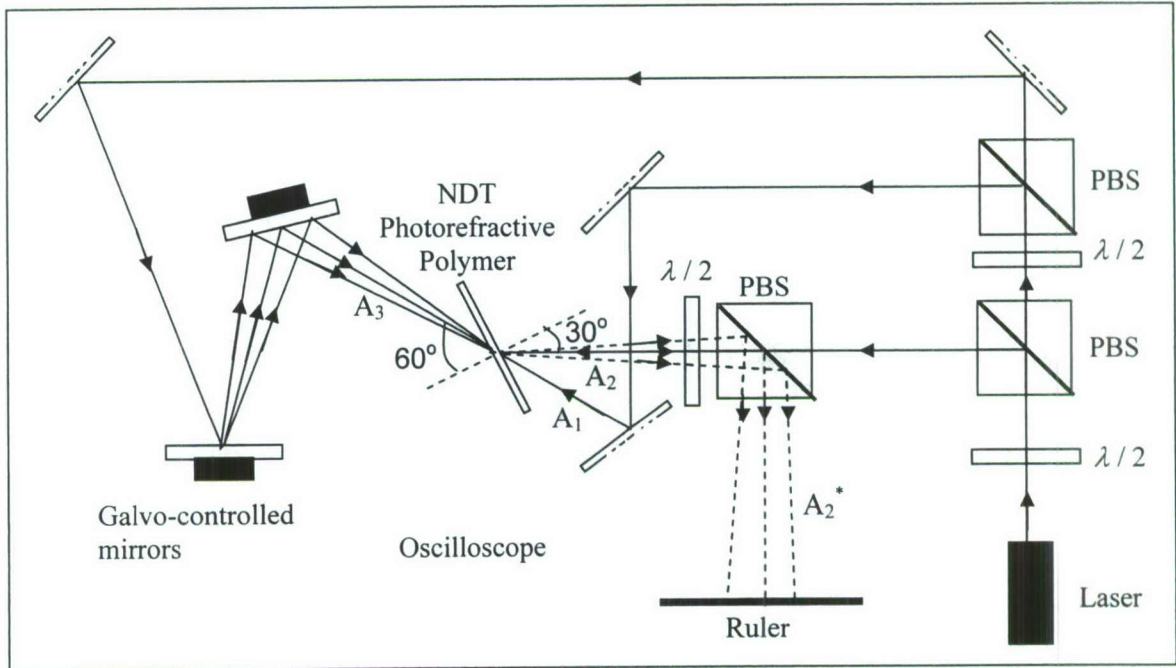Figure 4. Corrections to the vector diagram obtained from the coupled-wave theory

Figure 5. Experimental setup for measuring directional correlation between the probe and diffracted beams
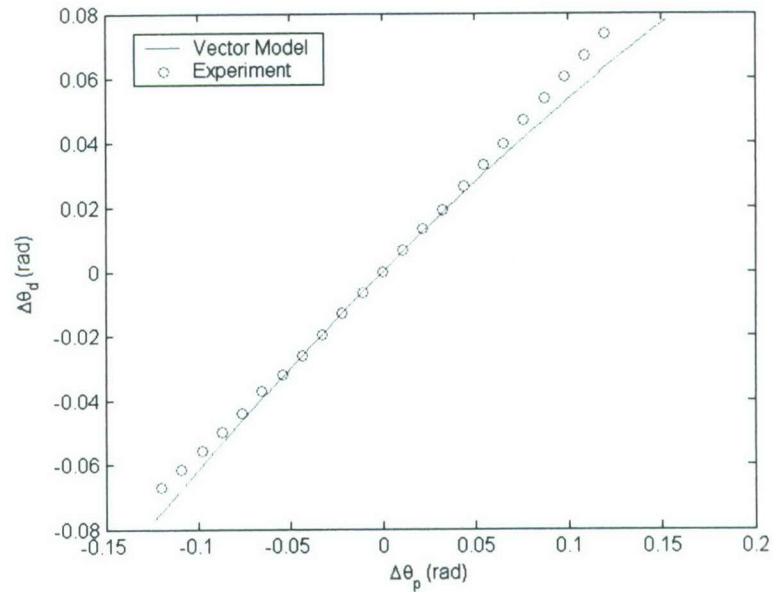

Figure 6. Theory curve from the bandwidth-uncertainty vector model and the experimental data points.

B.4 Prism-coupled lenslet array for a super-parallel holographic correlator and RAM

In many pattern-recognition and target-tracking applications, the speed of the detection system is of critical importance [1-3]. Optical correlation techniques in which data pages are compared in parallel may offer an improvement in speed over electronic digital signal processing methods that are serial in nature [4-8]. Volume holographic correlators represent a significant step in implementing optical parallelism via an angle-multiplexing scheme, so that all the data pages stored in one location are queried simultaneously. We have recently presented an initial demonstration of a super-parallel holographic optical correlator (SPHOC) that represents a further advancement of this parallelism [9-10]. This SPHOC uniquely identifies N images from a database using only $O(\sqrt{N})$ number of detector elements, and can process terabyte-sized data on a time scale that can be of the order of 1μ sec. The spatial location and the reference beam angle for the matched image are identified using a spatio-angular decoupling architecture that consists of a lenslet array, a holographic redirector, a demultiplexer, and two CCD arrays. The key component in the spatio-angular decoupling architecture is a prism-coupled lenslet array (PCLLA) that redirects and collimates the output correlation beams. The PCLLA can also be operated in reverse in a super parallel holographic RAM (SPHRAM) [11]. The SPHRAM can be used to send images to a real-time translation-invariant holographic correlator at a high speed or as a random-access memory supplying data in pages for optical or electronic processing systems [12]. Here, we first review the operation of the SPHOC/SPHRAM architecture, and then we derive the beam phase transformation that is required of the PCLLA for both plane waves and Gaussian beams. We also estimate the necessary parameters and dimensions for fabrication, and define methods for the construction of the full-scale PCLLA.

The architecture of the SPHOC is shown in figure 1 [9,11]. First, rXs (r by s) horizontally and vertically angle-multiplexed images (where r is the number of horizontally multiplexed images, and s is the number of vertically multiplexed images) are stored in each nXm spatial location of the holographic memory unit (HMU). The SPHOC operation starts by expanding the collimated beam from a read laser in order to match the size of the SLM. The target image is sent to the SLM via a high-speed data bus, and the beam reflected from the face of the SLM now carries this image. This reflected beam is then sent through the holographic demultiplexer/multiplexer (HDMX). The HDMX is a device that produces nXm copies of the input image, in as many angular directions. Such a device can be constructed simply by writing nXm plain wave holograms over the entire volume [13].

The output beams from the HDMX are now passed through the holographic redirector (HR) which redirects the beams so that they travel parallel to the optic axis, and impinge on the HMU, one at each spatial location. If there is a match with any of the images stored in a given location, a diffracted beam will emanate from that location at a particular angle. In order to maximize the storage capacity of the HMU, the angular separation between any two adjacent images will be very small. For example, for a 2 mm thick substrate, the angular separation can be as small as 0.25 mrad. Thus a device is

needed that can resolve these small angular differences within the constraints of the architecture. This task will be performed by the PCLLA.

Once the beams are separated and collimated, they pass through the rest of the architecture, which is comprised of two separate detection systems. One detector is used to determine which angle was matched, while the other determines which spatial position is matched. These two pieces of information identify which image was matched.

The operation of the SPHRAM is very similar to that of the SPHOC [11]. The beams now propagate from right to left as shown in figure 2. The goal of the SPHRAM is to allow simultaneous readout of multiple spatial locations. A beam deflector is used to select a certain readout angle to be used at every spatial location of the HMU. This readout angle is then translated into spatial position (one of the possible "paths") by a redirector.

After this reference beam is copied into multiple readout beams by a holographic multiplexer/demultiplexer, another redirector sends the multiple reference beams towards the PCLLA. The PCLLA is used to translate the spatial position (or "path") of the readout beams back into a specific read beam angle. Thus every copy of the reference beam is directed to the HMU at the angle that was selected. Readout occurs at each spatial location, and a shutter array is then used to select a single location for output to a detector. By selecting an angle at the beam deflector and opening a single element of the shutter array, one image is retrieved. Because of the high possible response times (~1 μs) of the shutter array and beam deflector, readout of the HMU has the potential to achieve very high speeds.

We recall first the key component of the SPHOC/SPHRAM architecture, the prism-coupled lenslet array. Although in our original design a single lens was used to represent the functionality of the lenslet array and bulk optics were used for the experiment, for a demonstration of the complete architecture a more complex structure is required [9].

In the case of the SPHOC, a single lens would be able to resolve any of the diffracted correlation beams. Each beam has a different angle, which would lead to an array of possible correlation spots in the focal plane of the lens. However, in order to determine the angle and location that is matched, the diffracted beams must pass through the rest of the architecture as shown in Figure 1 and described in reference 9. For this, a more complicated lens structure is needed. For the operation of the SPHRAM, a single lens is not able to translate position to angle without also focusing the beam. Because spherical wave readout is not desired for the SPHRAM, this also indicates that a more complex optical device is necessary.

Figure 3 illustrates one unit of the PCLLA that corresponds to one spatial location of the HMU in an SPHOC. Taking $z = 0$ to be at the holographic substrate, there is a primary lens at $z = f_1$ to separate the cone of possible overlapping correlation beams into a 2D focal array pattern. The secondary array of much smaller lenses is at $z = 2f_1 + f_2$, with each lens coupled to its own prism. Each prism is shaped to a different angle, which corresponds to the angle of the diffracted beam that will pass through it. The large primary lens will separate the beams according to their individual spatial frequencies, while the secondary array of small lenses and prisms will collimate and redirect the beams. Each spatial location of the HMU has a corresponding unit of the PCLLA to redirect and collimate the possible correlation beams. An example of a three spatial

location HMU and corresponding PCLLA is shown in figure 4. Figure 5 demonstrates the two-dimensional nature of the PCLLA device, showing the secondary lens/prism array. Because angle-multiplexing in both dimensions will be used in order to maximize the storage capacity of the HMU, all the elements of the SPHOC/SPHRAM architecture must be two-dimensional. The lenses that make up the secondary array are shown by the dotted circular lines. The prism elements are shown with the exit surface shaded. Prism elements along the main horizontal and vertical axes, shown by the dotted cross in figure 5, only need to redirect in one dimension. Prism elements outside of these two axis must redirect towards the central optic axis and therefore need to redirect in two planes.

We will use figure 3 to analyze the phase transformation the diffracted beam undergoes as it propagates through the PCLLA. We consider a single spatial location with diffracted beams in two dimensions. The large lens imparts a quadratic phase to an incoming beam. We account for this by writing the transfer function of the lens as

$$t_{lens}(x) = \exp\left(-i\frac{k}{2f_1}|\bar{\rho}|^2\right)$$

(1)

where $|\bar{\rho}|^2 = x^2 + y^2$. We can express the complex amplitude of a plane wave traveling at an angle θ by $U = \exp(i2\pi\upsilon_0 x)\exp(i2\pi\upsilon_1 y)$ where $\upsilon = \sin\theta/\lambda$ and υ_x corresponds to the spatial frequency (angle) in the x direction and υ_y represents the spatial frequency (angle) in the y direction. Therefore, the field distribution just after the lens is:

$$U_{after} = \exp(i2\pi\upsilon_x x)\exp(i2\pi\upsilon_y y)\exp\left(-i\frac{k}{2f_1}|\bar{\rho}|^2\right)$$

(2)

where we have dropped the constant phase factors. The field in the focal plane of the lens ($z = 2f_1$) is given by [14,15]:

$$U_f(x,y) = \frac{e^{ikz}}{i\lambda z}e^{i\frac{k}{2z}(x^2+y^2)}\iint U_{after}(\xi,\eta)e^{i\frac{k}{2z}(\xi^2+\eta^2)}e^{i\frac{2\pi}{\lambda z}(x\xi+y\eta)}d\xi d\eta$$

(3)

After completing the integration, we find that the field distribution is a delta function in x and y, shifted by an amount corresponding to the spatial frequencies of the input beam.

$$U_f = \delta\left(\frac{x}{\lambda f_1} - v_x\right)\delta\left(\frac{y}{\lambda f_1} - v_y\right)$$

(4)

Using equation (3) to find the field in the $z = 2f_1+L$ plane as well, we find:

$$U_{2f_1+L} = \exp\left(i\frac{k}{2L}(x^2+y^2)\right)\exp\left(-i\frac{kv_x\lambda f_1}{L}x\right)\exp\left(-i\frac{kv_y\lambda f_1}{L}y\right)$$

(5)

This field distribution yields the information on the focal lengths of the small secondary lenses we will need to cancel the quadratic phase terms, as well as the angles of the prisms needed to cancel the linear phase terms. The phase transformation required by the small lens and prism combination is then given by:

$$U_{lens+prism} = \exp\left(-i\frac{k}{2f_2}(x^2+y^2)\right)\exp\left(ik\sin(\theta_1)\frac{f_1}{f_2}x\right)\exp\left(ik\sin(\theta_2)\frac{f_1}{f_2}y\right)$$

(6)

This will exactly cancel both the quadratic and linear terms in equation (5), resulting in a collimated plane wave traveling parallel to the z axis (where f_2 is chosen to match L). We see from equation (6) that every lens L_2 in the secondary lens array has the same focal length, but each requires a different prism. The focal length f_2 is determined from the spacing of the beams in the focal plane. Equation (4) gives the spacing between focal spots.

In principle, there could be several thousand angle-multiplexed images stored in a single spatial location. For a typical 2mm thick holographic substrate, 1000 images in one location leads to the focal spots being as close as 10 microns. Current commercially available micro-optical manufacturing techniques can produce closely-packed lenses as small as 20 microns in diameter, and the industry is moving towards even smaller feature sizes [16]. Techniques are available to make both refractive and diffractive micro lenses and micro prisms in one- and two-dimensional arrays [16-19].

In designing a lens and prism array where the dimensions of each individual element are beginning to approach the wavelength of light, it is important to consider the diffractive properties of the beam itself. In this limit, many laser beams can be modeled accurately as Gaussian beams. The depth of focus, or Rayleigh range, for these beams is a measure of how far the beam can propagate and still be considered in the plane wave limit. The Rayleigh range is defined as [20]:

$$z_0 = \frac{\pi w_0^2}{\lambda} \tag{7}$$

In equation (7), w_0 is the waist, or radius, of the beam. For a 1 mm beam waist at 500 nm, the depth of focus is about 6 mm. For a 10 micron beam waist, the depth of focus is now less than 1 micron. It is clear that the Gaussian nature of these beams must be accounted for. Figure 6a illustrates a Gaussian beam propagating through a system comprised of two lens in the so-called "4-f" imaging system. In designing a PC-LLA at dimensions where the Gaussian nature of the beam will show, we must examine the propagation of the Gaussian beam through the proposed system to determine if any modification of the design is required. For the PC-LLA, the beams will be at an angle, as shown in Figure 6b.

Figure 6b illustrates the geometry that will be used in this analysis. U_0, U_1, and U_2 represent the complex amplitude of the beam at $z=0$, $z=2f_1$, and $z=2f_1+2f_2$. A Gaussian beam can be written in the form:

$$U(x,y) = \frac{w_0}{w(z)} e^{\frac{-(x^2+y^2)}{w^2(z)}} e^{\frac{-jk(x^2+y^2)}{2R(z)}} e^{jkz+j\varsigma(z)}$$

$$w(z) = w_0 \left[1+\left(\frac{z}{z_0}\right)^2\right]^{1/2} \quad ; \quad R(z) = z\left[1+\left(\frac{z_0}{z}\right)^2\right] \tag{8}$$

$$\varsigma(z) = \tan^{-1}\left(\frac{z}{z_0}\right)$$

Here, w_0 is the initial beam waist, $w(z)$ and $R(z)$ are the waist and radius of curvature as functions of z, and $\varsigma(z)$ is the Gaussian phase. Following figure 6b, the Gaussian beam of interest is incident at an angle θ, propagating along the axis z'. The angled axes x' and z' are related to the optical axes of the system x and z by:

$$x' = x\cos\theta - z\sin\theta$$

$$z' = x\sin\theta + z\cos\theta \tag{9}$$

For the following analysis, we will assume that $R(z') \approx R(z) \equiv R$ and $w(z') \approx w(z) \equiv w$, which is valid in the paraxial limit. By inserting the expressions for x' and z' into the standard Gaussian form shown in equation (8), we arrive at the expression for U_0:

$$U_0(x_0, y_0) = \frac{w_0}{w}\exp\left[-\left(\frac{2R + jkw^2}{2Rw^2}\right)\left(x_0^2\cos^2\theta - 2zx_0\sin\theta\cos\theta + z^2\sin^2\theta + y_0^2\right)\right]$$

$$\cdot \exp\left[jk\left(x\sin\theta + z\cos\theta\right)\right] \tag{10}$$

In order to determine the complex amplitude at $z=2f_1$ and $z=2f_1+2f_2$, we will use the equation for transmission through a thin lens from the front focal plane to the back focal plane, as derived using the Fresnel integral [14]:

$$U_{out}(x_{out}) = \tilde{U}_{in}(x_{in})\Big|_{f_x = \frac{x_{out}}{\lambda f}} \tag{11}$$

For the case of an image or beam traveling from the front focus of a thin lens to the back focus, the lens transformation is simply a Fourier transform of the incoming wavefront, scaled by the focal length of the lens and by the wavelength of light. Performing this transform, we arrive at the expression for U_1:

$$U_1(x_1, y_1) = \phi(z)\exp\left[\frac{-\pi^2}{a_1\lambda f_1}x_1^2 - j\sin\theta\cos\theta\frac{8\pi z}{a_1\lambda f_1 w^2}x_1\right] \otimes \delta\left(\frac{x_1}{\lambda f_1} - \gamma_1\right)$$

$$a_1 = \cos^2\theta\left(\frac{1}{w^2} + \frac{jk}{2R}\right) \tag{12}$$

$$\gamma_1 = \frac{k}{2\pi}\sin\theta - \frac{kz}{2\pi R}\sin\theta\cos\theta$$

In this equation, $\phi(z)$ contains the collected constants and constant phase terms, while the "$\otimes$" operator indicates convolution. Equation (12) shows that a Gaussian beam traveling on an angle through a lens is offset in the focal plane just as in the case of a plane wave. Here however, the amount of displacement is proportional not just to $f_1\sin\theta$, as in the plane wave scenario. In this case, the displacement is $\lambda f_1\gamma_1 = f_1\sin\theta - (z/f_1R)\sin\theta\cos\theta$. For a Gaussian beam with its waist in the front focal plane of a lens, the new Gaussian beam after the lens will have its waist in the back focal plane of the lens. Because of this, $R(z)$ for $z=2f_1$ will be very large and the second term is small enough to ignore. Thus we see that the Gaussian nature of the beam does not affect the location of the focal spots in this case.

A second Fourier transform is performed on the beam after traveling through the second lens with a focal length f_2. After this second transform, the beam is now:

$$U_0\left(x_0, y_0\right) =$$

$$\phi(z)\exp\left[-\left(\frac{2R + jkw^2}{2Rw^2}\right)\left(\frac{f_1^2}{f_2^2}x_0^2\cos^2\theta - 2z\frac{f_1}{f_2}x_0\sin\theta\cos\theta + z^2\sin^2\theta + y_0^2\right)\right] \quad (13)$$

$$\cdot\exp\left[jk\left(x\frac{f_1}{f_2}\sin\theta + z\cos\theta\right)\right]$$

Thus the resultant beam after the 4f system is still a Gaussian beam propagating at an angle with respect to the optic axis of the system, except that it is scaled by the ratio of the focal lengths of the lenses, as expected.

We have performed a simple simulation to show the feasibility of the design. In this simulation , the secondary lenslet array is constructed of closely-packed 100 micron diameter lenses, each with a 300 micron focal length. Using a 1 cm diameter lens as the primary lens with a 4 cm focal length allows 100 angles to be multiplexed in one dimension in one spatial location. For a reasonably well-collimated correlation beam, the beams at the output of the lenslet array can have a Rayleigh length of several centimeters, which is sufficient for the optical components of the rest of the SPHOC architecture. We plan to construct an SPHRAM based on these dimensions to test the design of the PCLLA.

The full-scale implementation of the PCLLA will require customized components to be fabricated by outside vendors. Before embarking on this venture, we have decided to test the basic feasibility of the PCLLA architecture by using off-the-shelf components that are readily available. Figure 7 shows one component of this small-scale PCLLA: a one dimensional array of lenses and prisms. Currently, three of these units are being employed to test a small scale SPHRAM.

In conclusion, we have proposed a design for a prism-coupled lenslet array that will play a key role in super-parallel architectures for a holographic correlator/RAM. We have performed the analysis of the required phase transformations of the beams using the Fourier optics approach, and have defined the steps to be used for a large scale implementation. A small scale implementation of the PCLLA has been achieved, and tests are underway to evaluate its performance in the SPHOC and the SPHRAM..

References:

1. R.O. Duda, P.E. Hart, and D.E. Stork, *"Pattern Classification"*, Wiley-Interscience (2000).
2. S. Theodoridis, and K. Koutroumbas, *"Pattern Recognition, Second Edition"*, Academic Press (2003).
3. W.W. Goj, *"Synthetic-Aperture Radar and Electronic Warfare"*, Artech House (1993).
4. N. Collings, *"Optical Pattern Recognition Using Holographic Techniques"*, Pearson Addison Wesley (1988).
5. M. S. Alam (Ed.), *"Selected Papers on Optical Pattern Recognition Using Joint Transform Correlation"*, SPIE Milestone Ser. **MS157/HC**, SPIE Press (1999).
6. F.T.S. Yu (Ed.), *"Selected papers on Optical Pattern Recognition"*, SPIE Milestone Ser. **MS156/HC**, SPIE Press (1999).
7. M.J. Murdocca and B. Sugla, "Design of an optical random access memory", *Appl. Opt.* **28**(1) 182 (1989).
8. P.M. Birch, F. Claret-Tournier, D. Budgett, R. Young, and C. Chatwin, "Optical and electronic design of a hybrid digital-optical correlator system", *Opt. Eng.* **41**(1) 32-40 (2002).
9. M.S. Shahriar, R. Tripathi, M. Kleinschmit, J. Donoghue, W. Weathers, M. Huq, J.T. Shen "Superparallel holographic correlator for ultrafast database searches", *Opt. Lett.* **28**(7), 525-527 (2003).
10. A. J.-B. Hassaun, "Holographic Correlation Improves on DSP by Six Orders of Magnitude", *Laser Focus World* (July 2002).
11. M.S. Shahriar, R. Tripathi, M. Huq, J.T. Shen "Shared-hardware alternating operation of a super-parallel holographic optical correlator and a super-parallel holographic random access memory", *Opt. Eng.* **43**(8) 1856-61 (2004).
12. A. Heifetz, J.T. Shen, J-K. Lee, R. Tripathi, M.S. Shahriar, "Translation-invariant image recognition system using a super-parallel holographic memory," to appear in *Optical Engineering* (2005).
13. M.S. Shahriar, J. Riccobono, M. Kleinschmit, J.T. Shen, "Coherent and incoherent beam combination using thick holographic substrates," Opt. Comm. 220, 75-83 (2003).
14. J.W. Goodman, *"Introduction to Fourier Optics"*, McGraw-Hill (1996).
15. A. Vanderlugt, *"Optical Signal Processing"*, Wiley-Interscience (1992).
16. T.J. Suleski, R.D. Te Kolste, "Fabrication Trends for Free-Space Microoptics," *J. Lightwave Tech.* **23**(2) 633-646 (2005).
17. S. Sinzinger, J. Jahns, *"Microoptics,"* WILEY-VCH GmbH & Co. KGaA (2003).
18. T. Suleski, D.C. O'Shea, A.D. Kathman, and D. Prather, *"Diffractive Optics: Design, Fabrication, and Test,"* SPIE Press, (2003).
19. N.F. Borrelli, *"Microoptics Technology,"* Marcel Dekker (2005).
20. B.E.A. Saleh, M.C. Teich, *"Fundamentals of Photonics,"* John Wiley & Sons (1991).
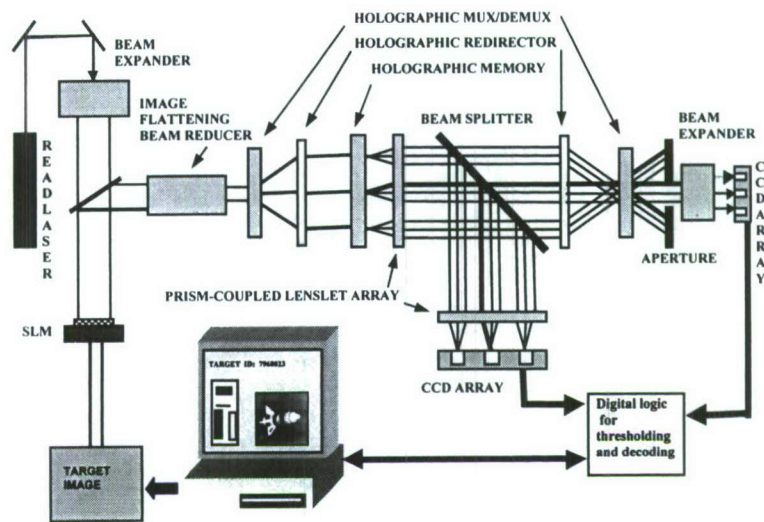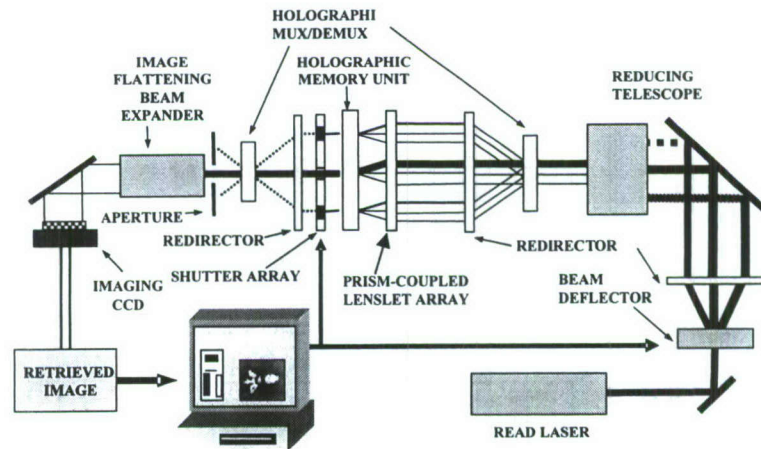
Figure 1: SPHOC Architecture
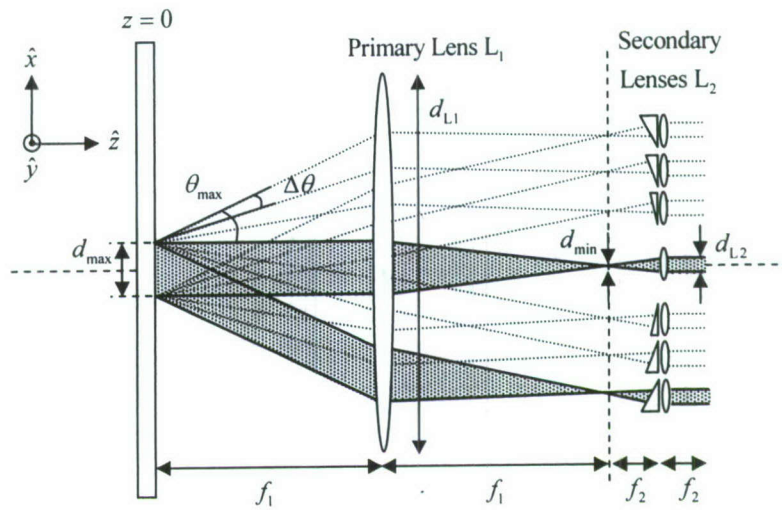

Figure 2: SPHRAM architecture

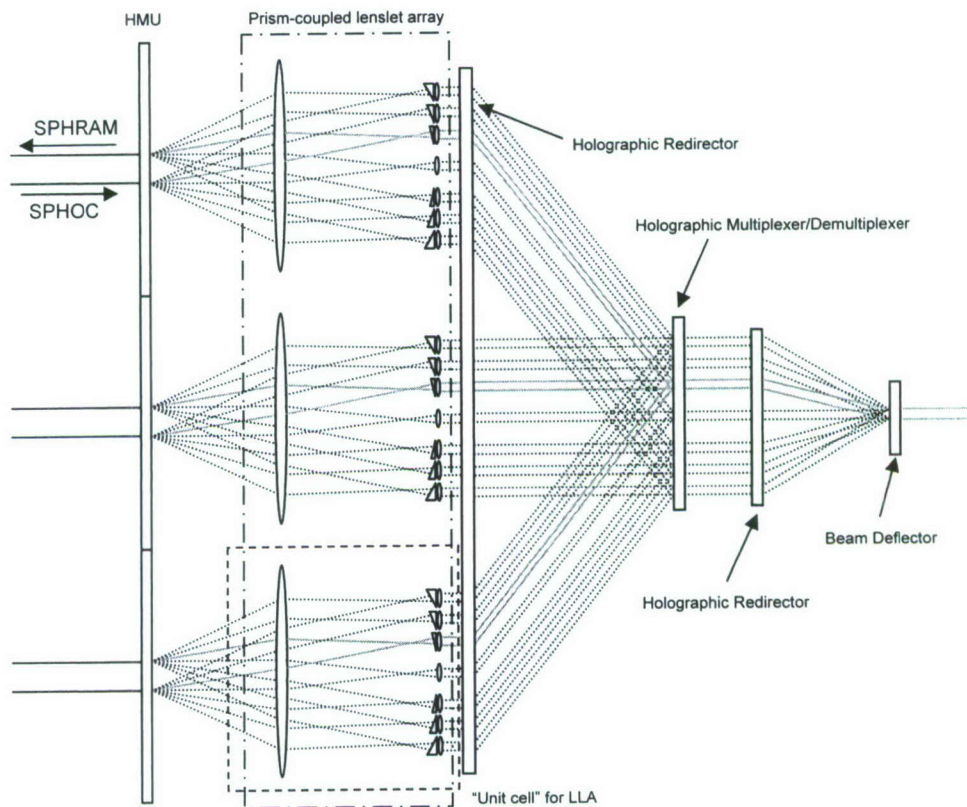Figure 3: Details of a "unit cell" of prism-coupled lenslet array

Figure 4: Prism-coupled LLA in a 3-spatial-location HMU SPHOC/SPHRAM architecture. Beams propagate left to right for SPHOC operation and right to left for SPHRAM operation.
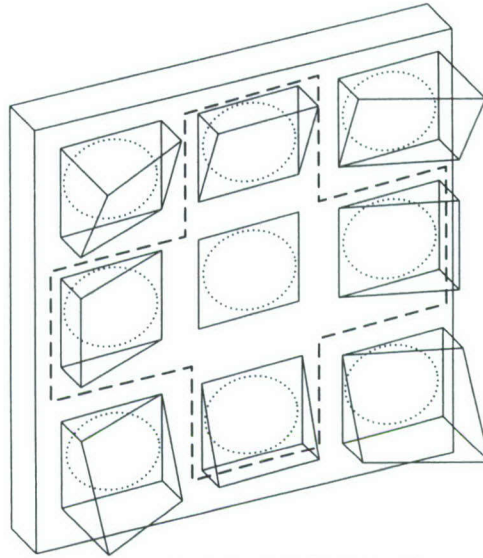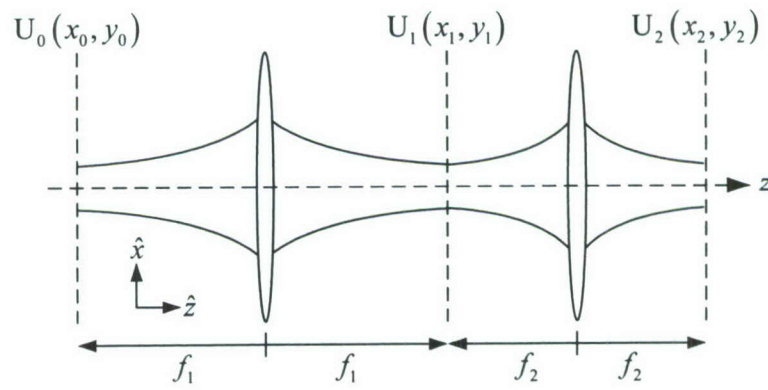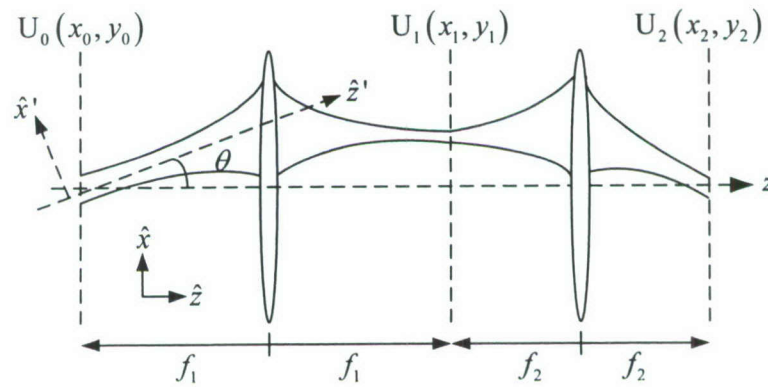
Figure 5: Schematic representation of a 3 by 3 PCLLA. See text for further description.

a.)

b.)

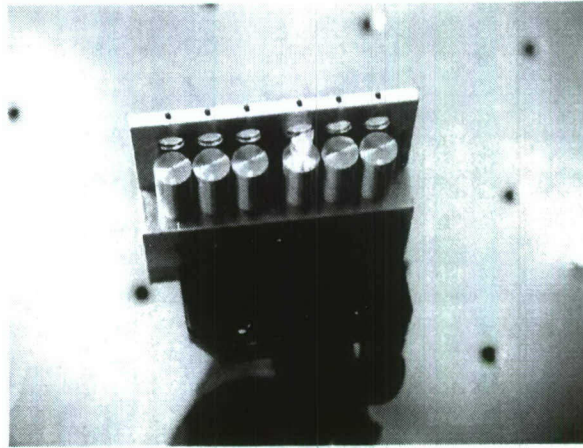Figure 6 a.) Gaussian beam, normal incidence b.) Gaussian beam, angled incidence

Figure 7. Picture of a 1x6 lenslet array we have constructed using commercially available components. This is currently being used to test the functionality of the PCLLA design in a small-scale SPHRAM.

B.5 Demonstration Of A Spectrally Multiplexed Holographic Stokesmeter

Polarization imaging [1,2] is useful in applications ranging from target recognition to vegetation mapping [3,4], and can be combined with our SPHOC/SPHRAM architecture to add additional image recognityion capabilities under conditions where an object may not be fully visible because of clouds or trees, for example. While current polarimeter architectures can be limited in speed or by the lack of an ability to determine the complete Stokes vector, a holographic Stokesmeter (HSM) [5] determines all four Stokes parameters in parallel and at speeds limited by the optical response of the holographic volume gratings.

A compact version [6] of this device consists of a pair of spatially separated gratings in a single substrate and two electro-optic modulators. After all four intensity measurements from the output beams diffracted by the holographic optical element are taken during the T_1 and T_2 period for each pixel of two focal plane arrays (FPA), we can construct the polarimetric image by manipulating the signals with precalibrated field programmable gate arrays.

The single hologram in each zone of the substrate for a compact architecture could be replaced by a set of angle multiplexed gratings. Each grating would be designed to produce a diffracted beam (orthogonal to the substrate) only for a specific band of frequencies at a specific angle of incidence, as shown in Fig.1. Thus, by scanning the angle of incidence without changing the position [7], it is possible to produce a polarimetric image for a desired wavelength band. Thus, it is possible to implement many such bands in a single device.

$$\Lambda = \lambda_G/(2^*\sin\theta_1) = \lambda_R/(2^*\sin\theta_2) = \dots = \lambda_i/(2^*\sin\theta_i)$$
$$\theta_s = 2(\theta_2 - \theta_1) = 2(\sin^{-1}(\lambda_G / (\lambda_R^*\sin\theta_1)) - \theta_1)$$
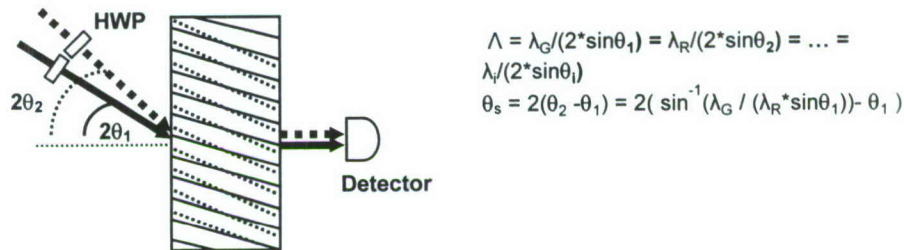
Figure 1

In order to demonstrate the feasibility of the spectrally multiplexed Stokesmeter, we have written a pair of spatially separated, angle-multiplexed gratings in a 2mm thick Memplex® sample with a 532nm frequency doubled Nd:YAG laser. We then measured the diffraction efficiencies for the same locations of the holographic substrate with two different wavelengths of 532 nm and 780nm as shown in Fig.2. The black (white) squares and triangles represent the diffraction efficiencies at the 1st location (2nd location) for the wavelengths of 532nm and 780nm, respectively. These diffraction efficiencies yield contrast ratios of 52.9% and 49.1% for 532nm, and of 86.1% and 85.0% for 780nm at two spatially separated locations. Based on these data, we can construct the measurement matrix of the system for each wavelength.
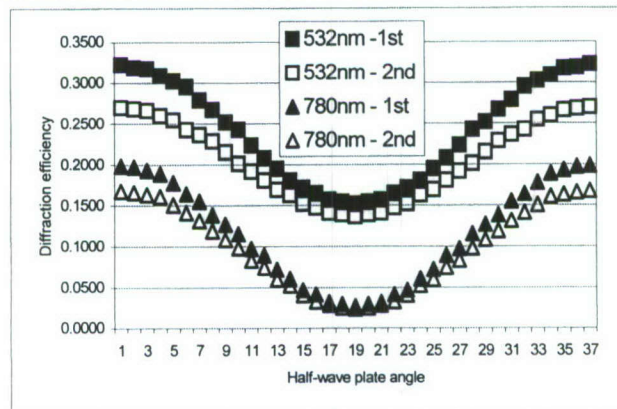

Figure 2

Fig.3 displays the measured average values and the standard deviations of I, Q, U and V using a pair of spatially separated angle-multiplexed gratings for each wavelength (532nm:'o', 780nm:'•') Here, we considered the linear polarization state and the elliptically polarization state of the input beam. The average values for each wavelength are approximately equal to the assumed values within the error range. This shows the feasibility of a spectrally multiplexed HSM in its compact architecture. The ability to combine spectral discrimination with polarization imaging in a single device makes this HSM a unique device of significant interest
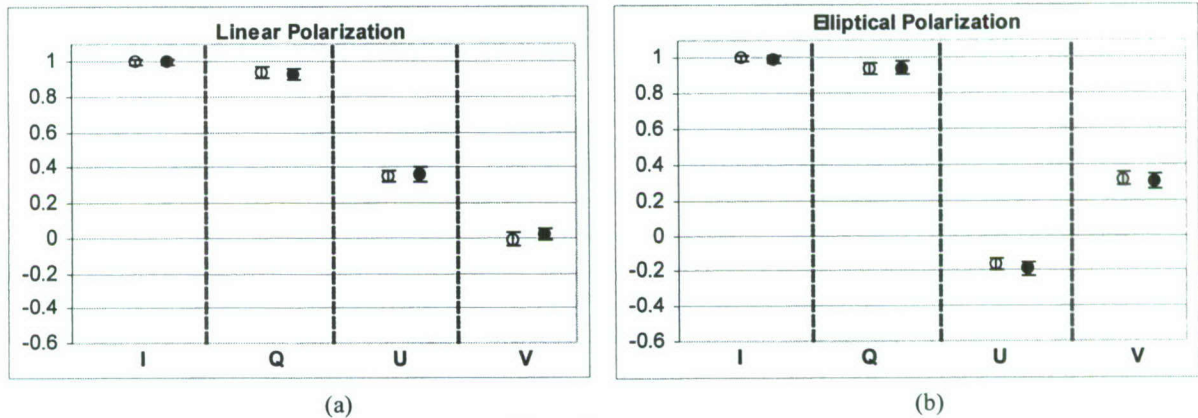

(a)   (b)

Figure 3

References

[1] K.P.Bishop, H.D.McIntire, M.P.Fetrow, L. McMackin, "Multispectral polarimeter imaging in the visible to near-IR, Targets and backgrounds : Characterization and Representation," *Proc. SPIE* **3699,** 49 (1999).

[2] G.P. Nordin, J.T. Meier, and M. W. Jones, "Micropolarizer array for infrared imaging polarimetry," *J. Opt Soc Am.* **A 16,** 1168 (1999).

[3] L.J. Denes, M. Gottlieb, B. Kaminsky, and D. Huber, "Spectro-polarimetric imaging for object recognition", *Proc. SPIE,*
   3240, 8 (1998).

[4] Curran, P.J., "Polarized visible light as an aid to vegetation classification", *Remote Sens. Environ.*, **12,** 491-499, 1982.

[5] M.S. Shahriar, J.T. Shen, R. Tripathi, M. Kleinschmitt, T. Nee, S.F. Nee, "Ultra-fast Holographic Stokesmeter for Polarization Imaging in Real Time," Opt.Lett, 29,208 (2004).

[6] J.-K. Lee, J. T. Shen, Alex. Heifetz, R. Tripathi, and M.S. Shahriar, "Demonstration of a Thick Holographic Stokesmeter," *Optics Communication,* in press (2005)

[7] M.S. Shahriar, R.Tripathi, M.Kleinschmit, J.Donghue,W.Weathers, M.Hug,and J.T. Shen, "Superparallel holographic correlator for ultrafast database searches," *Opt. Lett.* **28,** 7 (2003)

B.6 Demonstration of Landmark Identification Based Guidance Via Translation Invariant Image Correlations

GPS navigation provides the most accurate means of global location determination available today. However, the nature of the GPS system makes it vulnerable to jamming or spoofing. A need for an alternative to GPS navigation can be addressed through highly accurate landmark navigation. Here, we describe our recent investigation of the use of the holographic correlator demonstrated above for landmark identification based navigation (LIBN) of an UAV. Holographic correlation performs the two key tasks of LIBN simultaneously: the correlator identifies the landmark in the captured scene against a database of landmarks and also determine the relative position of the vehicle to the landmark, in a manner that is scale, orientation, and location invariant. This allows the UAV to update its inertial reference system. The basic idea is illustrated schematically in figure 1.

Figure 2 shows the first frames of two movie files illustrating the landmark identification process. The full movies can be downloaded from ftp://lapt.ece.northwestern.edu/ (*username:* lapt; *password:* lapt2005) in the directory "holo-targ-rec-new-movies." [*Note for Dr. Pomerenke:* this directory is new, and has movies that you have not downloaded before]. Each of these movies was produced by suspending a camera from the ceiling above a mock city block made of lego blocks. The camera was then rotated (for movie shown on the left) or translated (for movie shown on the right), simulating the flight motion of an UAV above a city. One of the buildings was selected as a target. The correlator technique described above was then used to identify the location of the building, The translation invariance was achieved automatically, while the rotation and scale variation was accommodated by simply recording many copies of the target object and searching through all of them.

In order to emulate a more realistic UAV flight, we used a remote controlled, helium-filled blimp, fitted with a wireless camera system under it, as shown in figure 3. The blimp was then made to fly around in a pre-designed trajectory above a mock city block. The trajectory was controlled precisely by using a set of four ultrasonic transmitters located on the corners of an optical table (see figure 4), along with an audio-receiver carried by the blimp. The images were captured in real time, and fed into the correlator for landmark identification. We have also developed a flight-simulator software module with hardware interface (see figure 5) that can analyze the correlation data, use it to determine the location of the blimp, and feed guidance information into the remote control system for navigating the blimp. The top picture is the firsts frame of a movie clip that can be downloaded from ftp://lapt.ece.northwestern.edu/ (username: lapt; password: lapt2005) in the directory "holo-targ-rec-new-movies." The bottom two pictures show close-ups of the propellers, the camera, and the audio-receiver.

Figure 6 shows the first frame of a movie that was produced with this system, illustrating the identification of a landmark as the blimp shown in figure 2 flew over a mock city block. Again, the movie can be downloaded from ftp://lapt.ece.northwestern.edu/ (username: lapt; password: lapt2005) in the directory "holo-targ-rec-new-movies."
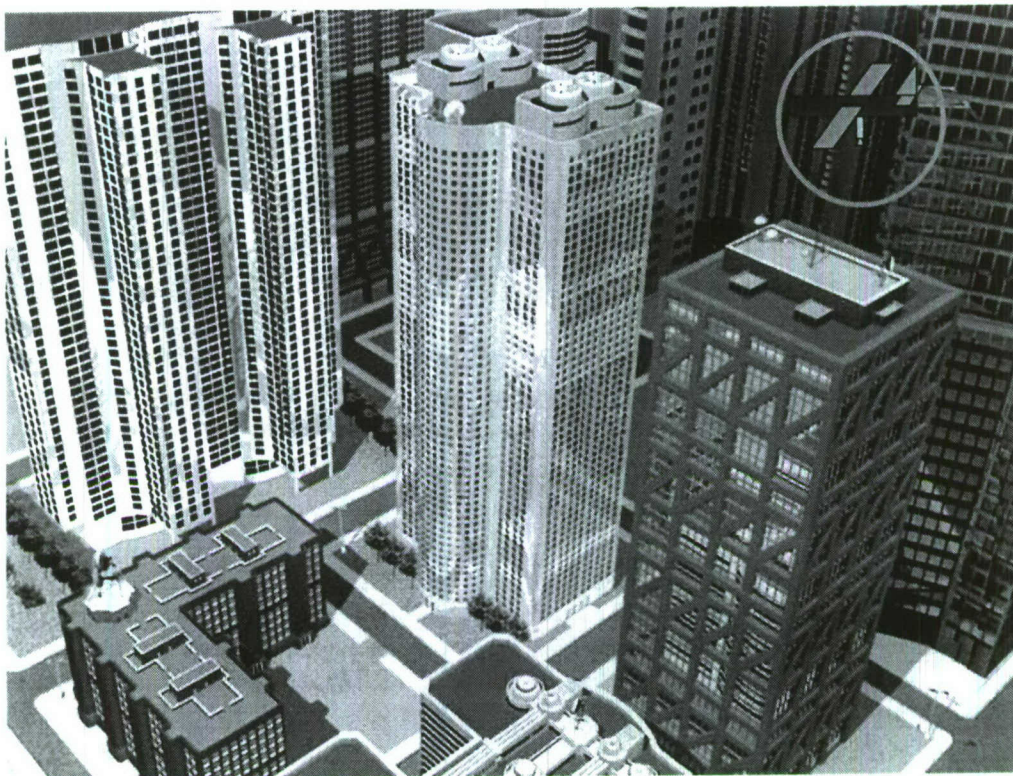
Figure 1: Basic idea behind landmark identification based UAV navigation using a translation invariant holographic correlator.
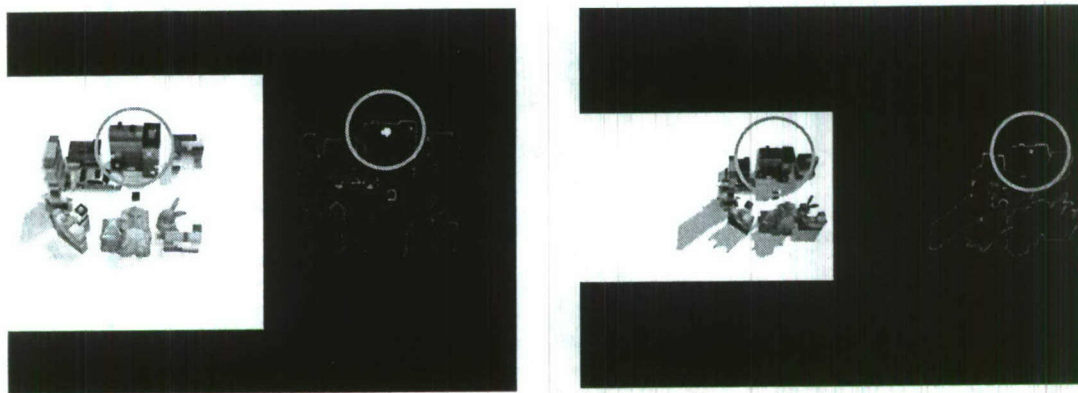

Figure 2: First frames of movie files showing the landmark identification. The full movies can be downloaded from ftp://lapt.ece.northwestern.edu/ (username: lapt; password: lapt2005) in the directory "holo-targ-rec-new-movies." Each of these movies was produced by suspending a camera from the ceiling above a mock city block made of lego blocks. The camera was then rotated (left) or translated (right), simulating the flight motion of an UAV above a city. One of the buildings was selected as a target. The correlator technique described above was then used to identify the location of the building, The translation invariance was achieved automatically, while the rotation and scale variation was accommodated by simply recording many copies of the target object and searching through all of them.
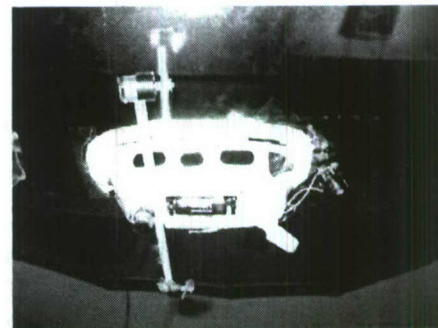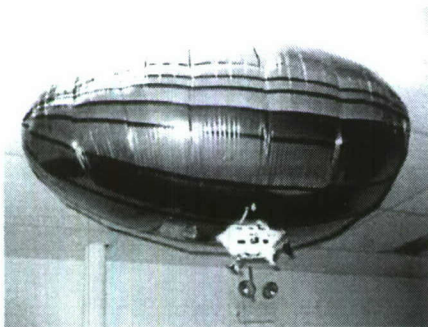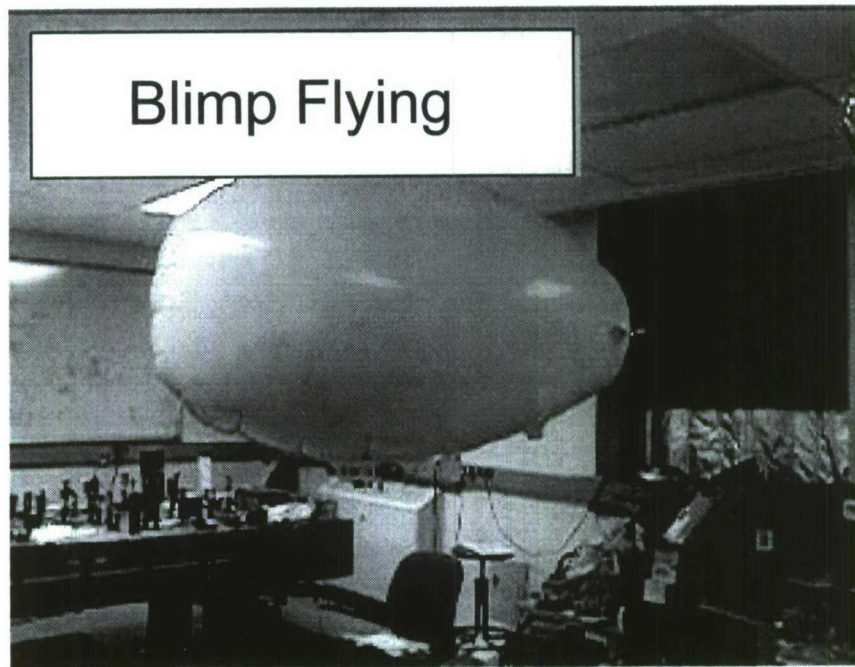
Figure 3: In order to emulate a more realistic UAV flight, we used a remote controlled, helium-filled blimp, fitted with a wireless camera system under it. The blimp was then made to fly around in a pre-designed trajectory above a mock city block. The trajectory was controlled precisely by using a set of four ultrasonic transmitters located on the corners of an optical table (see figure 4), along with an audio-receiver carried by the blimp. The images were captured in real time, and fed into the correlator for landmark identification. We have also developed a flight-simulator software module with hardware interface (see figure 5) that can analyze the correlation data, use it to determine the location of the blimp, and feed guidance information into the remote control system for navigating the blimp. The top picture is the firsts frame of a movie clip that can be downloaded from ftp://lapt.ece.northwestern.edu/ (username: lapt; password: lapt2005) in the directory "holo-targ-rec-new-movies." The bottom two pictures show close-ups of the propellers, the camera, and the audio-receiver.
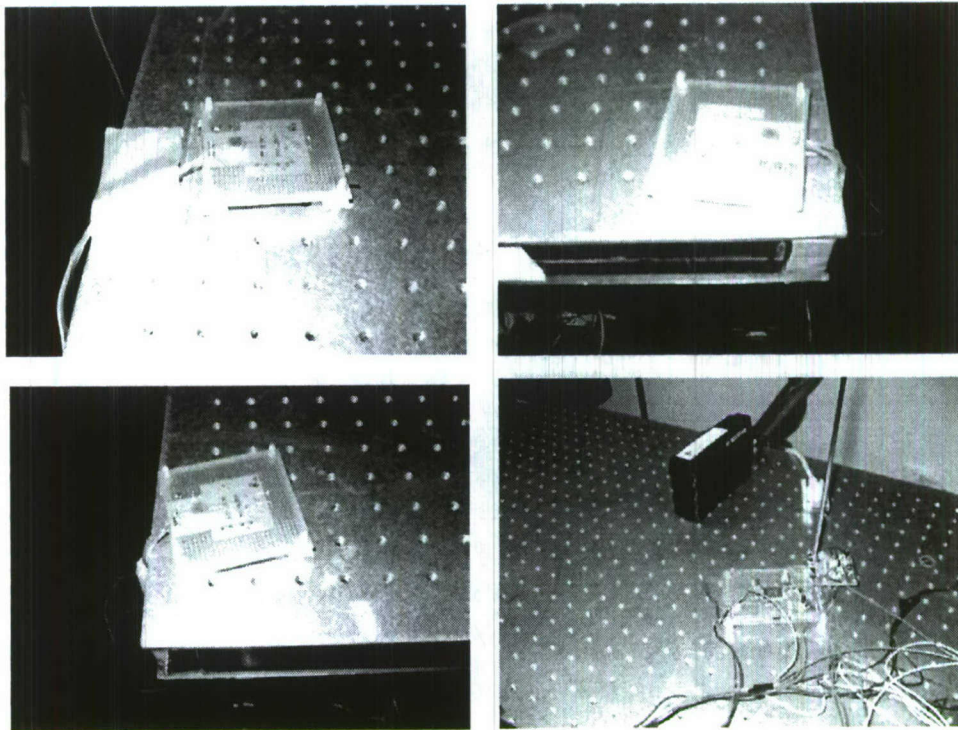
44

Figure 4: The four ultrasonic transmitter cards placed at the corners of an optical table to provide guidance for the blimp which carried an audio-receiver. See figure 2 caption for reference.
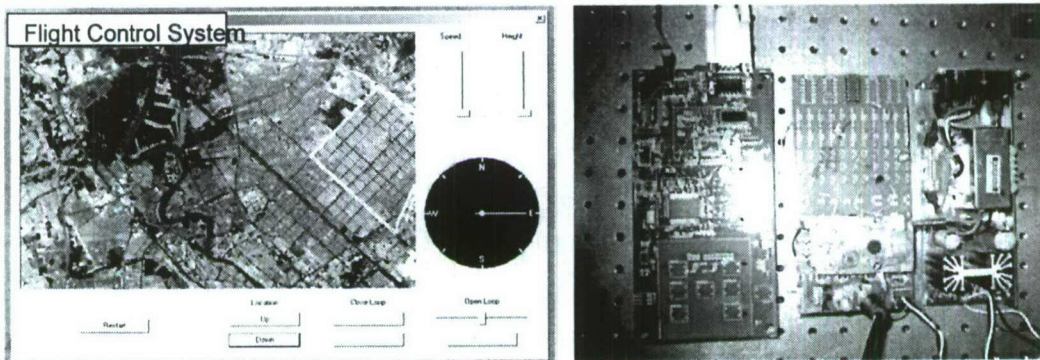

Figure 5: The software module (left) along with the hardware components (right) we have developed for a correlation guided navigation system for the blimp. See the caption of figure 2 for reference.
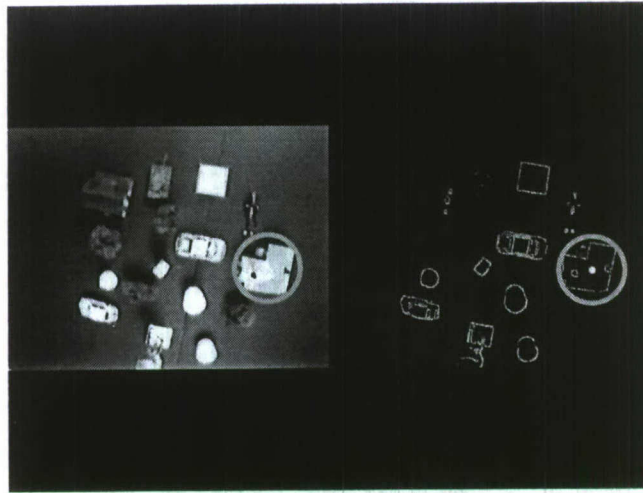
Figure 6: The front frame of a movie that was produced with this system, illustrating the identification of a landmark as the blimp shown in figure 2 flew over a mock city block. Again, the movie can be downloaded from ftp://lapt.ece.northwestern.edu/ (username: lapt; password: lapt2005) in the directory "holo-targ-rec-new-movies."
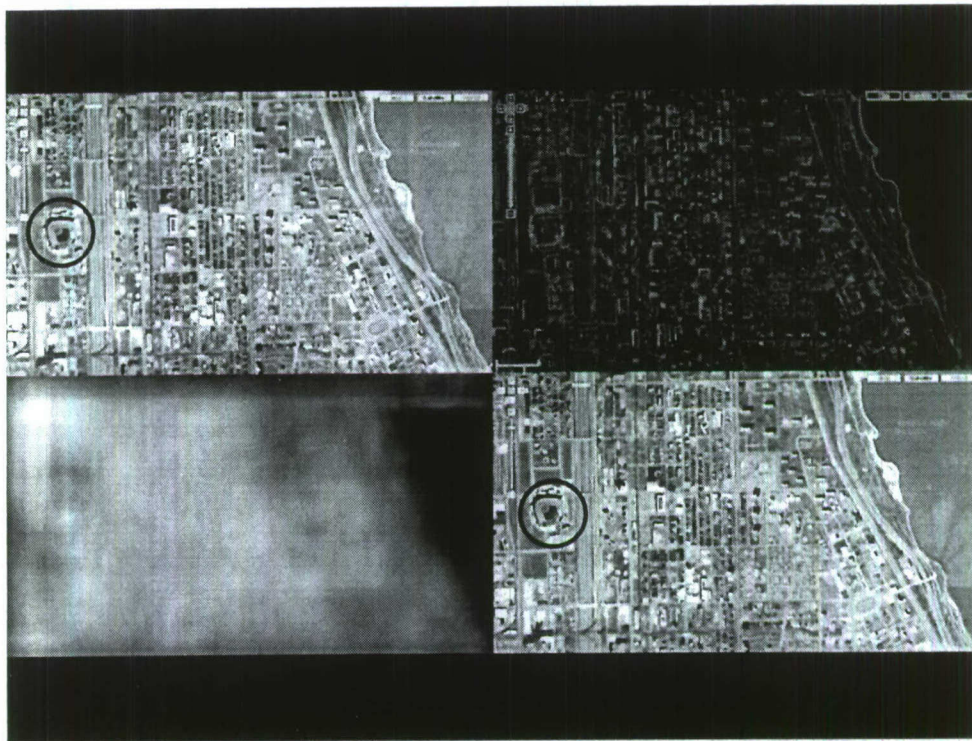

Figure 7. We have shown the feasibility of the landmark identification process by using digital images readily available from googleearth.com. This is the front frame of a movie that illustrates this process. The full movie can be downloaded from ftp://lapt.ece.northwestern.edu/ (username: lapt; password: lapt2005) in the directory "holo-targ-rec-new-movies.". In this movie, we have shown the identification of a landmark in Chicago, as the frames are shifted, simulating what would be seen from an UAV. As before, the process works in a translation an orientation invariant manner.
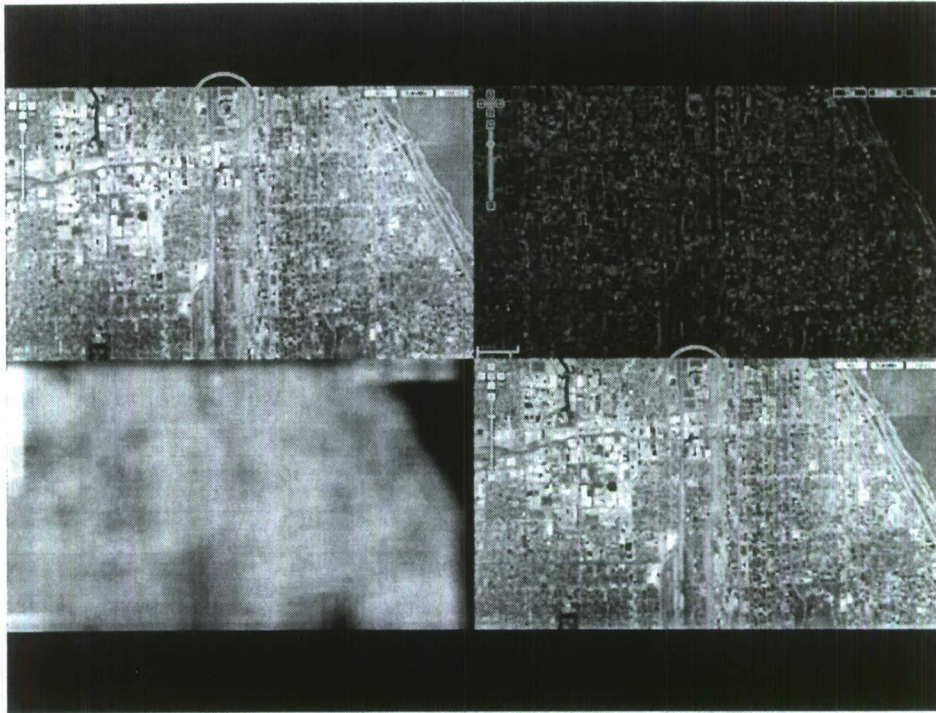
Figure 8: The front frame of another movie similar to the one shown in figure 6, which can be downloaded for viewing from the same URL. Here, we show tracking of the same Chicago landmark, but from a different perspective and a different height
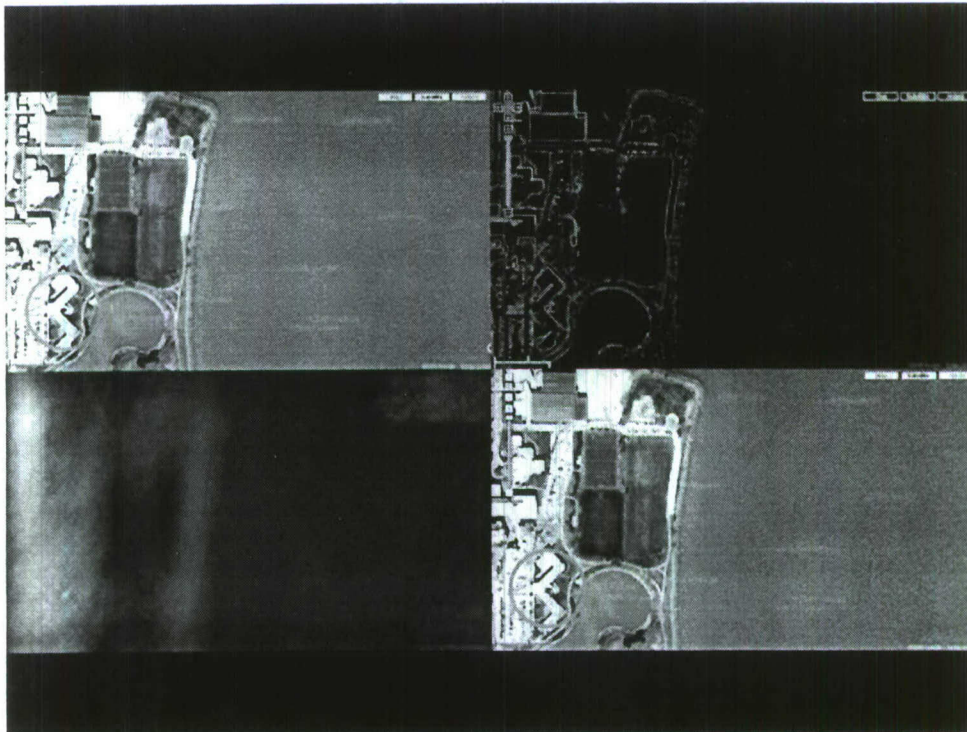

Figure 9: The front frame of another movie similar to the one shown in figure 6, which can be downloaded for viewing from the same URL. Here, we show tracking of the main building of the Northwestern University, Evanston campus.

Figure 10: The front frame of another movie similar to the one shown in figure 8, which can be downloaded for viewing from the same URL. Here, we show tracking of the same building , but from a different perspective and a different height.
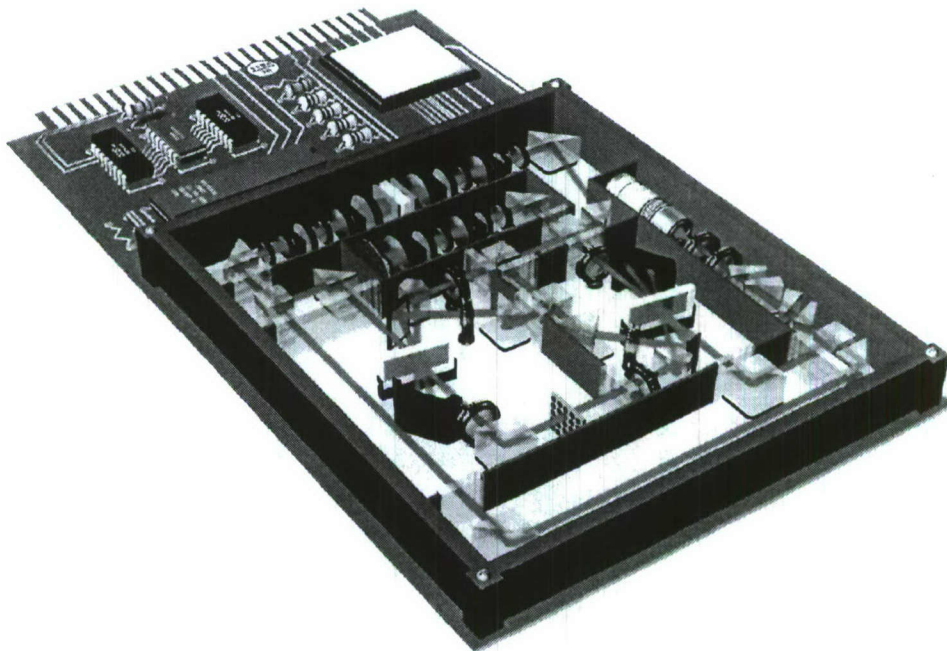
Figure 11: In the near future, our goal is to miniaturize the holographic correator based UAV navigator, in a manner that the whole optical system can fit on a small-foot-print card, as envisioned here in a schematic fashion.

48

Figure 7 illustrates the feasibility of the landmark identification process by using digital images readily available from googlearth.com. This is the first frame of a movie that demonstrates this process. The full movie can be downloaded from ftp://lapt.ece.northwestern.edu/ (username: lapt; password: lapt2005) in the directory "holo-targ-rec-new-movies." In this movie, we have shown the identification of a landmark in Chicago, as the frames are shifted, simulating what would be seen from an UAV. As before, the process works in a translation an orientation invariant manner. Figure 8 shows the first frame of another movie similar to the one shown in figure 7, which can be downloaded for viewing from the same URL. Here, we show tracking of the same Chicago landmark, but from a different perspective and a different height. Figure 9 shows the first frame of yet another movie similar to the one shown in figure 7, which can be downloaded for viewing from the same URL. Here, we show tracking of the ma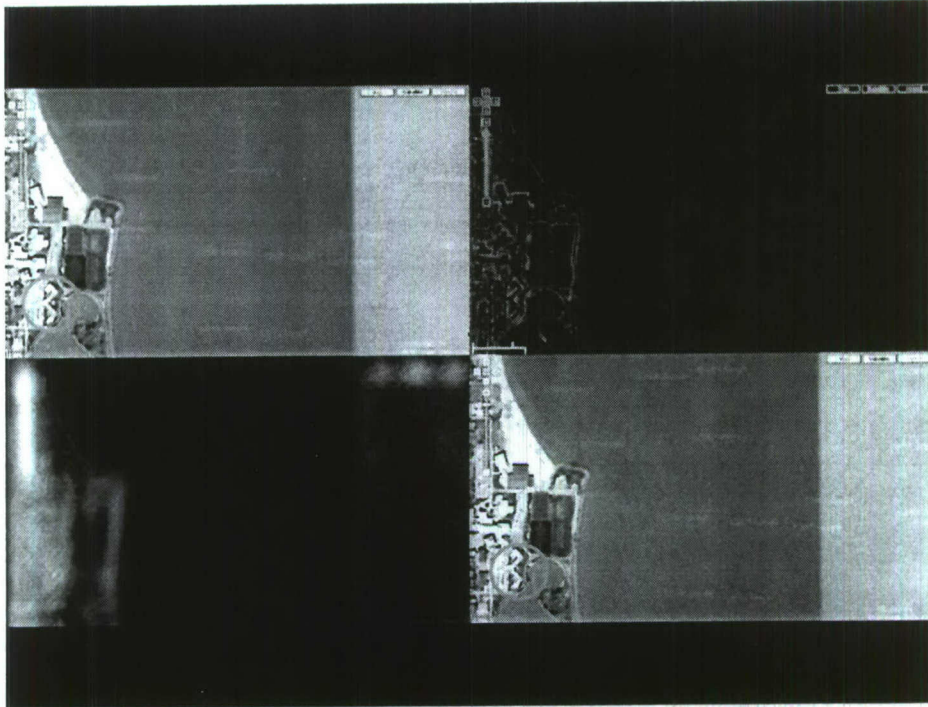in building of the Northwestern University, Evanston campus. Figure 10 shows first frame of a movie similar to the one shown in figure 9, which can be downloaded for viewing from the same URL. Here, we show tracking of the same building , but from a different perspective and a different height

In the near future, our goal is to miniaturize the holographic correator based UAV navigator, in a manner that the whole optical system can fit on a small-foot-print card, as envisioned in figure 11 in a schematic fashion.

SECTION 3: CONCLUSION AND OUTLOOK

A. Conclusion:

The overall objective of this project was to develop an ultrafast target recognition system using holographic techniques, as well as spin-off technologies with other applications. We report here a set of significant accomplishments towards this goal. These include:

- *(1) demonstrations of shared hardware operation of a super-parallel holographic correlator and RAM,*
- *(2) demonstrations of a ultra-fast holographic stokesmeter for polarization imaging*
- *(3) demonstrations of a coherent holographic beam combiner for imaging applications,*
- *(4) demonstrations of off-axis transmission and reflection holographic lenses for use in the super-parallel architecture,*
- *(5) demonstrations of a translation-invariant correlation of images stored via holographic angle-multiplexing in a thick photopolymer material,*
- *(6) development of a large-area, thick, optical quality holographic recording disc capable of storing up to 2 terabyte of data,*
- *(7) demonstration of real-time, pico-second speed, translation-invariant correlation using a novel photorefractive material,*
- *(8) demonstration of automatic target recognition of targets in a view from arbitrary altitudes and orientations during the flight of a remote-controlled aerial vehicle,*
- *(9) demonstration of a multi-spectral holographic stokesemetry based imaging system,*
- *(10) demonstration of spatially-multiplexed holographic lenses with each lens having two separate channels of distinct angular and spectral transmission properties, with applications to a tristimulus filter for an eye-protection system, and*
- *(11) development of a holographic lenslet array for use in the super-parallel architecture of holographic correlator and RAM.*

We have published 21 papers and made 24 conference presentation. Section 2 contains a brief description of these accomplishments. **Three students have received their Ph.D. degrees based on the work reported here.**

B. Technology Transfer:

No Technology Transfer has resulted from the work carried out under this project.

C. Outlook:

In many military as well as civilian applications, rapid target identification is essential. Targets are identified by comparing an incoming image with a database of target images, i.e., by correlating the images. Current image correlation techniques rely upon digital signal processing (DSP) elements which are often too slow for target intercept applications because the data is compared serially. A holographic optical correlator (HOC) offers parallel database searches much faster than DSP. The use of the HOC for practical applications has historically been limited by material and as well as other technical constraints. However, recent advantages in materials, architectures and components --- some of which resulting from the efforts of the PI under prior support

from AFOSR --- have now made it possible to consider HOC based devices for real-world applications. The work performed under this project has paved the way for new directions of research for this puprose. Two such avenues of research are as follows.

Polarimetry Enhanced Holographic Smart Eye for UAV Navigation: An UAV flying over a city or anyother terrain is generally guided by GPS and INS (Inertial Navigation System). However, INS is not very accurate, and GPS may sometimes becomes jammed, or is obstructed due to terrain constraints. Under such a scenario, it is necessary to provide guidance using visual information. One approach is to identify targets with known coordinates, and use this information to navigate the flight of the UAV. The Holographic Smart Eye (HSE) offers this capability. As an example, suppose an UAV such as the Predator is flying over Washington DC, and it has a picture of the Washington cathedral in its data base. It can identify the cathedral even though many other buildings are in its view. The HSE has two components: a Holographic Video Disc (HVD), and a Holographic Dynamic Correlator (HDC). The reference images from multiple (thousands) perpectives are stored in the HVD, which has a capacity close to two terabyte, or about 20 million images. During its operation, the HSE sends the UAV video-camera or SAR input into one channel of the HDC, and an image of the landmark of interest, retrieved from the HVD, into the other channel of the HDC. It may also produce the reference image in real time as it sees a new landmark of interest. The HDC compares these two inputs at a very high speed (pico-seconds), and identifies if the landmark is present, and if so, where. If there is no match, then the HSE scans through additional views of the same landmark. The HDC is translation invariant. Scale and rotation invariance is achieved by simply making use of a very large number of view of the same object, made possible by the massive storage capacity of the HVD. The same technology can also be used to implement general purpose computer vision, and for automated analysis of video data for content extraction, for example. We have demonstrated the feasibility of the HSE based UAV guidance with a helium-filled, radio controlled blimp flying around in the lab. For future work, we can develop a larger scale system that can be deployed in a real UAV. In addition, we can incorporate the capability for the HSE to operate even when the view may be partially obscured due to inclement weather, for example, by adding a Holographic Stokes-meter (HSM). The HSM analyzes the polarization properties of the images, and is thus capable of filtering out clutters produced by clouds, dust or vegetation. The HSM was invented by the PI, and its feasibility has been demonstrated in the laboratory. In a future venture, we expect to realize a version of the HSM that can work seamlessly with the HSE architecture.

Spatio-Spectral Holographic Correlator for Event Detection via Video Clip Correlation: Under some scenarios, it is important to be able to recognize an event within a video captured over a certain time period. Consider, for example, a surveillance operation where an UAV is flying over a territory, looking for unusual activities. The video captured by the on-board camera is to be analyzed in real time or later on, either automatically or by an analyst. The ideal case is that the video will be analyzed automatically and in real time, with an analyst simply entering a query. Suppose the analyst wants to identify the presence and the motion of an enemy vehicle on a road. With current technology, this is to be done in two steps. First, the presence of a given vehicle is to be established by searching through each frame. This is to be followed by an so-called optical flow analysis (OFA), which will attempt to determine the motion of the

vehicle by comparing consecutive frames. The OFA is extremely, slow, inefficient, and time consuming. Under future work, we could develop an automated, single-step method for achieving this goal, using the so-called video clip correlator (VCC), which will work as follows. The analyst will use a query video clip that shows the vehicle moving, for a duration of a few seconds, for example. This will be fed repeatedly into one channel of the VCC. The surveillance video captured by the UAV will be fed into the second channel of the VCC. If the surveillance video contains an event closely matching the query video clip, the output of the VCC will produce an affirmative signal, which will also identify the relative temporal location of the event within the surveillance video data.

The VCC could be created by combining the translation invariant spatial correlator described above (for the HSE) with the process of translation invariant temporal correlation. To illustrate the later, consider a medium that is inhomogeneously broadened. In such a medium, one can record a temporal bit stream by using a subsequent write pulse. The medium stores the Fourier transform of the combined temporal signal. A read pulse applied later on recalls the data stream. Alternatively, a matching data stream applied later on produces a single pulse, indicating data correlation. There is an exact analogy between this process and the holographic spatial correlator. The initial data stream corresponds to the object beam, and the write pulse corresponds to the reference beam, with the time separation being analogous to the the angle between the object and the reference beam. The matching pulse corresponds to the query image, and the output pulse corresponds to the correlation spot. Just as in the case of spatial holography, the process is translation invariant, meaning that the matching pulse can be applied any time after the recording. The two processes (of spatial and temporal correlations) can be multiplexed in the HDC (holographic dynamic correlator) inside the holographic smart eye described above, by making use of its temporal behavior. Specifically, the material used for the HDC can be viewed as inhomogeneously broadened, with the spectral width given by the inverse of its response time. In a future venture, we could establish the feasibility of realizing such a VCC by studying several candidate materials, commensurate with the parameters of the holographic smart eye.